Sox11 promotes neuronal regeneration or death: complexities from heterogeneity

Sox11 promotes neuronal regeneration or death: complexities from heterogeneity

A dissertation presented

by

Michael Norsworthy

to

The Division of Medical Sciences

in partial fulfillment of the requirements

for the degree of

Doctor of Philosophy

in the subject of

Biological and Biomedical Sciences

Harvard University

Cambridge, Massachusetts

September 2017

Sox11 promotes neuronal regeneration or death: complexities from heterogeneity

Abstract

The objective of achieving central nervous system (CNS) restoration after disease or trauma has bedeviled researchers and practitioners for decades. Some of the more recent advances are promising, but the prospect of restoring function after severe injuries remains elusive.

Here, I began with a screen of candidate genes from embryonic development, hoping to identify factors that could promote regeneration in retinal ganglion cells (RGCs). I found that AAV-delivered overexpression of *Sox11* could compel some RGCs to regenerate. Moreover, if *Sox11* was combined with mTOR activation, dramatic regeneration of RGC axons could be seen extending past the optic chiasm. Confusingly, *Sox11* killed other RGCs, including alpha RGCs. The differing abilities of CNS neurons to regenerate is only beginning to be characterized in the literature, and my findings provide the most extreme example to date. *Sox11* may be useful, combined with other regenerative therapies, if its negative effects can be overcome.

Considering the above, many currently promising regenerative approaches could have similar complexities or undetected problems. On the other hand, I argue that more rational engineering, aided by computational simulations, could reduce the search-space for workable therapeutics. I have implemented a basic example of such a simulator, which I name *Celletron*. By modeling the spatiotemporal environment of cells and tissues, with signaling networks too complex for any single person to understand, we might shave years off of screens and studies.

My findings suggest that future studies will need to detect and account for neuronal heterogeneity in regeneration. *Sox11* is a powerful and likely useful axon growth regulator, if its deficits can be addressed. Finally, I outline how developing improved computational tools could accelerate the engineering of CNS-restoring therapies.

Table of Contents

List of figures and tables

Opinion - The continuing need for CNS-restorative therapies

The central nervous system (CNS) executes all of the functions that makes us who we are: it senses the environment, controls motor and visceral outputs, processes internal and external signals, and for at least humans, gives rise to sapience. Many key CNS functions are also outside conscious control, such as sensing and responding to circadian rhythms, controlling heart rate, and decoding motor signals as they descend the spinal cord into instructions for muscle fiber contractions.

The diverse functions of the central nervous system are nearly matched by the diversity of diseases and injuries that can disrupt its operation. Disruptions, at the cellular level, can take the form of apoptosis or necroptosis, improper excitability, overgrowth, decay, improper connectivity, and complete disconnection e.g. the severance of axons, to name a few examples. The tangible presentations of these disruptions have many names including stroke, neurological disorders, cancers, neurodegeneration, and physical trauma. Patients suffering from these disruptions often have no hope of full functional recovery, unless the damaged areas of their CNS can be repaired and/or replaced.

The repair and replacement of CNS tissues is—at least at the surface—a simple directive that unifies the myriad causes of neuronal damage. What more is there, but to simply add some new neurons, and/or tell some neurons to reconnect to their neighbors? Or perhaps we could simply plug in a neuroprosthetic, to replace the damaged tissue's functions? These questions have been the subject of decades of research, and are being answered slowly at best. Clearly, something about the above questions is more complicated than their simplistic phrasing might imply. What are we missing?

In my thesis research, I, like many others, have grappled intensely with these questions. My project began in a fairly traditional way: with a screen, searching for genes that regulate axon regeneration. The rationale—that developmentally expressed transcription factors could regulate axon growth—has foundations in previous axon regeneration studies, even if the particular set of genes

screened was novel. *Sox11* was identified from this screen to promote axon regeneration of retinal ganglion cells (RGCs).

However, soon we found that *Sox11* modestly reduced the survival of RGCs in general, suggesting that it must act on some RGCs to promote their regeneration, and other RGCs to cause their cell death. This observation set *Sox11* apart from other known regenerative treatments including *Pten, Socs3*, *Klf6/7*, *Klf4/9*, *Dclk1/2*, and others. *Sox11*'s differential effects reassert that RGCs and other neurons are heterogenous, *and must be treated as such* to make full functional recovery of damaged nervous systems a reality. Likewise, the inadequacy of previously published regenerative genes may be partially explained through this lens: acknowledging the existence of side-effects, neuronal heterogeneity, and other complexities will help us move forward.

Experimental tools are starting to catch up. Single-cell and *in-situ* RNA sequencing provide snapshots of individual cells' regulatory states, for example. Meanwhile, live imaging of cells can provide readouts of cellular activity over time, albeit at lower throughput. Such observations can characterize results from mechanistic experiments, and provide new lists of candidates for follow-up studies. We are also aided by recently developed transgenic mouse lines that label specific subtypes of neurons. Such mouse lines have recently allowed researchers to selectively observe relatively homogenous populations of neurons in live animals or fixed tissues.

Even with these tools, however, the potential search space for interventions that could restore a nervous system is astronomical. Currently, as biologists, we still lack the means to design and test an intervention as more than an educated guess, and any guess requires months of hands-on time to evaluate. More data, more genetic screens, and more experimental readouts may not achieve full recovery of nervous system function, unless these are accompanied by more comprehensive and predictive modeling. The human nervous system is the most complex system known to exist in the universe, and biologists lack a sufficient CAD application. If the aerospace industry does not rely on

guesses and hand-drawn arrow diagrams to engineer its (relatively simple) products, then we should heed their example.

My thesis research is far from solving these problems. But, I hope that the principles and concepts concerning *Sox11*, RGC and other neuronal heterogeneity, and the development of new computational tools will help provide new ideas on how researchers can ultimately succeed at fully restoring patients' nervous system functions.

Chapter 1 - Background

Retinal development and function

Motivation for regenerative biology

Neuronal regeneration is, in some respects, a chicken-and-egg problem. Neurons would ideally reconnect to their exact prior targets, requiring that they retain some memory of their adult committed state and function; yet, they must regrow and properly navigate axons, likely using regulatory mechanisms similar to their earlier development. We will therefore begin our understanding of retinal axon regeneration with a broad overview of how the retina comes to exist, and how its development progresses to ultimately support functions in the adult.

Formation of the neuroretina

Vertebrate embryogenesis canonically depends on three major germ layers, the ectoderm, mesoderm, and endoderm. Ectoderm on the dorsal surface of a developing embryo folds inwards, forming the neural tube, which will yield most of the cells that eventually form the central nervous system. The caudal portion of the neural tube contributes to spinal cord formation, whereas the rostral portion undergoes sophisticated movements, including inflation of several fluid-filled ventricles that mechanically support and guide the brain's morphogenesis, e.g.(Lowery and Sive, 2005). These chambers include the diencephalon, which gives rise to several structures including specialized collections of cells, the eye fields, which shortly form optic vesicles. These cells expand outwards from the rest of the diencephalon, projecting laterally to contact the inner face of the surface ectoderm. From here, additional movements yield the optic cups, which remain connected to the diencephalon via narrow optic stalks.

The optic cups are the first obvious embryonic features that are recognizable precursors to the eyes. The neuroretina occupies most of the optic cups' surface, and a spherical precursor to the lens is

also present. The neuroretina, at this stage, consists of retinal progenitor cells (RPCs), arranged as a pseudostratified neuroepithelium adhered to a basement membrane. These RPCs proliferate and differentiate into the full complement of neuroretinal cell types required in the adult.

Initial commitment of RGCs from retinal progenitors

Retinal progenitor cells (RPCs) proliferate in the outer nucleoblastic layer throughout retinogenesis. Divisions of RPCs appear to occur three different ways: (1) symmetrically to yield two mitotic RPCs, (2) asymmetrically to yield another RPC, and a postmitotic daughter fated to differentiate, and (3) symmetrically to yield two postmitotic, differentiating daughters. In early retinogenesis, the plurality of RPC divisions is symmetric mitotic, followed by a shift towards asymmetric division, and finally late retinogenesis favors symmetric postmitotic division (Livesey and Cepko, 2001).

Temporally, early differentiation events tend to favor retinal ganglion cells (RGCs), horizontal cells, amacrine cells, and cones, whereas later differentiation tends to favor rods, bipolar cells, and Müller glia. In particular, the early generation of RGCs mainly occurs through asymmetric RPC divisions (Cepko, 2014; Poggi et al., 2005). Such divisions are signaled by the expression of *Math5*/*Atoh7*, in the precursor RPC and/or the RGC that follows, along with migration of the cell towards the ganglion cell layer (GCL).

Math5, a bHLH transcription factor, is critical, though not sufficient, for induction of RGC fate (Brown et al., 2001; Cepko, 2014). *Math5* expression is dependent on *Pax6* (Riesenberg et al., 2009), and *Math5* regulates RPC cell cycle progression and inhibits a homologous transcription factor, the pro-amacrine gene *NeuroD1* (Le et al., 2006). It is also necessary for expression of other RGC-associated downstream genes, including *Brn3b* and *Isl1* (Mu et al., 2005; Vetter and Brown, 2001). Confusingly, despite the differing fates of cells that express *Math5* and *NeuroD1*, mice with a *NeuroD1* knock-in of the *Math5* locus rescued RGC production, and did not increase amacrine cell numbers (Mao et al.,

2008a). As *Math5* and *NeuroD1* have diverged significantly in amino acid sequence, these observations defy trivial explanation. In any case, in normal retinogenesis, *Math5* expression plays an important role in the specification of RGCs within a complex gene regulatory network.

The neuroretina begins to express *Sox11* and *Sox4* following *Math5* expression onset, and a *Math5* deletion partially downregulates their expression (Jiang et al., 2013; Mu et al., 2005). *Sox11* and *Sox4* are close homologs in the *SoxC* group of transcription factors, and are initially expressed broadly, but at low levels, in progenitor cells beginning around E10-E11 in mice (Jiang et al., 2013; Usui et al., 2013). Their expression intensifies in cells differentiating into RGCs, and consequently, the developing inner nucleoblastic layer expresses *Sox11* and *Sox4* more intensely than the outer nucleoblastic layer. While *SoxC* genes might not directly regulate the termination of proliferation in RPCs (Usui et al., 2013), they can influence the overall balance of cell types in the retina. Their importance in post-mitotic RGC development is more evident: *Sox11* and *Sox4* together are absolutely critical for formation of the optic nerve (Jiang et al., 2013), even though their double deletion does not prevent the formation of putative *Brn3b+* RGCs. Apoptosis of retinal cells seems to increase as a secondary, not primary, consequence of *Sox11* or *Sox4* deletion (Jiang et al., 2013; Usui et al., 2013), perhaps related to their inability to connect to required targets, or to incomplete differentiation.

Molecular regulation of RGC axon growth

After induction of *Sox11* and *Sox4*, differentiating RGCs localize towards the nascent ganglion cell layer, and begin to project their axons. Initial axon specification in neurons depends on GSK-3β (Polleux and Snider, 2010). GSK-3β locally regulates key cytoskeletal actuators including APC, Tau, and Map1b (Polleux and Snider, 2010). Other factors such as Par3/Par6, PI3K/PTEN, and Akt/PKB are also involved in axon specification (Polleux and Snider, 2010). Subsequently, extension of specified axons requires a growth cone, a structure that locally executes the neuron's navigation decisions through

regulations that influence the mechanics of the cone's internal cytoskeleton and its external adhesion to the surrounding environment. In CNS neurons including RGCs, the cytoskeletal regulator *doublecortin*/*DCX* is necessary for correct extension and guidance of the growth cone. *Sox11* and/or *Sox4* regulate *DCX* and many other genes implicated in axon specification and extension including *Tubb3* and *Map2* through either direct or indirect mechanisms (Bergsland et al., 2006; Usui et al., 2013). These considerations establish *Sox11* and *Sox4* as key players in the specification and extension of axons in differentiating RGCs.

As axons extend, they integrate a variety of external and internal cues to successfully navigate from a differentiating neuron's cell body to its target. Growing RGC axons first extend through the retina's nerve fiber layer (NFL), limited on the inner face by the end-feet of Muller glia, and on the outer face by GCL repulsion. Navigation within the NFL is mediated in part by NCAM and Slit-Robo signaling (Erskine and Herrera, 2007). Slit signaling is necessary to contain RGC axons within the NFL, but is dispensable for overall directionality of growth: its loss of function permits RGC axons to escape the NFL, but the axons still grow towards the optic disk (Erskine and Herrera, 2007).

Interestingly, some overall navigational cues may come from the 'inwards-out' pattern of overall retinal differentiation. For one, growing RGC axons will tend to fasciculate with already-existing axons. This may make more peripheral RGCs, seemingly with more demanding navigation requirements, able to simply follow well-worn paths created by previously differentiated RGCs (Oster et al., 2004). Additionally, a variety of central-peripheral attractive and repulsive cues provide navigation information. For one example, neuroretina is initially high in CSPG expression, such that for any differentiating RGC, relatively peripheral tissue will repel nascent axons with CSPGs. As well, *Shh* is expressed higher in central retina, and provides an attractive growth cue (Erskine and Herrera, 2007). Eventually, axons reaching the optic disk turn towards the optic nerve. This turn requires local glial cells to express netrin-

1, with axons expressing its receptor, DCC (Deiner et al., 1997; Erskine and Herrera, 2007; Petros et al., 2008).

As retinal axons reach the midline at the optic chiasm, most will cross contralaterally, while some will remain ipsilateral. The ability of axons to cross the optic chiasm midline is in part explained by homotypic NrCAM interaction between cells at the chiasm and by growth cones (Petros et al., 2008). Plexin A-1, Sema, and Slit signaling are also implicated (Kuwajima et al., 2012; Petros et al., 2008). Interestingly, *SoxC* genes have recently been shown to promote contralaterality of differentiating RGCs, suggesting that *Sox11* and its homologs may have roles in axon guidance in addition to its other regulatory targets (Kuwajima et al., 2017). On the other hand, ipsilateral-projecting axons express *EphB1*. Growth cone-localized EphB1 receptor interacts with midline-expressed ephrinB2 repulsively, such that ipsilateral-projecting axons are always repelled by the midline (Williams et al., 2003). *Zic2* expression is sufficient to drive *EphB1* expression and induce ipsilateral projection in RGCs (Lee et al., 2008).

Thereafter, axons project into the targets such as the SC and LGN, with stereotyped retinotopic patterns. The retinal nasal-temporal axis is signified with a gradient of EphA expression, while its dorsal-ventral axis is signaled with EphB gradients (Triplett and Feldheim, 2012).

More generally, the transcription factors *Brn3b* and *Isl1* are important regulators of RGC axon navigation, and are both targets of *Math5* regulation (Pan et al., 2008). They are expressed immediately upon RGC commitment, and remain expressed throughout development. Embryonic mice with homozygous *Brn3b* deletions initially develop with an approximately normal number of RGCs, but axons extending from RGC cell bodies tend to wander unsteadily in the retina, and occasionally fail to turn towards the optic disk (Erkman et al., 2000). Further *Brn3b*$^{-/-}$-induced axon navigation defects occur at the optic chiasm, the LGN, and in topographic mapping, such that nearly all RGCs ultimately fail to innervate their correct targets and undergo cell death in postnatal and juvenile mice (Erkman et al.,

2000). *Isl1* appears to have a similar role in RGC axon pathfinding; its deletion results in misdirection of axons at the optic chiasm, and causes delayed RGC death (Pan et al., 2008). Moreover, the combined loss-of-function of *Brn3b* and *Isl1* results in the near-complete absence of the optic nerve by adulthood (Pan et al., 2008). Interestingly, some gene targets are shared between *Brn3b* and *Isl1*, including *Stmn2* and *Gap43*, which are implicated in cytoskeleton and growth cone regulation (Li et al., 2014). Considering the above, *Brn3b* and *Isl1* appear to be important regulators at many steps of axon growth and guidance in RGCs.

Mechanical regulation of axon outgrowth

In addition to the molecular mechanisms in the previous section, the biomechanical environment contributes to the regulation of axon growth and guidance. Biomechanics could conceivably influence growth in at least two ways: first, by imposing physical constraints (i.e., either barriers or permissible channels), and second, by providing mechanical cues for mechanosensitive signaling pathways. Recently it was demonstrated *in vivo* that Xenopus *Piezo1* senses the mechanical environment in RGC axons growing in the optic nerve, and that it is necessary for correct navigation towards relatively soft brain tissue targets (Koser et al., 2016). Mechanics and mechanosensing may be of substantial interest for future studies in both neuroregeneration and neuroprosthetics.

Developmental RGC specialization into subtypes

For visual functions in the adult, RGCs must specialize into subtypes with different dendritic structures, connections to other cells, gene expression, projections to different target centers in the brain, etc. Specialization in RGCs begin around the initial commitment and differentiation steps during retinogenesis. Furthermore, decisions made throughout development, like whether to cross the optic chiasm contralaterally, or to remain ipsilateral, likewise support specialization. On the other hand, it is

less clear whether specific developmental timing affects the preference for any particular RGC subtype (De la Huerta et al., 2012; de Melo et al., 2005).

A study on direction-selective RGCs exemplifies this early decision process towards specialization (De la Huerta et al., 2012; Livesey and Cepko, 2001). Specifically, a specific subtype of oods-RGCs is predicted by early expression of *Cdh6* (De la Huerta et al., 2012). Expression begins in a small subset of retinal progenitor cells (RPCs) by E10-E12 (De la Huerta et al., 2012), and it is likely that these cells correspond to *Cdh6*-expressing RGCs which are born around E10-E12 (De la Huerta et al., 2012). These *Cdh6*-expressing RGCs largely express CART, a more classical marker of oods-RGCs, and stratify with amacrine cells in the IPL in the expected manner (De la Huerta et al., 2012). Interestingly, *Cdh6* expression is restricted to only one type of oods-RGC; while nearly all *Cdh6*+ RGCs are oods-RGCs, around half of oods-RGCs are *not Cdh6*+, e.g. they might express *MMP17* instead, and correspond to a different type of oods-RGC (De la Huerta et al., 2012). Similarly, another type of ds-RGC, the 'J'-RGC, was found to express *JAMB* by E10 in mice (De la Huerta et al., 2012).

Also expressed early in RGC development is *Tbr2*/*Eomes* (Mao et al., 2008b). *Tbr2* is expressed in committed, differentiating RGCs localized to the GCL by E14.5, and is a regulatory target of *Brn3b*/*Pou4f2* (Mao et al., 2008b). While *Tbr2* loss-of-function has multiple effects such as increased apoptosis and axon misguidance (Mao et al., 2008b), it is particularly notable for its apparent restriction to non-image-forming RGCs, including M1-, M2-, and M3-ip-RGCs (Sweeney et al., 2014; Triplett et al., 2014). Interestingly, *Tbr2* appears to be anti-correlated with *Brn3a*/*Pou4f1* expression: *Brn3a* is expressed in most RGCs, whereas *Tbr2* expression covers most of the remainder (Sweeney et al., 2014; Xiang et al., 1995).

Further possibilities for early specialization include relative balances of *Brn3a*, *Brn3b*, and *Brn3c* expression. These are ultimately expressed combinatorially in morphologically distinct subsets of RGCs in adults (Badea and Nathans, 2011; Nadal-Nicolás et al., 2012; Xiang et al., 1995). As these are some of

the earliest genes invoked in RGC differentiation, their relative expression levels, combined with other mechanisms, are likely involved in the initial generation of RGC subtypes (Gan et al., 1996; Xiang et al., 1995). As well, this differential gene expression pattern could contribute to the maintenance of RGC subtype identities and/or target innervation in adulthood.

Visual targets of RGC subtypes after gestation

Many different subtypes of RGCs have been identified in mice over the years, through various methods and degrees of detail. Some have been linked to analogous, or perhaps homologous, RGC types in other animals such as primates. Recently, the number of defined RGC subtypes has grown to over 30 in the mouse (Baden et al., 2016; Martersteck et al., 2017). Equally complicating to this picture, the number of retinal axon targets has grown beyond the canonical targets like the LGN, SCN, and SC, and these targets' functions and mechanisms of processing are often unknown (Martersteck et al., 2017; Morin and Studholme, 2014).

Nevertheless, the major target for image-forming vision is the LGN, which subsequently sends signals through the optic radiations to the visual cortex (V1). Briefly, a variety of RGC subtypes project to the LGN, including alpha/parasol RGCs (Crook et al., 2008; Huberman et al., 2008), oods-RGCs (Kay et al., 2011), and M3-, M4/ON-alpha-, and M5-ip-RGCs (Ecker et al., 2010; Matynia, 2013). In primates, a given LGN will receive input from half of both eyes; specifically, the visual fields from both eyes overlap in support of binocular vision (Casagrande and Boyd, 1996). Within the LGN, different layers are responsible for processing inputs from the ipsilateral and contralateral eyes, as well as complex arrangements of inputs from different RGC subtypes (Casagrande and Boyd, 1996; Kim et al., 2010). The LGN also receives input from the visual cortex and other central nuclei (Casagrande and Boyd, 1996). All of these layers are generally aligned retinotopically, and together might contribute to the processing behind binocular vision (Casagrande and Boyd, 1996).

A second major target of many different RGC types is the SC, which helps control eye and body movements towards visual stimuli. Interestingly, for controlling gaze shifts, the SC represents the displacement of a target from the fovea according to a topographic map: large displacements (where a target is visible at the peripheral retina) are reflected in caudal SC activation, whereas small displacements activate the rostral SC (Soetedjo et al., 2002). This topographic encoding helps specify eye saccades and head movements, but may be updated too slowly to provide continuous motor feedback (Klier et al., 2001; Soetedjo et al., 2002). There appears to be significant overlap in terms of RGC subtype input to the SC and dLGN including oods-RGCs and alpha-RGCs / parasol RGCs (Crook et al., 2008; Huberman et al., 2008; Kim et al., 2010), though the SC in mice may be privileged to additional RGC subtypes that tend to be more sensitive (Ellis et al., 2016). This contrasts with observations in primates, where the dLGN instead appears more privileged in receiving small-field, sensitive inputs (Ellis et al., 2016).

Other important targets include the suprachiasmatic nucleus (SCN) and olivary pretectal nucleus (OPN), which both respond to ambient light levels. The SCN is responsible for entraining the circadian clock, dependent on retinal input from a minority of RGCs that express melanopsin and are intrinsically photosensitive (Berson et al., 2002; Freedman et al., 1999; Hattar et al., 2002; Moore et al., 1995), whereas the OPN regulates pupillary constriction, as well as indirect regulations of reflexive blinking and tear secretion (Fogerson and Berson, 2012). The OPN receives ip-RGC and perhaps also non-ip-RGC inputs (Chen et al., 2011).

More specifically, ip-RGC input to the SCN is approximately 80% from M1-ip-RGCs, and 20% from M2-ip-RGCs, whereas the OPN receives mixed ip-RGC (45% M1 and 55% M2) and non-ip-RGC inputs (Baver et al., 2008). However, without signaling from M1-ip-RGCs, the OPN is mostly unable to induce pupillary restriction (Chen et al., 2011). Signaling and behavioral phenotypes stemming from M2-

ip-RGCs is less clear, but is known to integrate inputs from both melanopsin and more canonical rod- and cone-expressed signaling (Baver et al., 2008).

Clearly, vision is a complex phenomenon (or, rather, a complex collection of phenomena). We have recently started to understand the basic mechanisms and neuroanatomy behind visual processing, but much more work will be required to compile, and then reverse-engineer, the specifics of how all retinal signals are encoded, integrated in central targets, cross-referenced to other visual (and non-visual) signals, and then understood by an animal as its view of the world.

CNS restoration

Regeneration: embryonic development all over again?

In the previous sections, we have discussed general principles in RGC development, and named a few genes with important roles in the process. Clearly, neural development is complex, involving gene networks, context specificity, and temporally dynamic regulatory states. The goal of neural development is the same as that of any CNS restoration strategy – both seek to yield a fully functional nervous system, involving the production, survival, and connectivity of neural tissue. Complexities aside, it is natural to suppose that embryonic genes might recapitulate their developmental roles if re-used during CNS-restoring treatments.

An important implementation of this strategy has explored the use of manipulating several *Klf*-family transcription factor homologs in CNS regeneration. Initially, *Klf4* was identified as an inhibitor of neurite outgrowth, from a candidate list of developmentally regulated genes (Moore et al., 2009; Wang et al., 2007). Overexpression of *Klf4* decreases outgrowth of both axons and dendrites, and causes growth cone enlargement (Moore et al., 2009). Normally, *Klf4* expression increases through E21, peaks postnatally, and remains high in adulthood (Moore et al., 2009). Its deletion improves axon outgrowth in adult optic nerves (Moore et al., 2009). Similarly, *Klf1*, *Klf2*, *Klf5*, *Klf9*, *Klf13*, *Klf14*, and *Klf16* all reduced

outgrowth of neurites if overexpressed in culture, and most of these reach their highest expression levels in postnatal or adult mice (Moore et al., 2009). Conceptually, inhibitory *Klfs* might promote maturation of axons and dendrites, ceasing any ongoing extension.

On the other hand, *Klf6* and *Klf7* enhance neurite outgrowth, and are expressed highest in embryogenesis (Moore et al., 2009). Furthermore, a separate group observed elevated expression of *Klf7* in *Math5*-expressing, differentiating RPCs/RGCs, relative to non-*Math5*-expressing cells (Gao et al., 2014). These data provide an earlier snapshot of the RGC transcriptome than Wang et al, 2007's data, placing *Klf7* expression as beginning during the earliest commitment of putative RGCs. Interestingly, overexpression of an engineered form of *Klf7* in adult mice can promote modest CNS regeneration (Blackmore et al., 2012). From the above, the *Klf* family of genes appears to validate the idea of overexpressing early-development genes, or suppressing late-development genes, to partially recapitulate the genes' developmental roles to improve regeneration. That said, the current examples of *Klf* treatments yield modest phenotypes, affecting only a handful of regenerating fibers.

Hyperactivation of the mTOR pathway is another example of a cell-intrinsic genetic therapy which can result in some neurogenic cellular behaviors. Deletion of *Pten* or *Tsc* increases mTORC1 pathway activation, resulting in increased RGC axon outgrowth and survival (Park et al., 2008). Interestingly, elevated mTORC1 activation is characteristic of earlier RGC development, as illustrated in a developmental time-course of p-S6 staining in embryonic, postnatal, juvenile, and adult RGCs (Park et al., 2008). As well, the mTOR pathway is necessary to regulate cell growth, survival, and proliferation in a variety of other embryonic contexts (Murakami et al., 2004; Zhu et al., 2013). Considering the above, mTOR hyperactivation illustrates the potential usefulness of recapitulating embryonic signaling for adult regeneration.

Another, more classic example of regeneration recapitulating development is that of *Gap43*, whose protein product is transported to growth cones during embryonic development, but is normally

downregulated in neurons of the adult CNS (Skene and Willard, 1981). However, *Gap43* overexpression either by itself, or in conjunction with *L1* overexpression, has rather limited effectiveness in promoting regeneration of Purkinje cell axons (Zhang et al., 2005). Moreover, a *Gap43* knockdown reduces RGC regeneration in zebrafish, although its phenotype is outclassed by knockdown of *Ascl1a*, an upstream transcription factor (Williams et al., 2015). Therefore, while this serves as another example of regeneration recapitulating neurogenesis, *Gap43* also suggests another point: the potency of using an embryonic gene for regeneration will depend on the specific mechanisms involved, and the usage of 'upstream regulators' to activate several pathways simultaneously may sometimes be desirable.

Many other regenerative treatments published thus far can be related to recapitulating roles in embryonic development. The comparisons are imperfect, and some interventions such as lens injury certainly do not fit this mold (Lima et al., 2012). Furthermore, zebrafish optic nerve regeneration partially recapitulates developmental signaling, but not completely (Veldman et al., 2007). Nevertheless, this regime may be helpful to advance overall understanding (Filbin, 2006).

Extrinsic versus intrinsic regeneration strategies

Classic experiments found that grafting peripheral nerve tissue into a CNS lesion improved regeneration (David and Aguayo, 1981). Since then, many studies have implicated the extracellular environment as playing important roles during CNS regeneration, and these studies seem to favor the importance of molecular signaling over physical blockage of axon growth (Fitch and Silver, 2008). However, other findings suggest the roles of some of these inhibitory mechanisms, including the famous *Nogo*, are less clear than previously thought (Grados-munro and Fournier, 2003; Lee et al., 2010).

Environmental inhibition may be, in part, developmentally programmed, rather than exclusively a function of post-trauma glial scar formation. For example, laser-axotomized central neurons regenerate inefficiently in a scar-minimal environment, indicating that prevention of a scar is not

sufficient to induce regeneration (Canty et al., 2013). On the other hand, young but not old neurons efficiently extend axons on myelin-associated glycoprotein, suggesting that in this context developmental maturation is sufficient to limit regeneration (Cai et al., 2001). Moreover, the age of Schwann cells accounts for age-related decline in PNS regeneration (Painter et al., 2014). We can see that interactions between neurons and their environment are complex and developmentally regulated.

Many of these extracellular signals act as cues for intracellular transduction pathways. For example, the developmental decline of neuronal growth on myelin-associated glycoprotein can be ameliorated through elevated cAMP signaling, or worsened through PKA loss-of-function (Cai et al., 2001). Similarly, inflammatory agents promote RGC regeneration in a manner that depends on CNTF as well as intracellular JAK/STAT3 signaling (Leibinger et al., 2009). STAT3 signaling is strongly upregulated by a SOCS3 deletion, and SOCS3 deletion potently promotes regeneration of RGCs either by itself (Smith et al., 2009) or in combination with PTEN deletion (Sun et al., 2011).

Considering the above, it appears possible to regulate axon regeneration at many levels, and that divisions between environmental and cell-intrinsic therapies may be somewhat artificial. Interestingly, there are examples of simultaneous intrinsic and extrinsic manipulations – such as loss-of-function of *Pten* and *Nogo*, which had a complex, but positive regenerative phenotype (Geoffroy et al., 2015), or of zymosan, *Pten* loss-of-function, and cAMP elevation (Lima et al., 2012). Therefore, we should be mindful of these and all the other possible treatments before us, and attempt to select the most promising options, regardless of mechanism, for possible synergistic effects.

Neuroprosthetics: a 'stimulating' field

In contrast to recent recovery of partial vision in mice from axonal regeneration (Bei et al., 2016; Lim et al., 2016; Lima et al., 2012), the use of direct surgical interventions to evoke visual sensation in humans, bypassing the optic nerve, is ancient history. The first reports of these sensations, or

phosphenes, were by Löwenstein and Borchardt (1918), Krause (1924), and Otfrid Förster (1929). It was found that phosphenes were perceived according to a retinocortical map, and that phosphenes could be grayscale or colored (Lewis and Rosenfeld, 2016; Penfield, 1947; Piotrowska and Winkler, 2007). The concept, even if primitive by today's standards, of using these findings for a neuroprosthetic was patented soon afterwards (Lewis and Rosenfeld, 2016; Shaw, 1955).

One of the earliest publications that demonstrated the power of cortical visual prosthetics was by Brindley and Lewin (1968), who found in human subjects the ability to discriminate several different letters. In a review, Lewis and Rosenfeld (2016) comment that, at the time, the Brindley and Lewin publication was so impactful that "the UK Medical Research Council formed the Neurological Prosthesis Unit", that it resulted in increased funding of the field by the precursor of the NIH's NINDS, and that "there was a steady increase in the development of neuroprosthetic and specifically visual prosthetic technologies throughout the 1970s" (Lewis and Rosenfeld, 2016). The principle of this result – multi-phosphene evocation from visual cortex stimulation – was upheld by subsequent publications in humans and non-human primates (Dobelle and Mladejovsky, 1974; Dobelle et al., 1974). Furthermore, Schmidt et al (1996) report on some ability of evoked phosphenes to be perceived as colored. Interestingly, when former participants of neuroprosthetic studies were interviewed, many participants described "feelings of loss" after their studies concluded (Lane et al., 2013). Thus, even the current capabilities afforded by neuroprosthetics are emotionally meaningful to patients.

Compared to neuroregenerative approaches, involving complex and potentially tumorigenic signaling networks, the potential side-effects of a neuroprosthetic are limited and well characterized. Occasional microbial infections were reported, but this problem appears largely solved (Rushton et al., 1989). There have also been some reports of implant-induced seizures (Lewis and Rosenfeld, 2016; Naumann, 2012; Pudenz, 1993), though Pudenz (1993) notes stimulation amplitudes around 2.5

milliamps, compared to a more recently published current on the order of tens of microamps (Callier et al., 2015).

Local neuronal damage has also been reported from intracortical neuroprosthetic stimulation (McCreery et al., 2010), but it appears that such collateral damage does not greatly diminish neural function over time (Chen et al., 2014). Encouragingly, visual and other sensory stimuli appear functional after at least two years post-implantation (Callier et al., 2015; Davis et al., 2012). This contrasts with recording/ descending-type neuroprosthetics: recording requires fine sensitivity to relatively small signals, whereas stimulation is at liberty to induce relatively larger electrical charges. Therefore, stimulation/ascending-type neuroprosthetics (i.e., for vision, proprioception, etc.) are likely tolerant to the formation of glial scars, despite the reputation of some neuroprosthetic designs to cause scarring.

Despite these advances, visual cortical prosthetics (and, by extension, other neuroprosthetics) are limited by several unanswered questions, including at least: (1) How does visual processing normally function in intact tissue? (2) Where, within three-dimensional layered tissue, should electrodes or other stimulators best target for particular signaling goals? (3) How can neuroprosthetics 'learn' (digitally, physically, or biochemically) to emulate synaptic refinement and pruning? (4) What physical and biochemical considerations can sufficiently reduce undesired physiological reactions to implants? (5) Can surrounding tissues be bioengineered to more readily accommodate neuroprosthetics? (6) What engineering differences might there be between neuroprosthetics for image-forming vision, versus non-image-forming vision e.g. circadian entrainment? And (7) are any new analysis, fabrication, or engineering techniques or tools needed to support answers for the previous questions? While answering the above questions should not be required for partial functional recovery, answering them should accelerate and improve partial recovery, and make full functional recovery possible.

A complex, interdisciplinary problem

I propose that for full functional recovery of visual systems, we should consider integrating mixed treatments of cell-signaling/genetic therapies to promote cell survival and neurite regrowth at innervation targets, regulation of the surrounding tissue context, and precisely designed neuroprosthetics that process raw incoming light signals into appropriate spatiotemporal depolarization patterns. In all these aspects, it will be important to respect cell, tissue, and signaling heterogeneity. Much more scientific exploration will be needed to characterize, understand, and model these complex systems, and this must be matched by equally challenging engineering and validation work across all disciplines. Acknowledging challenges posed by such interdisciplinary research in terms of cognition and communication, I additionally advocate for building tools and pipelines that facilitate decentralization of expertise and engineering efforts. After all, “Nothing is particularly hard if you divide it into small jobs” (Henry Ford).

Chapter 2 - *Sox11* Expression Promotes Regeneration of Some Retinal Ganglion Cell Types but Kills Others

Summary

At least 30 types of retinal ganglion cell (RGC) send distinct messages through the optic nerve to the brain. Available strategies of promoting axon regeneration act on only some of these types. Here we tested the hypothesis that over-expressing developmentally important transcription factors in adult RGCs could reprogram them to a "youthful" growth-competent state and promote regeneration of other types. From a screen of transcription factors, we identified *Sox11* as one that could induce substantial axon regeneration. Transcriptome profiling indicated that *Sox11* activates genes involved in cytoskeletal remodeling and axon growth. Remarkably, α-RGCs, which preferentially regenerate following treatments such as *Pten* deletion, were killed by *Sox11* overexpression. Thus, *Sox11* promotes regeneration of non-α-RGCs, which are refractory to *Pten* deletion-induced regeneration. We conclude that *Sox11* can reprogram adult RGCs to a growth-competent state, suggesting that different growth-promoting interventions promote regeneration in distinct neuronal types.

Introduction

Neurons in the adult central nervous system (CNS) regenerate poorly after damage. Both extrinsic inhibitory factors and intrinsic constraints on growth in mature and injured neurons contribute to this regenerative failure. Recent studies have identified several methods that can activate growth-associated signaling pathways and promote neuronal survival and axon regeneration after injury (Benowitz et al., 2017; Bradke et al., 2012; Crair and Mason, 2016; He and Jin, 2016). However, the regeneration effects observed to date are still limited. For example, the activation of mTOR by deleting *Pten* or over-expression of osteopontin (OPN; *Spp1*) and insulin-like growth factor (*Igf1*) promotes the selective regeneration of α-RGCs (Duan et al., 2015; Park et al., 2008), which comprise only ~6% of RGCs

in intact retinas (Duan et al., 2015; Sanes and Masland, 2015). Thus, new strategies are needed to promote regeneration of other types of RGCs.

We reasoned that manipulation of transcription factors that act as master controlling factors of axon growth during development might represent another avenue for promoting axon regeneration in adults. In fact, previous studies have shown that manipulations of Krüppel-like family of transcription factors (KLFs) promoted axon regeneration (Moore et al., 2009). However, the observed regeneration after KLF manipulations are relatively modest. A possible clue is that KLF expression changes significantly during the early postnatal period, coincident with dramatically decreasing axon growth ability in the neonatal age (Goldberg et al., 2002). Thus, KLFs might maintain an axon growth program once it has been activated by other factors, rather than initiating such a program. Based on this reasoning, we focused here on transcription factors that regulate the early differentiation of RGCs, during which axon growth is initiated (Livesey and Cepko, 2001; Mu and Klein, 2004).

Results

Identification of Sox11 as a regeneration-promoting transcription factor

We tested 7 transcription factors for their ability to promote optic nerve regeneration. Genes were delivered by intravitreal injection of AAV serotype 2 vectors (AAV2) to mouse retinas; our previous work showed that this protocol can lead to transduction of > 90% of RGCs (Nawabi et al., 2015; Park et al., 2008). As a control, we injected AAV-Plap (placental alkaline phosphatase, hereafter “AAV-Control”), an unrelated protein with no detectable effect on retinal structure or regeneration (Bei et al., 2016; Nawabi et al., 2015). Two weeks after virus injection, the optic nerve was crushed. After another two weeks, axon regeneration was monitored by an anterograde tracer fluorescent-conjugated cholera toxin subunit B (CTB).

Overexpression of *Sox11* significantly increased regeneration of RGC axons (Figures 2.1.A, 2.1.C, S.1.A, S.1.B). *Sox4* (a *Sox11* homolog) and *Brn3b* (Figure 2.1.A-C) also increased axonal regeneration, but these effects did not reach statistical significance. The four other genes screened did not detectably increase regeneration (Figure 2.1.A-C). We verified expression of AAVs either in retinas or in culture (Supplemental Figures S.1.A-B and S.5, and data not shown). Interestingly, although some of these factors such as *Sox2* have been shown to be able to reprogram terminal differentiated fibroblasts into multipotent neuronal stem cells (Ring et al., 2012), in our hands, their over-expression failed to promote axon regeneration after injury. We therefore focused on *Sox11* in subsequent studies.

In a separate experiment, we found that at 4 weeks after injury, *Sox11*-induced axons frequently extended more than 4 mm past the crush site at this time (Figure S.1.C-D). However, *Sox11* expression failed to increase neuronal survival and instead modestly decreased RGC survival (Figure 2.1.D and 2.1.E), as revealed by immunostaining retinal sections with antibodies to the pan-RGC marker RBPMS (Rodriguez et al., 2014). Thus in contrast to other interventions such as the deletion of *Pten* and/or *Socs3*, which increase both neuronal survival and axon regeneration (Park et al., 2008; Sun et al., 2011), *Sox11* over-expression promoted axon regeneration but not survival.

Figure 2.1: Over-expression of Sox11 promotes optic nerve regeneration

(A, B) Representative images of optic nerve sections showing CTB-labeled axons in wild type mice with intravitreal injections of AAV-Plap (AAV-Control), AAV-Sox4, and AAV-Sox11 (A), and AAV-Pax6, AAV-Math5, AAV-Sox2, AAV-Brn3b, and AAV-Isl1 (B) at 2 weeks after optic nerve injury. The crush site is indicated with a red asterisk. Scale bars in (A) and (B) represent 250 µm.

(C) Quantification of regenerating axons from A and B. Data are expressed as mean ± SEM (n = 3-12). *** $P < 0.001$ (ANOVA with Bonferroni posttests; relative to AAV-Control).

(D) Representative retinal sections stained with anti-RBPMS antibodies from intact retina, or the retina at 2 weeks after injury with prior injection of AAV-Control or AAV-Sox11. Scale bar represents 100 µm.

(E) Quantification as in D. RBPMS-positive cells in the ganglion cell layer were imaged and quantified for two sections per retina, and normalized to length counted. Data are expressed as mean ± SD (n = 3-4). * $P < 0.05$, ** $P < 0.01$ (ANOVA with Bonferroni posttests).

Figure 2.1 (Continued)

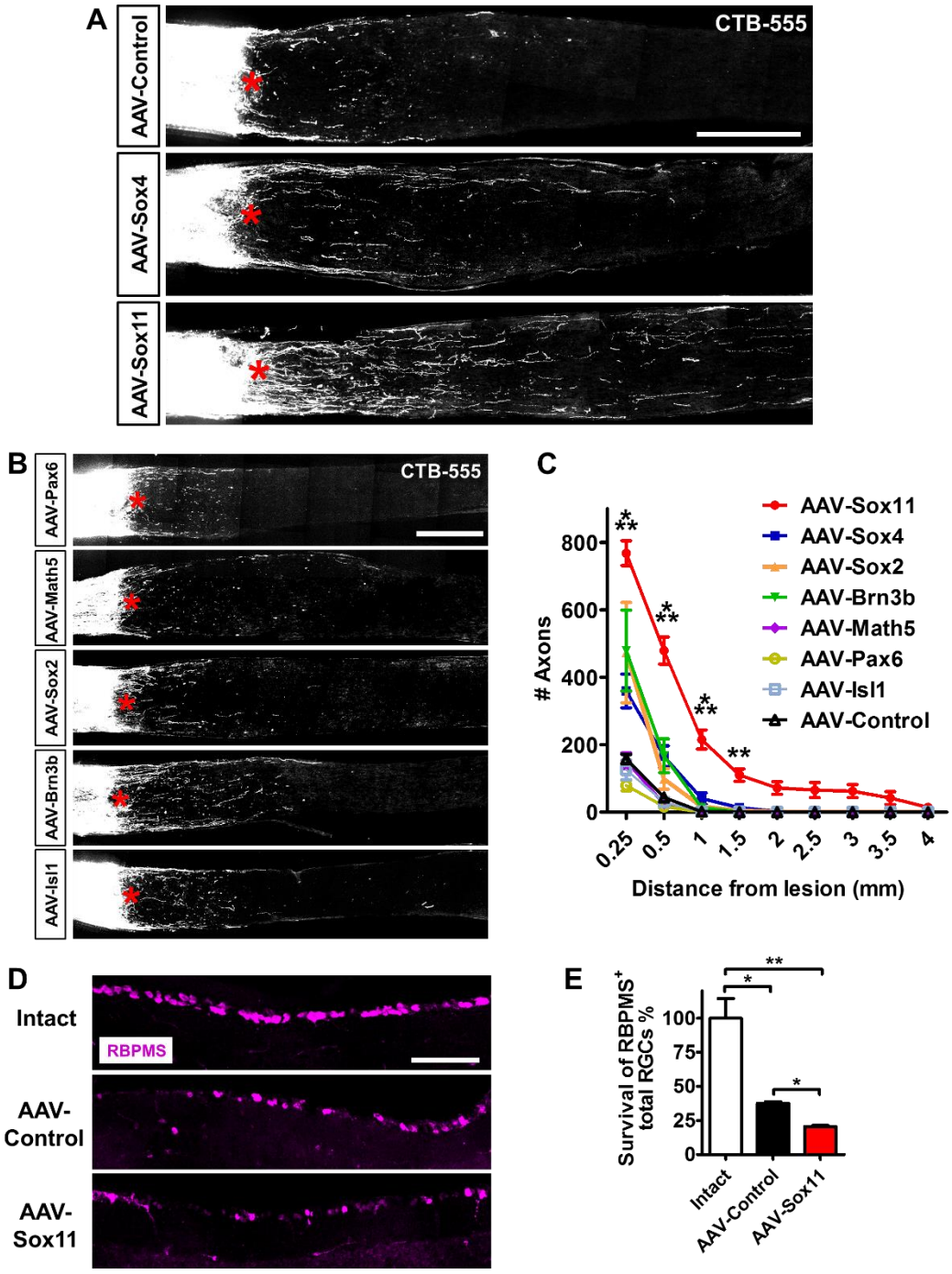

Sox11 kills α-RGCs and promotes axon regeneration from non-α-RGCs

Recent studies have shown that some interventions such as PTEN inhibition or co-expression of osteopontin and *Igf1* selectively promote axon regeneration from α-RGCs (Duan et al., 2015). We asked whether the same was true for *Sox11*. We marked α-RGCs with YFP using Kcng4-Cre mice crossed with a reporter line Thy1-fl-STOP-fl-YFP (Duan et al., 2015). We injected AAV-Control or AAV-Sox11 into the vitreous bodies of Kcng4-Cre; Thy1-fl-STOP-fl-YFP mice, crushed the optic nerve crush and labeled all regenerating axons with CTB as described above. Although many regenerating CTB+ axons were found in *Sox11*-treated eyes, none of these were YFP positive (Figure 2.2.A, 2.2.B). In addition, we found a total absence of YFP+ fibers proximal to the crush site whereas YFP+ fibers are evident in the control group (Figure 2.2.A, 2.2.B). Moreover, few YFP-positive RGCs were present in *Sox11*-overexpressing retinas at 2 weeks after injury (Figure 2.2.C-D).

The apparent absence of YFP-labeled α-RGCs could be explained either by the down-regulation of their molecular markers (*Yfp* expression from the *Thy1* locus) or by cell death. To distinguish between these possibilities, we used two additional markers. First, we used another reporter, Rosa26-CAG-fl-STOP-fl-tdTomato, which expresses the fluorescent protein tdTomato under the control of a constitutive promoter (Madisen et al., 2010). Second, we immunostained retinas with an endogenous marker of α-RGCs, Osteopontin (Duan et al., 2015). In AAV-Control treated eyes, we confirmed the presence of α-RGCs through tdTomato expression coincident with osteopontin. In contrast, AAV-Sox11 led to the elimination of tdTomato+ or osteopontin+ RGCs, both in intact retinas and following nerve crush (Figure 2.2.E, 2.2.F). Thus, *Sox11* expression likely induces the death of α-RGCs. This result implies that axons regenerating after *Sox11* over-expression must arise from non-α RGCs.

Figure 2.2: *Sox11* ablates α-RGCs and promotes axon regeneration from non-α-RGCs

(A-D) Axon regeneration (A, B) and survival of α-RGCs (C, D) in Kcng4-Cre mice crossed with Thy1-fl-STOP-fl-YFP at 2 weeks post crush (wpc). α-RGCs and their axons are labeled with YFP. Regenerating axons distal to the crush sites (asterisk) are anterogradely traced by CTB (red). Retina whole-mount staining confirms there is almost complete ablation of YFP-positive α-RGCs in *Sox11*-treated retinas (C, D). Scale bars in A and C represent 300 μm.

(E, F) Survival of *Sox11*-treated α-RGCs labeled by either crossing Kcng4-Cre mice with Rosa26-CAG-STOP-tdTomato or staining with an antibody against osteopontin (OPN). 4 weeks after AAV-Sox11 injection, few α-RGCs were observed either with optic nerve crush (2 wpc) or without crush. Scale bar in E represents 100 μm. Data are expressed as mean ± SD (n = 3-5). *** $P < 0.001$ (ANOVA with Bonferroni posttests).

Figure 2.2 (Continued)

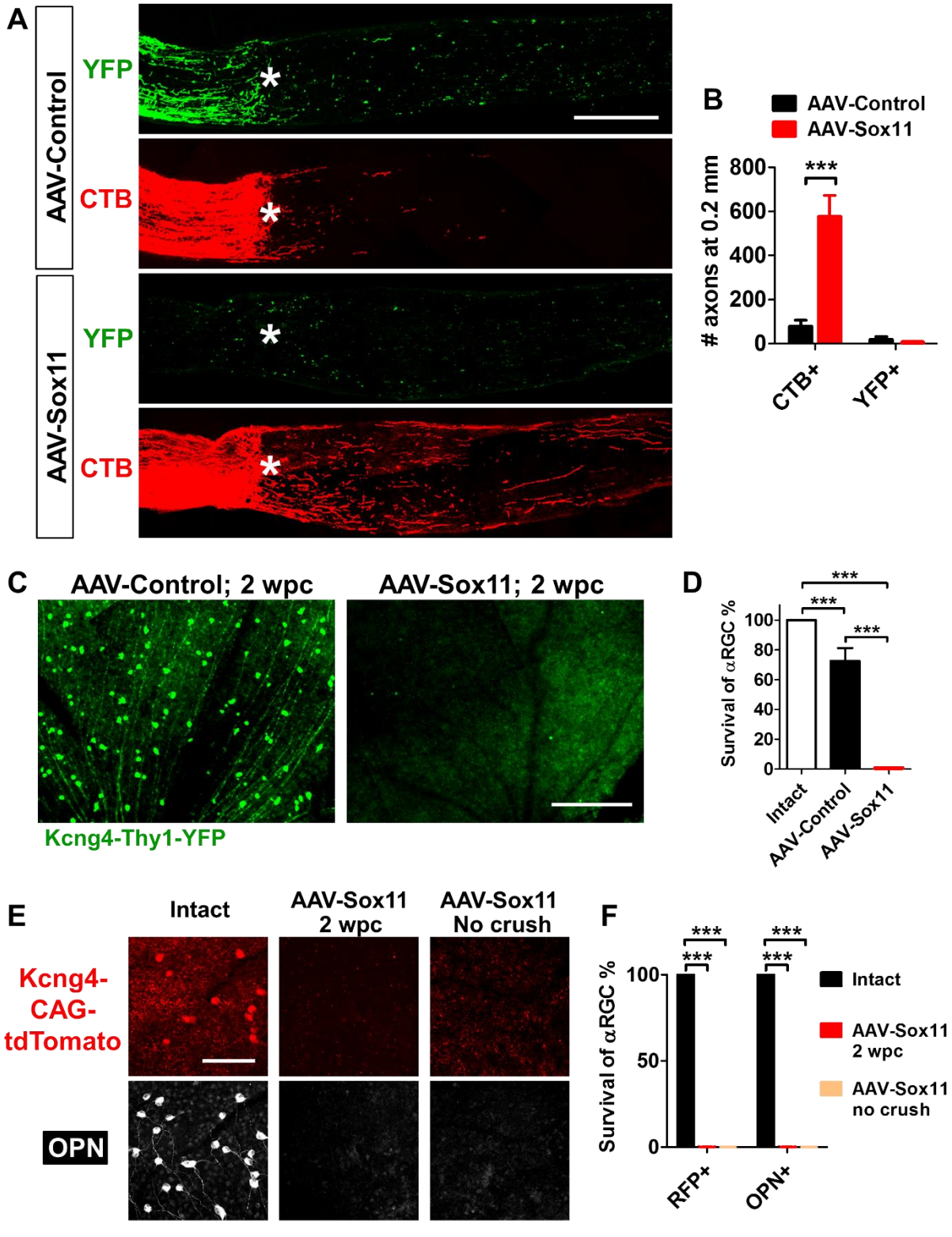

In addition, we tested the effect of *Sox11* in transgenic mice overexpressing *Bcl2*, a well-established anti-apoptotic molecule that increases RGC survival after nerve crush (Bei et al., 2016; Bonfanti et al., 1996). As expected, AAV-Sox11 improved regeneration over AAV-Control in the Bcl2 background (Figure S.2.A). However, the extent of *Sox11*-induced regeneration in *Bcl2*-overexpressing mice was not appreciably different from that observed in wildtype animals (compare Figure S.2.A to Figure 2.1.C). Further, even with *Bcl2* co-treatment, *Sox11* still failed to increase RGC survival (Figure S.2.B) and *Bcl2* failed to rescue the *Sox11*-induced loss of Osteopontin+ α-RGCs (Figure S.2.C). It is possible that other cell death mechanisms, such as pyroptosis or necroptosis, are at work (Moujalled et al., 2014), or that *Sox11* regulates a balance of cell death machinery sufficient to overwhelm *Bcl2*'s protective effects.

Intravitreally injected AAV2 vectors can transduce RGCs as well as other retinal cells (Park et al., 2008). To determine whether *Sox11* acts directly on RGCs to promote regeneration, we injected AAV2-FLEX-Sox11 into the vitreous bodies of Vglut2-Cre mice, in which *Cre* is expressed in RGCs selectively (Ellis et al., 2016), and subjected these mice to an optic nerve injury. We found that AAV-FLEX-Sox11 induced regeneration was comparable to those induced by non-conditional AAV-Sox11 (Figure S.2.D, S.2.E, as compared with Figure 2.1.A, 2.1.C). Likewise, AAV-FLEX-Sox11 reduced pan-RGC survival essentially indistinguishable from non-specific AAV-Sox11 (Figure S.2.F), and was expressed well in surviving RGCs (Figure S.2.G). Thus, *Sox11*-induced axon regeneration is likely regulated in a cell autonomous fashion.

Developmental axon growth programs activated by Sox11 in adult RGCs

To gain mechanistic insights into the effects of *Sox11*, we performed gene expression profiling analysis in RGCs. To this end, we injected AAV-Sox11 or AAV-Control into the vitreous bodies of wild type mice, waited two weeks and performed optic nerve injury. Three days later, we dissociated RGCs,

labeled them with antibodies against the RGC-selective marker THY1, and purified them by FACS (Figure 2.3.A). By immunostaining, we verified the presence of α-RGCs in the samples prepared from both AAV-Control and AAV-Sox11 treated retinas at this time point (Figure S.3.A, S.3.B).

Messenger RNAs from the purified cells were then used for library preparation and sequencing (Figure 2.3.A, Figure S.3.C). From 26,691 annotated transcripts, we identified 2797 differentially expressed (DE) genes at the threshold of FDR < 0.1 (Figure S.3.D, S.3.E, and Supplemental Table S.1). Gene ontology (GO) analysis showed that two groups of similar GO terms account for a large fraction of the up-regulated transcripts (Figure 2.3.B, Supplemental Table S.2). The first group is related to the biosynthesis and metabolism of ceramide (Figure 2.3.B). In light of evidence for a role of the ceramide-sphingolipid in cell death (Mencarelli and Martinez-Martinez, 2013), these results might point to a possible mechanistic link to *Sox11*-triggered death of α-RGCs. The second group includes axon growth-related cellular functions, such as cell-cell adhesion, cell morphogenesis involved in differentiation, neuron process development and axonogenesis (Figure 2.3.B), suggesting that *Sox11* is able to re-activate axon growth programs. On the other hand, the majority of genes down-regulated by *Sox11* were associated with synaptic transmission (Figure 2.3.B). As previous studies showed that during development, axonal growth loss is associated with the switching from an axon growth mode in embryonic stages to the synapse growth mode in mature stages (Enes et al., 2010; Goldberg et al., 2002), these results support the model that *Sox11* over-expression reprogram adult RGCs into an immature stage.

In further support of the notion that *Sox11* activates an axon growth program, we found that among the most significantly altered genes (Figure 2.3.C), several are cytoskeletal regulators: for example, doublecortin (*Dcx*) (Gleeson et al., 1999; Schaar et al., 2004), microtubule-associated protein 1B (*Map1b*) (Hammarback et al., 1991; Opal et al., 2003), Ras GTPase-activating-like protein *Iqgap1* (Hart et al., 1996), and Rho Guanine Nucleotide Exchange Factor 26 (*Arhgef26*) (Samson et al., 2013).

Dcx was of particular interest because it is crucial for axon growth and neuronal migration during development (Gleeson et al., 1999; Schaar et al., 2004); it is expressed by newly differentiated neurons and then quickly down-regulated during neuronal maturation (Gleeson et al., 1999). Moreover, we showed recently that over-expression of *Dcx* promotes optic nerve regeneration (Nawabi et al., 2015). We therefore used immunostaining with anti-DCX antibodies to validate the effect of *Sox11* on *Dcx* expression. As expected, DCX staining was barely detectable in RGC cell bodies from control uninjured eyes, but *Sox11* overexpression increased DCX staining of RGCs in both intact retina and following optic nerve crush (Figure 2.3.D). These results support the idea that *Sox11* promotes axon regeneration by activating the axon growth program used during development.

Figure 2.3: Sox11 overexpression induces changes in transcripts with roles in cell stress, axon growth, and other functions

(A) Overview of RNA-sequencing and analysis.

(B) Partial listing of Gene Ontology (GO) Biological Process terms. GO terms were generated separately for genes up-regulated or down-regulated (thresholded at FDR < 0.05) by AAV-Sox11 relative to AAV-Control. After Bonferroni correction, 57 terms were significantly enriched in up-regulated transcripts, and 144 in down-regulated transcripts. This panel shows the 20 GO terms with the largest sum of Fold Enrichment from up- and down-lists, then sorts the terms by direction of enrichment. Numbers in black indicate the overall number of genes in the GO term definition; numbers in blue and red indicate the number of differentially expressed genes at FDR < 0.05 that are listed in the given GO term definition. Bars indicate the Fold Enrichment over the number of genes expected to appear if genes were randomly selected. Asterisks indicate significance of GO term enrichment: *, $P < 0.05$; **, $P < 0.01$; ***, $P < 0.001$. The full list of significant GO terms is provided in Supplemental Table S2, alongside the enrichment scores and *P*-values.

(C) Heatmap showing a selection of differentially expressed genes between AAV-Control and AAV-Sox11 after crush. The 15 most significant genes (by smallest FDR value) are given for genes that are either up-regulated (red) or down-regulated (blue) by AAV-Sox11 relative to control. Color values indicate log2 transformations of expression values as specified in the color key (bottom), where all values are relative to the average expression in the AAV-Control Crush group. The columns correspond to individual samples, with each treatment group performed in triplicate.

(D) Retinal sections were immunostained for Doublecortin/DCX in either intact or post-crush samples as indicated. Scale bar: 50 μm.

Figure 2.3 (Continued)

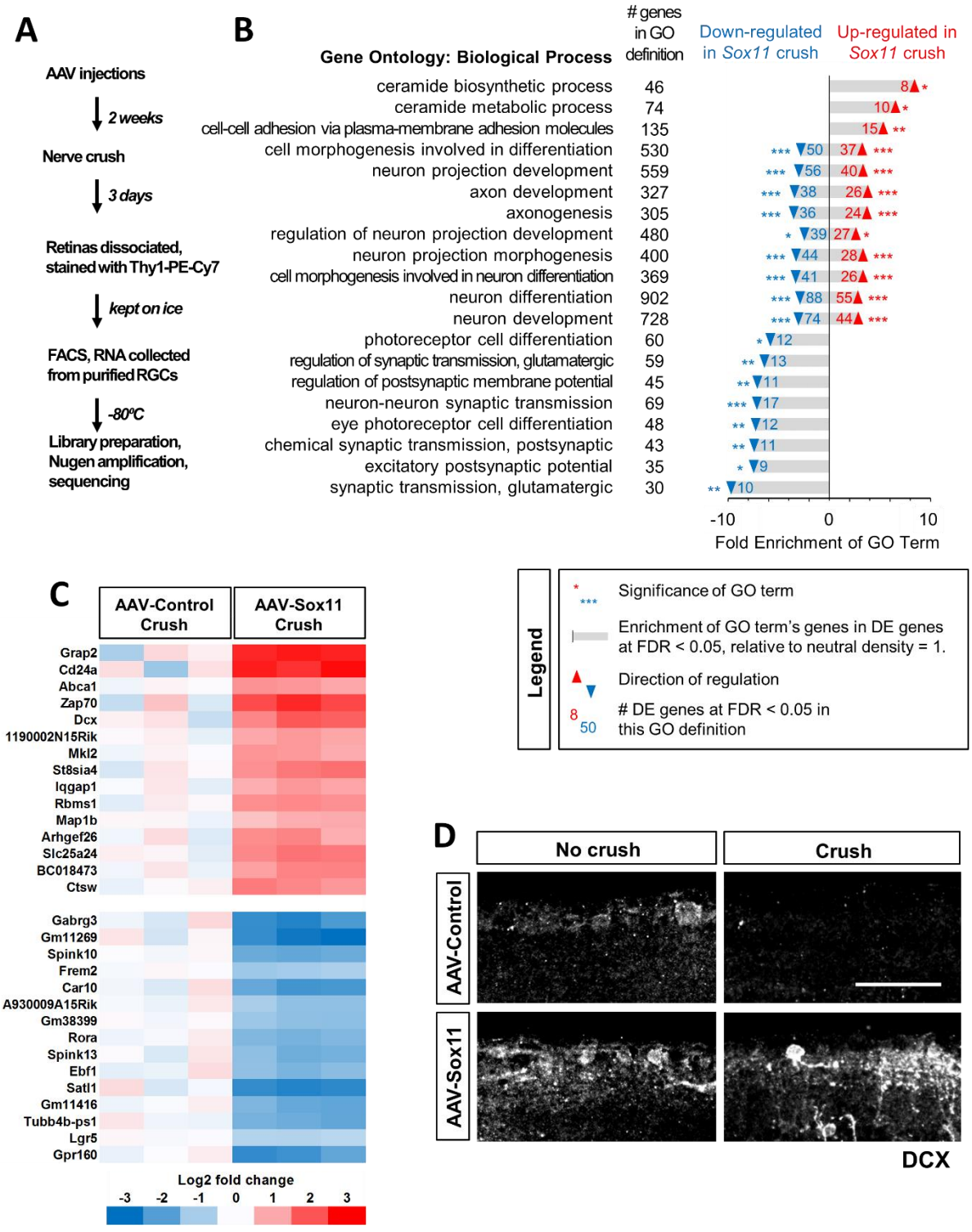

Pten deletion further enhances the regeneration-promoting effects of Sox11 from non-α-RGCs

Previous studies showed that *Pten* deletion dramatically enhances survival of RGCs, and selectively promotes regeneration of α-RGCs (Duan et al., 2015; Park et al., 2008). In contrast, results presented above show that *Sox11* leads to death of α-RGCs and promotes regeneration of non-α-RGCs. These distinct effects led us to explore the functional interaction of *Sox11* and *Pten* deletion. In $Pten^{f/f}$ mice, we deleted *Pten* using AAV-Cre mixed with either AAV-Control (hereafter "ΔPten/Control"), or AAV-Sox11 (hereafter "ΔPten/Sox11"). Optic nerves were injured two weeks later and axon regeneration was analyzed by CTB tracing 2 or 7 weeks after injury. In the ΔPten/Control group, many regenerating axons project for a relatively short distance (Figure 2.4.A-B for 2 weeks and Figure S.4.A-B for 7 weeks). In the ΔPten/Sox11 group fewer axons regenerated but they grew for much longer distances than those in the ΔPten/Control group (Figure 2.4.A-B, S.4.A-B), or in mice with *Sox11* over-expression only (Figure 2.1). By 7 weeks after injury, many regenerating axons were observed in the optic tract after crossing the chiasm (Figure 2.4.A-C); this length of regeneration was seldom observed in mice following either *Sox11* expression or *Pten* deletion alone. Notably, as in wild-type mice, *Sox11* decreased the survival of RBPMS+ RGCs in *Pten*-deleted mice (Figure 2.1.D, 2.1.E, 2.4.D). The number of SOX11-expressing RGCs and the intensity of the expression were moderately increased in *Pten*-deleted retinas as compared with *Pten*-preserved ones, when all retinas were treated with AAV-Sox11.

Figure 2.4: Pro-regenerative effect of *Sox11* in non-α-RGCs is enhanced by *Pten* deletion

(A) Representative images of optic nerves showing regenerating axons from different groups at 6-7 weeks after injury.

(B) Quantification of regenerating axons shown in (A).

(C) Images showing regenerating axons in ΔPten/Sox11-treated mice in the optic tract.

(D) RGC survival results at 6-7 weeks after injury.

(E) Retinal sections from ΔPten/Sox11-treated mice with FluoroGold (FG) injection to the distal optic nerve, and stained with RBPMS or TUJ1 antibodies.

(F) Quantification showing percentages of RBPMS- and TUJ1-co-stained cells among FG-positive cells shown in (E).

(G, H) Retinal images (G) and quantification (H) showing co-staining of FG-labeled RGCs with anti-OPN or SMI32. In ΔPten-treated animals, 80% of FG-labeled cells are both OPN-positive and SMI32-positive; however, none of the FG-labeled cells are co-stained with either OPN or SMI32 in ΔPten/Sox11-treated animals. Scale bar in (A) represents 500 μm. Scale bars in (C), (E) and (G) represent 100 μm. Data in (B) are expressed as mean ± SEM while data in (D), (F) and (H) are expressed as mean ± SD (n = 3-5). Significance levels in (B) are indicated by *, $P < 0.05$; **, $P < 0.01$; ***, $P < 0.001$ by ANOVA with Bonferroni posttests. Significance in (D) is indicated by ***, $P < 0.001$ by Welch's *t*-test.

Figure 2.4 (Continued)

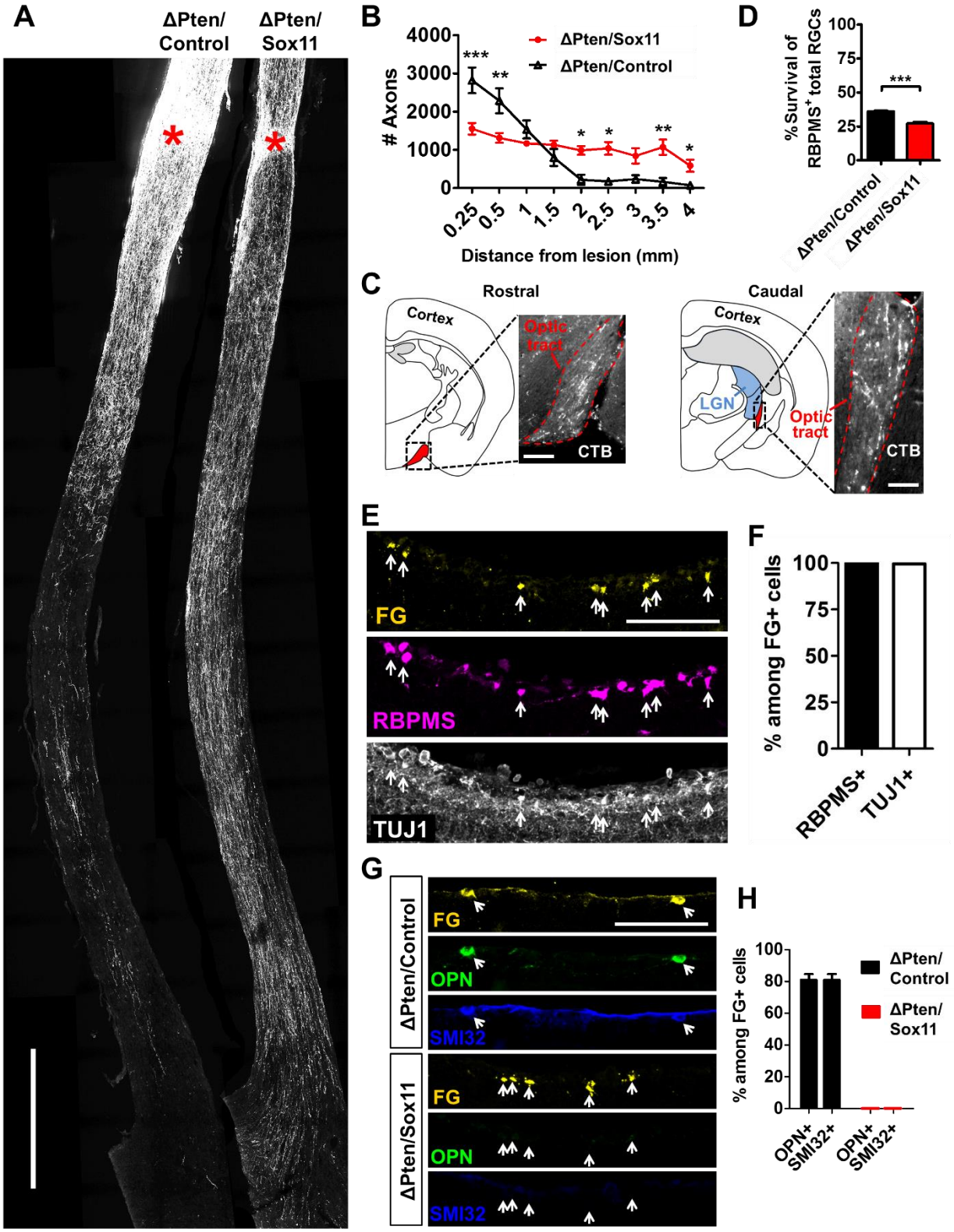

We next wanted to ask whether regeneration induced by ΔPTEN/Sox11 acted upon α- or non-α-RGCs, and whether *Sox11*-regulated mechanisms were conserved in ΔPten/Sox11 regenerating RGCs. Thus, we developed a protocol to retrogradely label RGCs with regenerating axons by injecting the tracer FluoroGold in the distal optic nerve and then analyzed FluoroGold-positive RGCs in the retinal sections. With this protocol, many RGCs were labeled in intact wild type mice but none of RGCs were labeled in the mice after injury (Figure S.4.C). In the ΔPten/Control group, FluoroGold-positive RGCs were observed across the retina sections. Consistent with previous results (Duan et al., 2015), the majority of these individually examined RGCs (over 200 cells) were α-RGCs as they were co-stained with the α-RGC marker OPN as well as a second α-RGC marker SMI32 (Figure 2.4.G-H).

In the ΔPTEN/Sox11 group, many RGCs were also labeled with FluoroGold (Figure 2.4.E). All these FluoroGold-positive RGCs expressed the RGC markers RBPMS and class III beta-tubulin or TUJ1 (Figure 2.4.E-F), but none were from α-RGCs (Figure 2.4.G-H). In fact, few OPN or SMI32-positive RGCs were observed in all ΔPTEN/Sox11-treated retinas, suggesting a near-total loss of α-RGCs (Figure S.4.F). Finally, as expected, many of these FluoroGold-labeled RGCs also expressed DCX (Figure S.4.D), a young-neuron marker up-regulated by *Sox11* alone (Figure 2.3.C and E) and phospho-S6 (Figure S.4.E), an mTOR-activity indicator up-regulated by *Pten* deletion (Park et al., 2008). Together our results indicate that *Pten* deletion could further enhance axonal regeneration from non-α-RGCs induced by *Sox11* over-expression.

Discussion

Repurposing developmental programs for regeneration

Multiple factors have been shown to be key in the differentiation of RGCs during development (Livesey and Cepko, 2001; Mu and Klein, 2004). However, it remains unclear which factors are most relevant to the axon growth program. Our results suggest *Sox11* is one such critical factor. Both *Sox11*

and *Sox4* are members of the Sry-related high mobility group (HMG) box (*Sox*) family of transcription factors which have been implicated as critical regulators of cell fate, differentiation, and survival during development (Chang et al., 2017; Kuwajima et al., 2017; Sarkar and Hochedlinger, 2013). *Sox11* promoted strong and significant axonal regeneration, and *Sox4* likely promoted regeneration albeit with marginal significance. These results are consistent with the notion that *Sox4* and *Sox11* have redundant biological effects (Jiang et al., 2013). Previous studies have also implicated *Sox11* in promoting regeneration of PNS (Chandran et al., 2016; Jankowski et al., 2009; Jing et al., 2012) and corticospinal axons (Wang et al., 2015). Gene profiling showed *Sox11* activates a set of developmental axon growth-related genes in RGCs, consistent with the possibility that it is a master regulator of the axonal growth program. *Sox11* also down-regulates genes involved in synaptic transmission and related functions, consistent with previous observations on the development-dependent switching from axon growth mode immature neurons to dendrite/synapse growth mode in mature neurons (Enes et al., 2010; Goldberg et al., 2002). However, it remains to be determined whether the inhibition of dendrite/synapse function is required for *Sox11*-mediated activation of axon growth programs.

Along with its beneficial effect on promoting axon regeneration, *Sox11* expression had the distressing effect of leading to the death of nearly all α-RGCs. In this regard, our gene profiling studies indeed revealed that *Sox11* over-expression could up-regulate the biosynthesis and metabolism of ceramide, a critical regulator of neuronal stress response and cell death (Mencarelli and Martinez-Martinez, 2013). In addition, Welsbie et al show that *Sox11* is involved in *Dlk*/*Mapk*-mediated RGC death (Welsbie et al., 2017). Furthermore, a previous study showed that despite promoting some CST regrowth, *Sox11* over-expression resulted in worsening of motor performance outcomes (Jayaprakash et al., 2016; Wang et al., 2015); we speculate that *Sox11*-mediated cell death might have contributed to such behavioral impairments. On the other hand, it has been shown that, during development, *Sox11* and *Sox4* are critical for preventing the death of RGC (Jiang et al., 2013), sympathetic (Potzner et al.,

2010) and DRG neurons (Lin et al., 2011). How *Sox11* shows such differential survival effects on different neuronal types remains unclear. This is further confounded because *DCX*, in addition to its pro-regenerative effects, improves the survival of RGCs after injury (Nawabi et al., 2015) – so, *DCX*'s pro-survival effect must somehow be overwhelmed or modified by other *Sox11* target genes. To speculate, it is possible that *Sox11*'s effects on ceramide signaling, interaction with different combinations of Brn3a/b/c factors, or regulation of heterogenous oxidative stress pathways might play a role in such differential survival. To take a more cell-centric (rather than *Sox11*-centric) view, it is also possible that *Sox11* overexpression is stressful to most RGCs, whereas some are more protected e.g. due to a lower rate of firing/depolarization, or lower metabolism. In any case, any attempts to use *Sox11* or other reprogramming methods as neural repair strategies (Li and Chen, 2016) will need to take account of these double-edged effects.

Neuronal subtype-specific control of axon regeneration

Our recent studies showed that *Pten* deletion or overexpression of osteopontin and *Igf1* selectively promotes the axon regeneration from α-RGCs (Duan et al., 2015). In view of this result, it was surprising that *Sox11* expression both promoted axon regeneration and killed virtually all α-RGCs. The implication, which we supported by retrograde labeling from regenerating axons, is that *Sox11* promotes regeneration of RGC types that are otherwise unresponsive to the effects of mTOR activation. Moreover, even in combination with mTOR activation (*Pten* deletion), *Sox11* kills α-RGCs and promotes regeneration from non-α-RGCs. There are at least 30 RGC types in mouse, each with distinct morphological, molecular and functional properties (Baden et al., 2016; Sanes and Masland, 2015). It will be challenging to identify which RGC types are affected by *Sox11*, but the availability of increasing numbers of markers and transgenic lines (Dhande and Huberman, 2014; Sanes and Masland, 2015) provides a means of addressing this issue.

These results provide new evidence for the idea that distinct neuron types differ in their regenerative responses to certain manipulations (He and Jin, 2016). The presence of resilient and susceptible populations of RGCs is particularly intriguing in this regard, because most RGCs are similar in many respects: their somata are in the ganglion cell layer, their dendrites arborize in the inner plexiform layer, their axons run through the optic nerve to the brain, they are glutamatergic, and they express markers such as RBPMS, THY1, and BRN3 class transcription factors. These similarities, then, make the remaining differences between RGC types all the more compelling. By comparing RGC types before and after injury, and following interventions such as *Sox11* or *Pten* deletion it should be possible to identify the critical factors required for survival or regeneration following injury.

Methods:

Experimental models

Mouse lines

Mouse lines including Kcng4-Cre and Thy1-fl-STOP-fl-YFP were generated and characterized in our laboratories (Duan et al., 2015). Kcng4-Cre was crossed with Thy1-fl-STOP-fl-YFP or Rosa26-CAG-fl-STOP-fl-tdTomato (Jackson Laboratory) to label α-RGCs. Wild-type mice were purchased from Charles River Laboratories. Bcl2 mouse line was described previously (Bei et al., 2016). Vglut2-Cre mice were obtained from Jackson Laboratory (016963). In experiments where a transgenic mouse line was not specified, mixed-background wildtypes were used.

Mouse husbandry

All experiments were performed in compliance with protocols approved by the IACUC at Boston Children's Hospital. Mice were given *ad libitum* access to food and water, and housed in cages under

positive-pressure filtered air supplies with bedding changed frequently. Mice were not permitted to breed before or during their inclusion in *in vivo* experiments.

In vivo procedures and reagents

Production of AAVs

Vectors of AAV-Pax6 and AAV-Isl1 were made by inserting mouse *Pax6* cDNA (Addgene #32932) and mouse *Isl1* cDNA (Addgene #32929) respectively into an AAV plasmid consisting of the cytomegalovirus enhancer fused to the chicken beta-actin promoter (CAG promoter) and Woodchuck hepatitis virus Posttranscriptional Regulatory Element (Wpre). The other vectors were assembled similarly, with coding sequences either cloned in-house from cDNAs or directly chemically synthesized. All pAAVs, as listed in the Key Resources Table, were then packaged into AAVs of serotype 2/2 (titers: > 5×10^{12} genome copies per milliliter) by the Boston Children's Hospital Viral Core.

Intravitreal injection and optic nerve crush

For intravitreal injection, adult animals were anesthetized with ketamine/xylazine (100/10 mg/kg) and then AAV (1-3 µl) or Alexa-conjugated cholera toxin beta subunit (CTB-555, 1 mg/ml; 1-2 µl) was injected intravitreally with a fine glass pipette attached to the Hamilton syringe using plastic tubing. CTB-555 injection was performed 2-3 days before euthanasia to trace regenerating RGC axons. For optic nerve crush in anesthetized animals, the optic nerve was accessed intraorbitally and crushed using a pair of Dumont #5 forceps (FST), two weeks after AAV injection. More detailed surgical methods were described by Park et al. (2008) and Bei et al. (2016).

Retrograde tracing of RGCs

Two weeks after optic nerve crush, a cranial opening was created over the frontal cortex and a distal segment of the crushed optic nerve was exposed intracranially through removing overlying brain tissues. 4% FluoroGold (Fluorochrome) was slowly injected into the optic nerve approximately 1-1.5 mm distal to the crush site using a fine glass pipette. Care was taken to minimize passive diffusion of FluoroGold solution back toward the crush site including removing overflowing FluoroGold solution.

Histology

Tissue preparation

Anesthetized animals were transcardially perfused with 4% paraformaldehyde (PFA). Dissected optic nerves, brains, and eyeballs were post-fixed in 4% PFA overnight, and then immersed in sucrose solutions at least two days before embedding and snap-freezing in OCT. Sucrose solutions contained 15% sucrose in PBS for optic nerves, or 30% sucrose in PBS for eyes and brains. Typically, 10-14 μm thick sections were cut for optic nerves, 16-20 μm thick sections for retinas and 25 μm thick sections for mouse brains. Sections were adhered to room-temperature charged microscope slides, dried, and frozen until further processing. Slides were then either washed and mounted for imaging with an anti-fade reagent, for example, for some CTB-traced optic nerves, or further processed for immunohistochemistry. Some retinas were dissected out *in toto* after post-fixing in PFA, washed with PBS, immunostained, cut radially with scissors to flatten the tissue, and then mounted for imaging.

Staining conditions

For immunohistochemistry, whole mount retinas were generally blocked for one hour in PBS with 5% donkey serum and 0.3% Triton X-100, and then incubated 0.5-2 days at 4 °C in primary antibodies diluted in PBS with 3% donkey serum and 0.3% Triton X-100, followed by treatment of

secondary antibodies (Jackson ImmunoResearch or Invitrogen) for 1-2 hours at room temperature after rinsing. Immunohistochemistry on sections was performed generally by blocking with 3% bovine serum albumin and 0.5% Triton X-100 in PBS, incubation with primary antibodies overnight at 4 °C in blocking solution, then incubation with secondary antibodies for 2 hours at room temperature.

Antibodies

Primary antibodies used were: Goat anti-DCX (1:400, Santa Cruz sc8066); chicken anti-GFP (1:1000, Abcam ab13970); rabbit anti-RFP (1:500, Abcam ab34771); goat anti-Osteopontin (1:1000, R&D Systems AF808); rabbit anti-phosphorylated S6 Ser235/236 (1:200, Cell Signaling 4857); rabbit anti-RBPMS (1:500, Abcam ab194213); guinea pig anti-RBPMS (P4-P24) (1:2000, Raygene custom order A008712 to peptide GGKAEKENTPSEANLQEEEVRC); mouse anti-SMI32 (1:1000, BioLegend/Covance SMI-32R); goat anti-Sox11 C-20 (1:200, Santa Cruz sc17347); mouse anti-TUJ1 (1:400, BioLegend 801202); rabbit anti-Tubb3 (1:400, Abcam ab18207). Fluorescent secondary antibodies used were generally from either Invitrogen/Thermo-Fisher Scientific or Jackson ImmunoResearch, raised in either goat or donkey against the primary antibody's host species, and conjugated to fluorophores of DyLight 405; Alexa Fluor 488; Cy3; or Alexa Fluor 647 as appropriate, and generally used at 1:800 final dilution.

Microscopy

For nerve sections and some whole-mount retinas, individual fluorescent images were acquired using a Ultraview Vox Spinning Disk Confocal Microscope (Perkin Elmer) and automatically stitched using Volocity software (Perkin Elmer). For some retina sections, images were taken using epi-fluorescent microscopy with a Nikon TiE Eclipse epifluorescent microscope with automated tiling or Zeiss LSM 700 fluorescent confocal microscopy. Z stacks were projected onto a single plane using either Volocity or ImageJ. Brightness and contrast of the images were adjusted and pseudo-colors applied for

presentation. When imaging was taken for quantification, image capture and processing were kept constant.

Experimental design

Inclusion and exclusion criteria

The vast majority of samples in all experiments were included in their respective final datasets. However, occasionally samples were rejected as follows: (1) At the time of sacrifice and dissection, eyes were rejected if lens injury or hardening of the vitreous humor was apparent. This generally resulted in rejection of zero to one retinas and/or optic nerves per experiment. (2) During sample preparation, a minority of samples were damaged from human error, such as cryosectioning severely orthogonal to the intended plane of sectioning, and excluded from further analysis. (3) Microscopy images of retinal or optic nerve sections were excluded if sectioning was orthogonal, similar to criteria 2 above. (4) Once experiments entered statistical analysis, no further samples were excluded by any formal or informal criterion.

Randomization and efforts to minimize systematic errors

Experiments involving mice included both adult males and females, generally between the ages of 6 to 10 weeks, and control and treatment groups were always balanced for female:male ratios, ages, different litters, and/or background as applicable.

Experimental design for histological samples involving surgeries, i.e. injections and nerve crushes, were always carefully balanced for possible unilateral-specific artifacts caused by the surgeon. More specifically, experiments always used one of two strategies: (1) using only one retina and nerve (e.g. the right eye) per mouse, for all treatment groups, or (2) using an equal 50:50 balance of left and right eyes for both treatment groups.

Blinding

Generally, phenotypes were sufficiently obvious and reproducible in the hands of multiple authors that blinding was judged unnecessary for analysis. However, during the initial screens that identified *Sox11*, blinding was used for our first characterizations of pan-RGC survival. Additionally, for some histological analysis of retinas involving Pten/Sox11, the results from non-blinded quantifications were repeated by a second investigator who was blinded. In such cases, the second investigator's conclusions would be considered final.

RNA-seq preparation

RGC enrichment and RNA isolation

Before beginning the experiment, we validated that an antibody, Thy1.2-PE-Cy7, was able to mark RGCs by checking it against the YFP-17 mouse line (Supplemental Figure S.6) (Sun et al., 2011).

Retinas were dissected, dissociated in serum-free media using papain, triturated carefully, then stained with Thy1.2-PE-Cy7 antibody (Affymetrix eBioscience 25-0902-82) and SYTOX live-dead cell stain, then flow sorted on a BD FACS Aria II using an 85 micron nozzle to a goal of approximately 100,000 events. Using the Arcturus PicoPure kit, RGCs identified by FACS were sorted directly into extraction buffer XB and lysed immediately after sorting according to the kit's instructions. RNA quality was verified with an Agilent BioAnalyzer 2100. All experimental steps through RNA extraction were performed in triplicate for the control and experimental group, with each replicate performed a different day. The samples within a replicate were prepared on the same day, in a different order each replicate, to avoid any systemic errors from differences in timing.

Sequencing reactions

RNA-sequencing was carried out for the RNAs with by the UCLA Neuroscience Genomics Core. Briefly, cDNA was generated using the Ovation RNA-Seq System V2 kit (NuGEN), followed by library preparation using the TruSeq Nano DNA Library Prep kit (Illumina). Samples were sequenced using an Illumina HiSeq-4000 sequencer with 69-base paired end reads resulting in a minimum of 50M reads per sample.

Quantification and Statistical Analysis

Quantifications involving regenerating axons

For quantifying regeneration of axons traced with fluorescent CTB, we took longitudinal sections of optic nerves and counted the total number of CTB+ axons at multiple distances along the optic nerve, anterograde from the crush site. The counts were transformed to a density of axons, then multiplied by the nerve's approximate cross-sectional area to estimate the total number of axons in each respective nerve. More specifically, we used four sections from each nerve to estimate that nerve's axon count, and took each estimate as a single biological sample for subsequent statistical testing. For quantification of fluorescent protein co-localization with regenerating axons in optic nerves, axons were counted with their number estimated according to a method described previously (Bei et al., 2016). In analyzing YFP-positive axons, care was taken to exclude fluorescent signals from tissue debris. We confirmed that axon regeneration counts, at several distances from the crush site, followed an approximately normal distribution by the Kolmogorov-Smirnov test ($P > 0.1$).

Quantification involving RGC cell bodies

For quantification of RGCs in sections, generally 2 sections were quantified per retina for a total quantified ganglion cell layer length of 3 to 4 mm per section. In intact control retinas, generally 300 to

500 RBPMS+ cells were counted per section. The cell count was normalized to the length of GCL counted (measured in ImageJ for every section), and one value was generated per retina for subsequent statistical analysis. For quantification of RGCs in whole mounts, each retina was sampled with generally six to eight fields of view focused on the ganglion cell layer (each ~0.4mm x ~0.4mm). Densities were calculated for each field of view, then averaged to generate one value for each retina for subsequent statistical analysis. We confirmed that RGC survival counts, in our experimental layout, followed an approximately normal distribution by the Kolmogorov-Smirnov test ($P > 0.1$).

Statistical testing of axon or RGC cell body quantifications

All statistical tests were two-tailed, and the sample size *n* was defined as the number of individual eyes, retinas, nerves, or mice as appropriate in the experiment. For such quantifications, generally a *t*-test or ANOVA with post-testing was used for analysis, as detailed in the corresponding figure legends. Asterisks, e.g. *, **, *** indicate significance levels as specified in the corresponding figure legends. Where applicable, graphs indicate either the SEM or SD with error bars (specifically labeled in the relevant figure legends). Analyses were performed in either PRISM or Excel, and checked against raw data by more than one author.

RNA-sequencing Analysis

Reads were aligned to the latest mouse mm10 reference genome using the STAR (ver 2.4.0) spliced read aligner (Dobin et al., 2013). Read counts for Ensembl genes were generated by HT-seq 0.6.1 (Anders et al., 2015). Transcripts with at least 10 read events in any sample were permitted into the dataset, for a total of 26,691 transcripts. Raw counts were normalized by upper quartile normalization followed by removal of unwanted variation using RUVSeq (Risso et al., 2014). Differentially expressed (DE) genes were obtained using the EdgeR bioconductor R package (Robinson et al., 2009). GO analysis

was performed separately for up- and down-regulated gene lists using the Gene Ontology Reference Genome Project's PANTHER Classification System (pantherdb.org) against the GO biological process complete annotation data set, with Bonferroni correction.

Data and software availability

Raw and processed RNA-seq data are deposited to Gene Expression Omnibus (GEO: GSE87046).

Author contributions

Michael Norsworthy, Fengfeng Bei, Josh Sanes, Giovanni Coppola, and Zhigang He designed experiments. Michael Norsworthy, Fengfeng Bei, Riki Kawaguchi, Qing Wang, Nicholas Tran, Yi Li, Benedikt Brommer, and Yiming Zhang performed the experiments and analyzed the data. Chen Wang performed optic nerve crush and AAV injections. Michael Norsworthy, Fengfeng Bei and Zhigang He wrote the paper with the inputs from all authors.

Chapter 3 - Sox11 promotes regeneration of intrinsically photosensitive RGCs, and may affect oxidative stress in alpha RGCs

Summary

To this point, we have established that Sox11 acts differently on at least two populations of RGCs, such that one population regenerates, while another population (definitively including alpha RGCs) is ablated. The next immediate question is: What type(s) of RGCs regenerate? Furthermore, what are the mechanisms that makes Alpha RGCs particularly vulnerable to Sox11-induced ablation, and equally important, what factors make other RGCs prone to regenerate upon Sox11 expression? Here, I provide evidence that intrinsically photosensitive RGCs regenerate given Sox11 and PTEN/Sox11 treatment. Furthermore, I implicate oxidative stress as a factor in Sox11-induced ablation of alpha-RGCs, and show that alpha RGCs differ from other RGCs in expression for an antioxidant gene. Future studies may find these data helpful in understanding heterogeneity in regeneration, and building more predictive models of signaling pathways that may be important regulatory targets.

Introduction

Differential RGC survival after injury

Our Tuj1+ and RBPMS+ RGC survival data imply that Sox11 probably does not increase survival of a different RGC subtype to compensate for the loss of Alpha RGCs. Therefore, we could use knowledge of the survival of other RGC subtypes in wildtype animals after nerve crush to identify candidates. We looked at a recent publication that characterized the survival rates of different RGC subtypes after nerve crush, using a variety of molecular and transgenic markers (Duan et al., 2015). In their study, the authors quantified relative numbers of RGC subtypes at 2 weeks and 4 weeks after injury. Though many RGC subtypes were not identified in this challenging study, approximately 50% of

RGCs surviving 4 weeks post crush were accounted for in wildtype animals. At this point, alpha-RGCs account for around 25% of surviving RGCs, M1-ipRGCs account for another 10-15%, and W3 RGCs account for around 10% (Duan et al., 2015). Therefore, ipRGCs and W3-RGCs were experimentally accessible candidates for Sox11-induced regeneration.

Vulnerability of some RGCs to oxidative stress in glaucoma

RGCs undergoing glaucomic stress experience higher oxidative stress, and express several genes in an attempt to ameliorate this stress (Kim et al., 2015). Interestingly, the first RGCs lost in a primate model of glaucoma tend to have large-diameter axons, which the authors interpret as representing Y-cells (Quigley et al., 1987). This anatomical description matches alpha RGCs (Krieger et al., 2017), and alpha RGCs have high firing and conduction rates (Cleland et al., 1975) which presumably requires elevated metabolic and oxidative demands. Therefore, differential vulnerability to oxidative stress is a candidate predisposing mechanism that could interact with *Sox11* for the ablation of alpha-RGCs.

Results

Sox11 promotes ip-RGC and not W3-RGC or oods-RGC regeneration

Using a mouse line with Cre expressed from the melanopsin (Opn4) promoter (a kind gift from Michael Do's lab), we labeled all classes of ipRGC by AAV delivery of FLEX-GFP. GFP fluorescence was visible in many cell bodies, dendrites, and axons. After nerve crush, I searched for regenerating ipRGC axons in the optic nerve through co-labeling of GFP and CTB tracer. Critically, I successfully identified multiple GFP+/CTB+ co-positive regenerative axons, indicating that Sox11 regulates regeneration in ipRGCs (Figure 3.1.A). However, we also observed a decrease in survival of GFP+ ip-RGCs (Figure 3.1.B, 3.1.C). Note that M4-ipRGCs are also Alpha RGCs, and will have been killed in our Opn4-Cre labeling in

Sox11 but not PLAP treatment. It is likely that ablation of M4 ip-RGC / alpha RGC ablation contributes to the Sox11-induced decrease in ip-RGC cell counts.

In a follow-up experiment, we used the same Melanopsin-Cre mouse line with AAV-FLEX-GFP and AAV-FLEX-Sox11 (Figure 3.1.D, 3.1.E). Interestingly, we observed regeneration of significantly more CTB+ axon fibers than in control animals, and also verified that many CTB+ fibers were positive for FLEX-GFP expression (Figure 3.1.D, 3.1.E). Comparing the estimated number of CTB+ regenerating fibers between Melanopsin-Cre / AAV-FLEX-Sox11 versus wildtype / AAV-Sox11 experiments (Figure 2.1.C, 3.1.E) opens the attractive possibility that a substantial fraction of total regenerating axons come from Melanopsin-Cre expressing cells.

Finally, we tested a combination of Melanopsin-Cre / PTEN-deletion / FLEX-Sox11 overexpression, and observed that PTEN/Sox11 synergize and can promote regeneration specifically of ip-RGCs. By two weeks after crush, these axons reach for several millimeters down the optic nerve (Figure 3.2.A). It will be interesting to see whether these specifically regenerating ip-RGCs can reach the SCN at a later post-crush time point, similar to what I have observed with pan-RGC regeneration into the SCN from the PTEN/Sox11 treatment at 6-7 weeks after crush (Figure 3.2.B).

On the other hand, in experiments on YFP-expressing W3-RGCs using the TYW3 mouse line, we found that Sox11 did not induce W3 regeneration (Figure 3.3.A). W3 axons appear to have retracted from the optic nerve stump in both AAV-Control and AAV-Sox11 animals (Figure 3.3.A). W3-RGC survival was low overall, and may be further modestly reduced by Sox11, though this decrease was not significant (Figure 3.3.B, 3.3.C). We also verified, using a CART antibody in retinal cryosections, that CART-expressing RGCs did not survive optic nerve crush in the Sox11 treatment group, confirming that CART+ RGCs likely are not regenerative (3.3.D).

Figure 3.1: Regeneration of intrinsically photosensitive RGCs

(A) Animals were treated with AAV-FLEX-GFP and either AAV-Control or AAV-Sox11, and regenerating axons were traced with CTB. Samples were sectioned, and GFP signal was amplified with anti-GFP immunofluorescence. Sections were then imaged. The "Intersect" visualization was performed in Photoshop with a sequence of filters. Settings were kept identical between PLAP and Sox11 images. (B) Visualization of GFP activation in the indicated treatments. (C) The number of GFP+ cells was counted in 4 random views per retina in the indicated treatments. Sox11-treated retinas have fewer GFP+ ipRGCs. Note that M4-ipRGCs are also Alpha RGCs, so the significant decrease in ipRGCs by Sox11 is partly explained by the known loss in Alpha RGCs. (D) In melanopsin-cre mice, eyes were injected with either FLEX-GFP + PLAP, or FLEX-GFP with FLEX-Sox11. Optic nerves were crushed, and axons were allowed to regenerate 2 weeks. Axons were traced with CTB-555 before sacrifice. Red dotted box indicates co-localization of GFP with CTB. We only detected GFP in some axons, and attribute this to limited detection sensitivity of GFP because it must be synthesized by each cell at high levels to be visible, compared to CTB which requires only transport through the axon. (E) Quantification of the experiment in D.

Figure 3.1 (Continued)

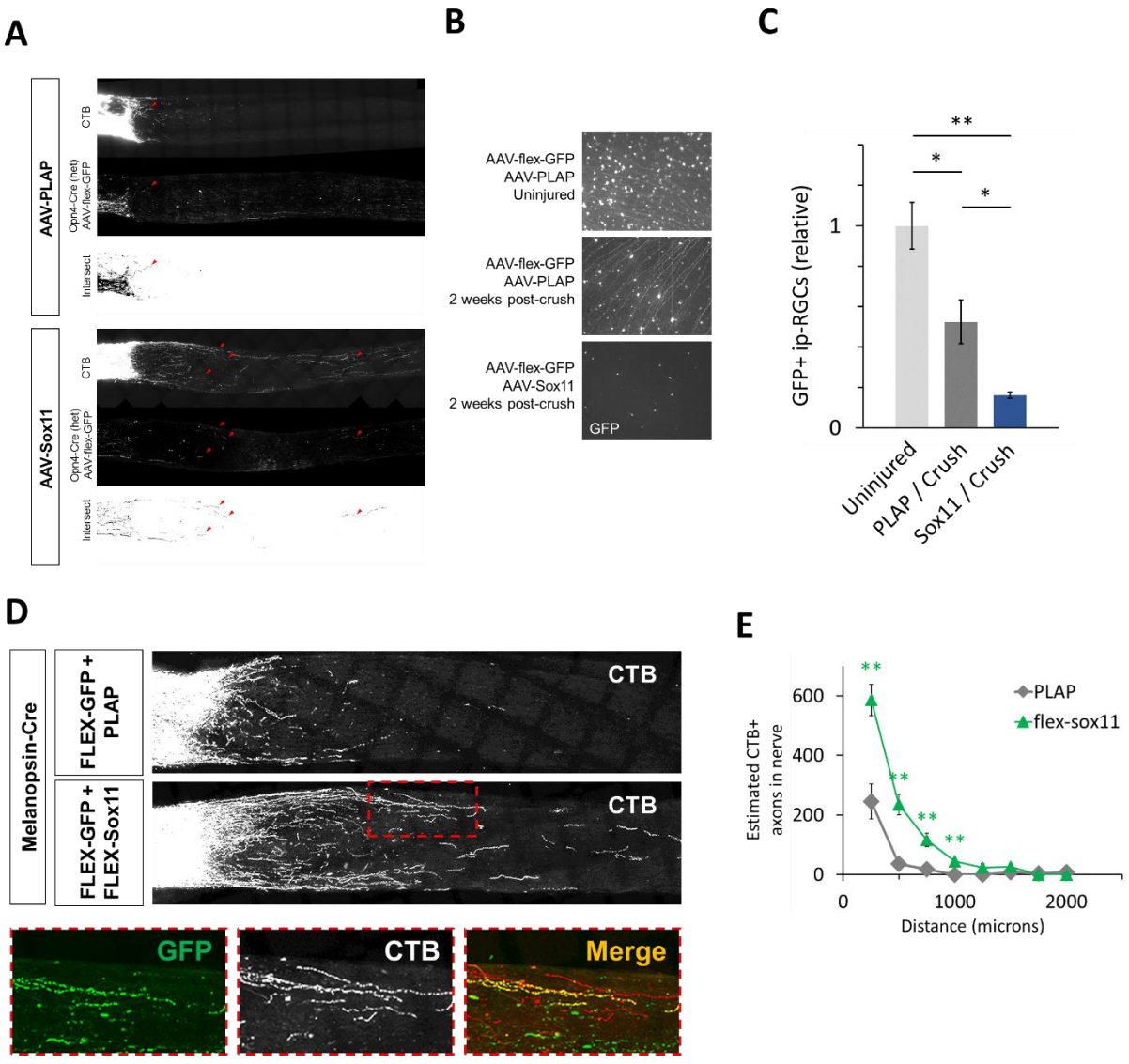

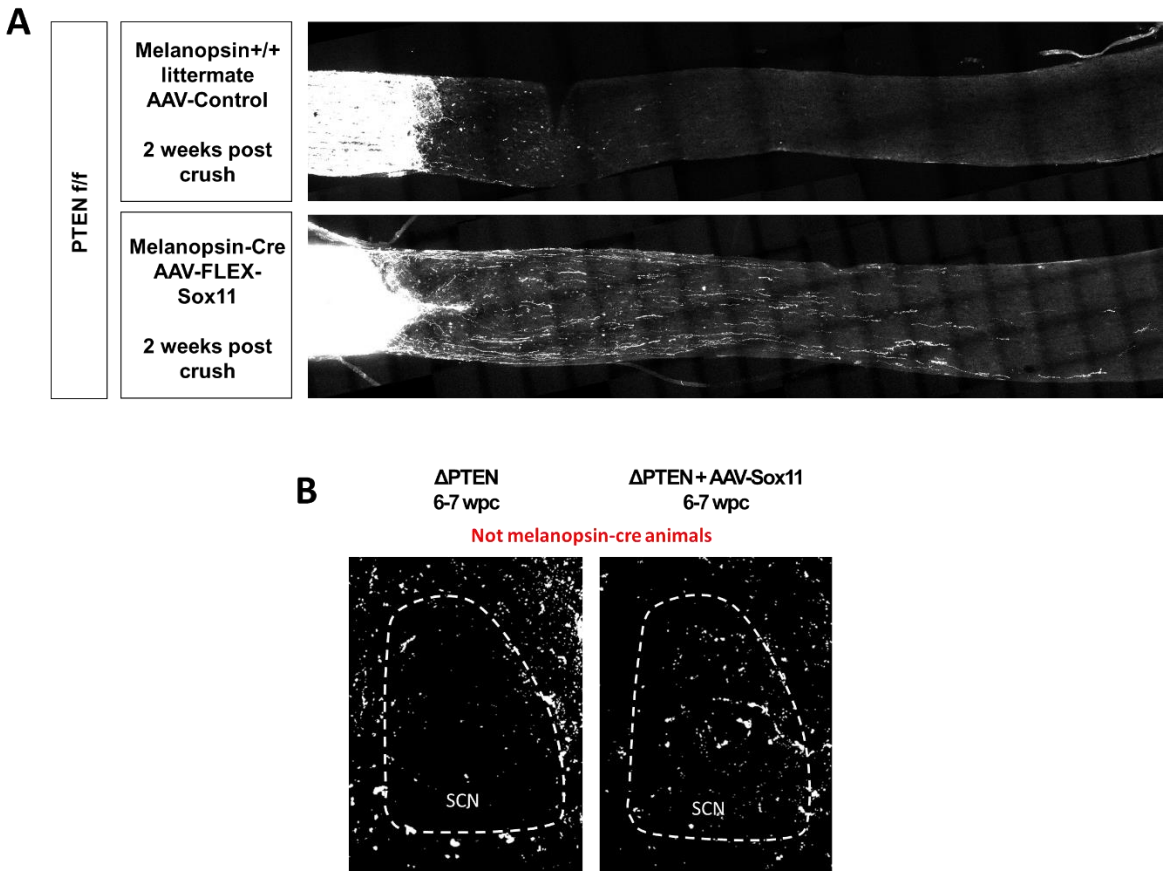

Figure 3.2: PTEN/Sox11 synergistic regeneration involving photoentrainment components

(A) In PTENf/f mice crossed to Melanopsin-cre heterozygotes, we took either Melanopsin+/+ mice or Melanopsin-Cre heterozygotes, and injected AAV-Control or AAV-Flex-Sox11. Nerves were crushed, regenerated 2 weeks, then regenerating axons were traced with CTB before sacrifice. (B) In PTEN mice, we injected either AAV-Cre + AAV-Control, or AAV-Cre + AAV-Sox11. Regeneration proceeded 7 weeks after crush, then regenerating fibers were traced with CTB. Brains were recovered and cryosectioned, and the suprachiasmatic nucleus was imaged.

Figure 3.3: Sox11 does not detectably promote CART or W3 regeneration

(A) In W3-YFP mice, we injected either AAV-Control or AAV-Sox11, then crushed optic nerves, and assayed regeneration after two weeks using CTB tracer. Co-localization of YFP with CTB indicates regenerative axons coming from W3 RGCs. A negligible number of CTB+ axons can be seen regenerating in the AAV-Control nerve, whereas AAV-Sox11 results in regeneration of several CTB+ axons. However, co-localization of YFP was not observed, and it seems unlikely that W3 RGCs meaningfully contribute to Sox11-induced regeneration. (B) Survival of W3 RGCs in the retina without injury (left), with AAV-Control and nerve crush (middle), and AAV-Sox11 and nerve crush (right). (C) Quantification of B. (D) Survival of CART+ RGCs in uninjured animals (top), in AAV-Control treated eyes four weeks after injury (middle), or in AAV-Sox11 treated eyes four weeks after injury (bottom). (E) Quantification of D.

Figure 3.3 (Continued)

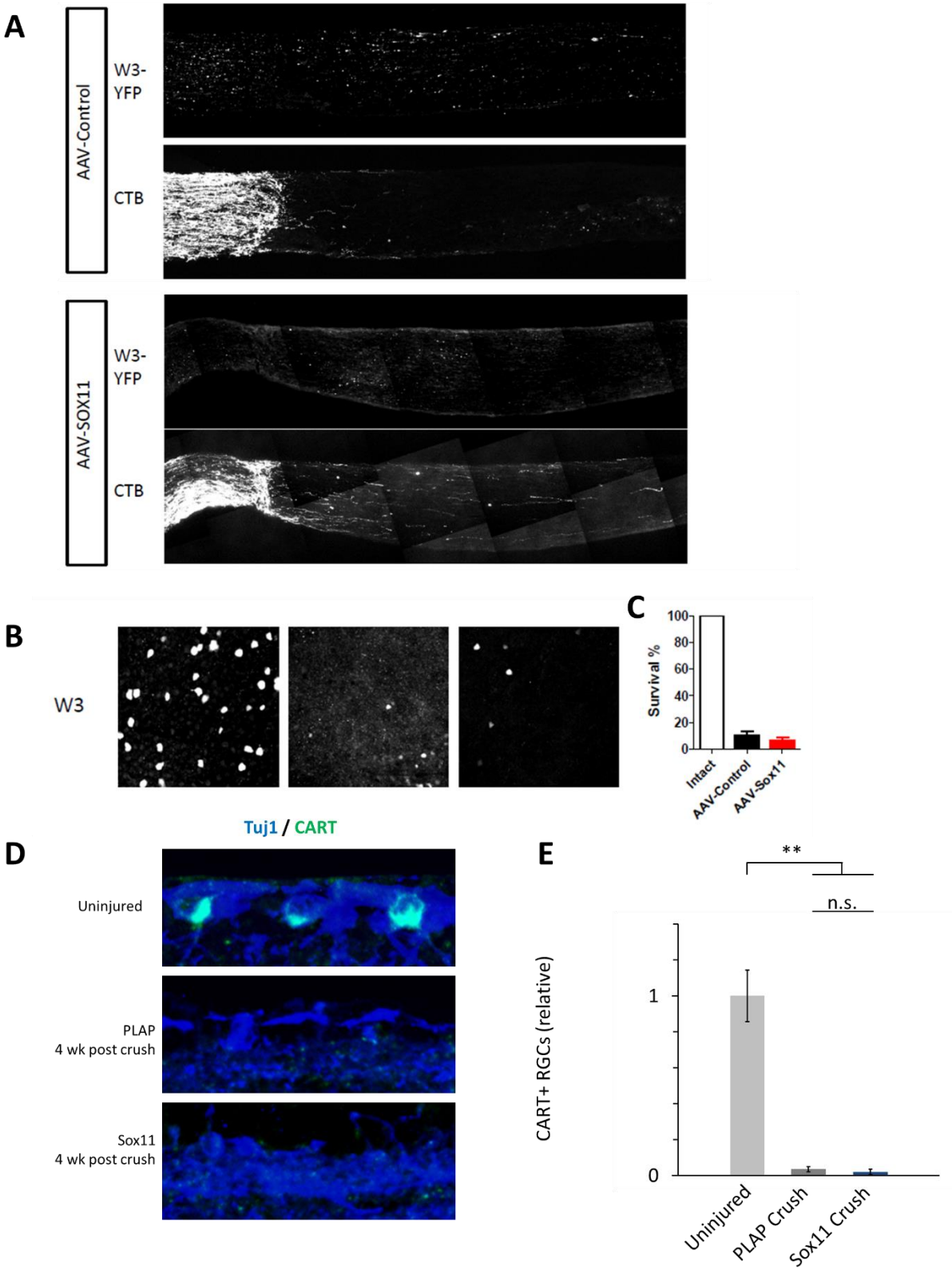

Alpha-RGCs are enriched for mitochondrial superoxide dismutase, *Sod2*, which could be regulated as a response to Sox11 expression.

I wanted to test whether alpha RGCs could be directly distinguished using markers of oxidative stress. In support of this, wildtype mice were perfused, and retinas were cryosectioned then stained for mitochondrial/manganese superoxide dismutase, *Sod2*, along with an alpha RGC marker, Osteopontin. Interestingly, the brightest *Sod2* expression was observed co-localizing with Osteopontin+ alpha RGC cell bodies. Distributed expression was also observed in some lamina in the inner plexiform layer, as well as nearby/within the outer plexiform layer (Figure 3.4.A).

This finding establishes that Alpha RGCs differ from other RGCs in terms of their ability to handle oxidative stress, and implicates at least *Sod2* in their stress response capacity. Next, I wanted to see whether *Sod2* might be a regulatory target of *Sox11*. Therefore, I stained *Sod2* on two groups of mice that were either injected with AAV-Control followed by nerve crush, or injected with AAV-Sox11 followed by nerve crush. Two weeks after nerve injury, mice were perfused, and retinas were stained as above for *Sod2* and *Ostpn* (Figure 3.4.A). While *Ostpn*+ alpha RGC cell bodies are still visible in control animals two weeks after crush, their expression of *Sod2* seems to have fallen. On the other hand, animals treated with AAV-Sox11 have very few *Ostpn*+ alpha RGCs remaining at 2 weeks after crush (for a total of 4 weeks after AAV infection), and no *Sod2* cell bodies are visible. This is expected: if *Sod2* expression is mainly limited to alpha RGC cell bodies, then the elimination of alpha RGCs should eliminate *Sod2*+ cell bodies as well.

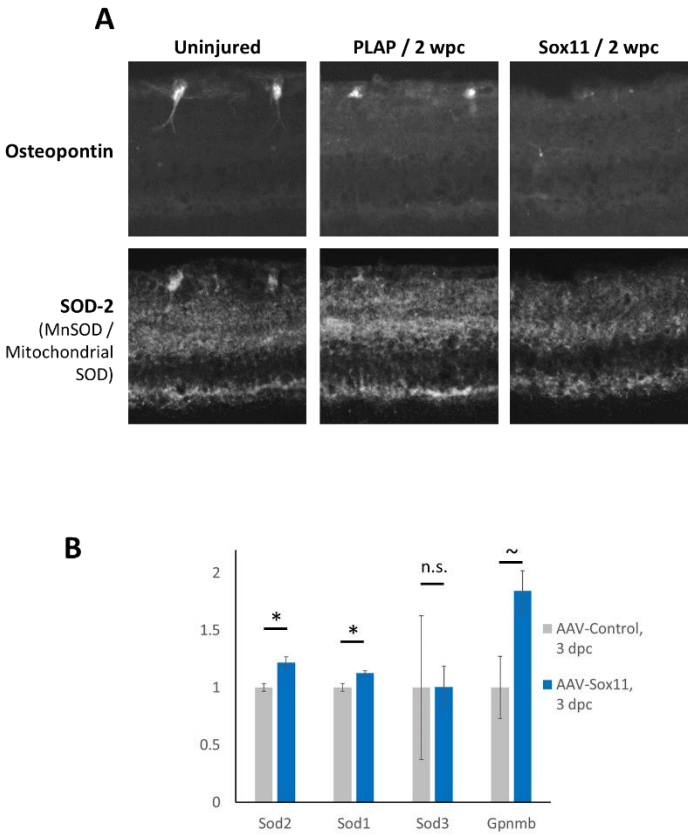

Figure 3.4: Oxidative stress in relation to Alpha RGCs and *Sox11*

(A) Retinas from wild-type, uninjured mice were cryosectioned and stained for Osteopontin and SOD-2. Co-localization of SOD-2 to Osteopontin+ cell bodies was readily apparent. Additionally, retinas were obtained from mice given either AAV-Control or AAV-Sox11 injections, then given optic nerve crushes for two weeks, and stained for SOD-2 and Osteopontin. Nerve crush may cause some loss of SOD-2 expression in Osteopontin+ cell bodies of AAV-Control treated eyes. More dramatically, no Osteopontin+ or SOD-2+ cell bodies are visible in the AAV-Sox11-treated eyes. (B) Selected expression data from RNA-seq data set (GEO: GSE87046) for SOD-2 and some other oxidative stress-related genes. Detailed methods for the RNA-seq are provided in Chapter 2. The expression data for *Sod2*, *Sod1*, *Sod3*, and *Gpnmb* was taken from this data set, and compared using Welch's *t*-tests.

This brings the question: can we see any indication of Sox11 modifying oxidative stress markers? The RNA-seq data set can help begin to answer this question (Figure 2.3, Supp Table S.1, S.2, and GEO: GSE87046). Our data set provides a snap-shot of RGCs at 2 weeks after AAV infection plus 3 days post-crush, for a total of 17 days after AAV infection, and many alpha RGCs are still alive at this time point (Supplemental Figure S.3.A, S.3.B). Therefore, we might be able to see any changes in oxidative stress genes before alpha RGC death runs to completion. From the RNA-seq data set, I tested *Sod2*, as well as homologs *Sod1* and *Sod3*, and the gene *Gpnmb* which rescues glaucoma normally found in the DBA/2J mouse model (Anderson et al., 2002; Kim et al., 2015). Interestingly, *Sod2* and *Sod1* are modestly increased by AAV-Sox11 in post-crush RGCs (Figure 3.4.B). *Gpnmb* may have increased with marginal significance due to *Sox11* overexpression ($p = 0.069$, Welch's *t*-test). *Sod3* expression was low (FKPM = 1.35, GEO: GSE87046) in both the control and Sox11-treated retinas and does not appear to be influenced by *Sox11* expression ($p = 0.9931$, Welch's *t*-test).

The above data indicate that genes involved in oxidative stress may increase as a result of *Sox11* overexpression, and that alpha RGCs may differ from other RGCs in their vulnerability to changes in this stress. While these data are only observational, they suggest that further exploration of the link between oxidative stress pathways and the differential survival of subtypes of RGCs would be worthwhile. Future studies may also wish to directly test whether the use of antioxidants could ameliorate *Sox11*'s preferential elimination of alpha-RGCs.

Discussion

Future exploration of RGC subtype differences in survival and regeneration

The above data suggest ip-RGCs represent a large fraction of the RGCs that regenerate upon Sox11 treatment. However, it is presently unclear what subtypes of ip-RGCs regenerate, and the identities of any non-ip-RGCs that regenerate are likewise unknown.

Intrinsically photosensitive RGCs consist of approximately 6 subtypes (Cui et al., 2015). M1 and M2 ipRGCs classically project to the SCN, and express sufficient melanopsin to be detected in immunofluorescence without amplification strategies. M3 ipRGCs also express melanopsin detectably, and are bistratified (Schmidt and Kofuji, 2011; Sweeney et al., 2014). Additional types – M4, M5, and M6 – are different in that they express melanopsin at relatively low levels. The functions of most of these types are unclear, but at least M4 ip-RGCs may play a role in the behavior of postnatal mice to avoid brightly lit, wide-open areas (Estevez et al., 2012; Sexton et al., 2015).

In terms of Sox11-induced ip-RGC regeneration, we can say M2 regeneration is unlikely because, in wild-type animals, M2-ipRGCs widely undergo cell death after nerve crush (Duan et al., 2015), and we have seen no indication that *Sox11* increases survival of any RGC subtypes. Furthermore, M4 ip-RGCs are most likely ablated, because M4-ipRGCs are also characterized as Osteopontin-expressing, ON-type alpha-RGCs (Estevez et al., 2012; Sanes and Masland, 2015). Therefore, we can surmise that some combination of M1, M3, M5, and M6 ip-RGCs is regenerating.

Future studies will better characterize the regenerative ip-RGC and non-ip-RGC cells that respond to Sox11 and other regenerative treatments, through the careful application of additional transgenic mouse lines, more selectively regulated overexpression vectors, utilization of distinguishing molecular markers and cell morphology, and perhaps retrograde tracing. After these characterizations are complete, it should be possible to identify the factors that enable these cells to survive optic nerve crush, to be less vulnerable to *Sox11*-induced ablation, and ultimately to regenerate.

Optimizing oxidative stress for regeneration

Interestingly, normal RGC development in zebrafish may utilize elevated hydrogen peroxide concentrations for axon guidance and regulate *Shh* signaling (Gauron et al., 2016). It is therefore possible that in reprogramming RGCs to embryonic-like growth, their reactive oxygen species

environment may necessarily change, and it may not be desirable to completely eliminate sources of oxidative stress. Further studies will be needed to understand how oxidative stress changes throughout axon regeneration, to characterize the phenotypic consequences of modified oxidative stress environments, and to appropriately optimize the oxidative environment for promoting regeneration and ameliorating cell death.

Methods

Methods used in this chapter were essentially the same as those used in Chapter 2. In addition, the following primary antibody was used: Rabbit polyclonal anti-SOD-2 (FL-222) (Santa Cruz sc-30080).

Author contributions

Michael Norsworthy, Fengfeng Bei, Josh Sanes, and Zhigang He designed experiments. Michael Norsworthy and Fengfeng Bei performed the experiments and analyzed the data. Chen Wang performed optic nerve crush and AAV injections. Michael Norsworthy and Fengfeng Bei assembled figures, and Michael Norsworthy wrote this text.

Chapter 4 – Towards computer-aided modeling and engineering of CNS restoration

Summary

A forming consensus, from literature and from our own studies, is that achieving the goal of full functional restoration of nervous systems will be exceptionally complex and difficult. Tools that enable better information gathering and usage, and integration of this information into models and engineered solutions, should support this goal while bypassing limits of human cognition. We therefore designed an example of a highly integrative cellular modeling tool, which should enable more precise understanding of mechanisms and prediction of outcomes from interventions. This tool, named *Celletron*, is designed to be a versatile platform for simulating cells and tissues over time. Its implementation allows tissues to change in shape over time, through defined physical forces, and for the transmission, processing, amplification, and destruction of information and biochemical metabolites. Included in this chapter are two demonstrations of how this model approach can yield emergent cell-like behaviors from simple rule sets. Ultimately, further improvements to this modeling approach may enable many researchers to define, share, and modify signaling networks during the course of their research, and for engineers to utilize these networks for designing the most promising sets of interventions before committing to in-vivo experiments.

Introduction

Axon regeneration and neuroprosthetics: a long way to go

Current regenerative therapies will need additional work before they can be considered practical. *Sox11* is an example of a powerful, but complex regenerative regulator (Jayaprakash et al., 2016; Norsworthy et al., 2017; Wang et al., 2015). *Klf* family members are limited in their regeneration-promoting capacities, and it is unclear how they could be productively combined into a synergistic treatment (Blackmore et al., 2012; Moore et al., 2009, 2011). Hyperactivating the *mTor* pathway e.g.

with *PTEN* deletion causes enlargement of cell bodies (Park et al., 2008), is associated with autism (Huang et al., 2016; Spinelli et al., 2015), and may have any number of unknown side-effects to characterize and solve before clinical usage.

Combinations of regenerative treatments, such as *PTEN/Socs3/Myc*; *PTEN/cAMP/*zymosan; or *PTEN/Sox11* have more impressive phenotypes (Belin et al., 2015; Lima et al., 2012; Norsworthy et al., 2017; Sun et al., 2011), but their caveats are even more poorly defined, and might not compensate for undesired side-effects caused by their constituents (Norsworthy et al., 2017). Indeed, neural regeneration is not simply a problem of extending axons long distances (Bei et al., 2016) – axons must be accurately targeted, accurately remyelinated, etc. This is an engineering problem, complete with complex interaction networks of many components that are often decently understood individually. Other disciplines, like mechanical engineering, already have dedicated, workhorse software suites, that handle most aspects of project lifecycles, including planning, editing, previewing, and even simulation. Perhaps, biology and bioengineering need such workhorse software most of all.

Current analytical tools are inadequate

One of the most well-known simulators to neuroscientists is NEURON. NEURON is a neurophysiology modeling program, leading to at least 1,840 publications since it was first introduced by Hines M (Hines, 1989, 1993). It excels at quantitative models of membrane currents and ion channel behavior, within the context of branched cell morphology endemic to neurons. It can also model networks of neurons with some representations of second messengers. Unfortunately, NEURON provides only a 'snapshot' of a neuron's implicit regulatory and morphological state, and therefore has limited usefulness for regeneration studies where these states are dynamic and hard to predict.

Separately, Karr and Sanghvi et al (Karr et al., 2012) reported a simulation of the single-cell organism *M. genitalium*. They modeled gene and metabolic networks through time, and were able to

recapitulate an emergent behavior of their system – cell division – by iterating through the logic defined in their network models. This concept provides another portion of what could be a comprehensive regeneration model, but is not directly applicable to cells with complex morphology since it has minimal consideration of 3D or local structures.

The goal of regeneration and functional recovery ultimately relies on reassembly of a nervous system's damaged areas. It relies on genetic logic, protein networks, neurotransmission, cell motility, growth cone navigation, reconnection to the correct circuits, and other functions – that is, an ideal regeneration outcome would require *all* functions of *all* cells in question to work within the environmental context of *all* signaling and physical cues. This modeling application is beyond the scope of the above computational tools, or any others currently available.

More specifically, I believe that addressing the following computational needs in an integrated framework will accelerate such studies: (1) integrating genetic and other molecular databases, and improving the coverage of reactions and molecular interactions in databases; (2) enabling entities or interactions in those databases to be simulated in a tissue-like context; (3) allowing users to directly adjust network models, distributing the workload of experimental validation and refinement; (4) linking simulations to real data, such as a microscope image of a crushed optic nerve with various inflammation markers, for more rapid model/hypothesis/experiment cycles; and ultimately (5) goal-seeking towards a healthy tissue, provided an initial injury, candidate treatment strategies, and a sufficiently accurate network model.

Concept of a new simulation algorithm

I have led design on such a framework, in support of more comprehensive cell and tissue simulation. This framework allows representation of sub-cellular structures, whole cells, and extracellular materials as volume-occupying fluids, composed of many particles with non-zero mass.

Within this representation, information or *"reagents"*, such as regulatory molecules, or ions, are assumed to have negligible mass and volume, and can spread within a given structure, or be transported to a different structure, and can be processed through reactions. On the other hand, structures or "*scaffolds"* can gain or lose mass, and can either generate or detect physical forces, as either inputs or outputs of reactions processing a cell's information. In this way, changes in a cell's regulatory state can be related to changes of cell morphology, and vice-versa, without literalistic modeling of individual molecules.

We implemented a basic proof-of-concept for this simulation strategy, named *Celletron*. *Celletron*, from the above particle/information framework, can qualitatively yield emergent behaviors characteristic of complex tissues, such as neurotransmission and synaptic integration, the growth and navigation of an axon, and a gene regulatory cascade induced through extrinsic signaling. So far, most emphasis has been placed on developing the engine, and imagining the ways users should interact with data and the program. With additional improvements, database incorporation, quantitative tuning, and implementing optional CAD tools and goal-seeking behavior, it will become conceivable to simulate, from start to finish, many of the signature aspects of RGC development and adult function, to forecast what aspects remain problematic in RGC regeneration, and to engineer likely solutions.

Implementation

Celletron is written in Java, using the Eclipse Integrated Development Environment. In-depth documentation accompanies the source code, but a brief overview is warranted to illustrate the current concepts and capabilities of the simulator (Figure 4.1). This overview eschews some properties of the Java language (e.g. the difference between references and objects) for the sake of clarity.

Overall framework

The current implementation specifies that similar particles, that is, particles that together might constitute a particular cellular structure, are treated as comprising a 'scaffold'. Each scaffold is held in an instance of class `ScaffoldSpace`. The collection of all physical substances includes many scaffolds, and is called `ScaffoldUniverse`.

Each particle is represented as an instance of `ScaffoldParticle`, and contains all of the following: (1) a floating-point location in 3D space, along with a vector indicating the particle's polarity direction; (2) a value of its mass; (3) a list of the current concentration values, called `ReagentElement`s, of all `ReagentType`s which may be present on that particle; (4) a list of the current physical interaction parameters, called `PhysicsElement`s, towards other particle types with defined physical interactions; and (5) a `PhysicsInstance` which accumulates calculated forces from interacting nearby particles, and is used to yield a net force, acceleration, velocity, and resulting movement.

Figure 4.1: *Celletron* implementation

(A) Example screen-shot of *Celletron* window. (B) Example of using particle-based scaffolds to represent a cellular structure, in this case, part of an axon. This enables the representation of key organelles and other compartments, in a fluid and dynamic way, without needing to simulate individual molecules. (C) Conceptual outline of how interactions between particles can proceed. Any interaction can be calculated in a pairwise fashion (directionally, if desired), and can be adjusted according to the distance between particles. (D) Interactions can either be physical (via force interactions) or informational (via exchange or conversion of reagent quantities). (E) An example physical model for pairwise particle interactions. Here, if a force is defined to represent electrical field repulsion, its strength will decay according to the square of distance between points. A simultaneous physical attraction can be rationalized as interactions between specific binding sites. In this case, such attraction would not behave as an ambidirectional electrical field, and therefore would not decay by the square of the distance. The competition between attraction and repulsion yields a particular distance where the net force approaches zero. Force vectors are summed for any given particle, resulting in a net force vector which is used to calculate acceleration and then velocity for any particular time step in the simulation.

Figure 4.1 (Continued)

A

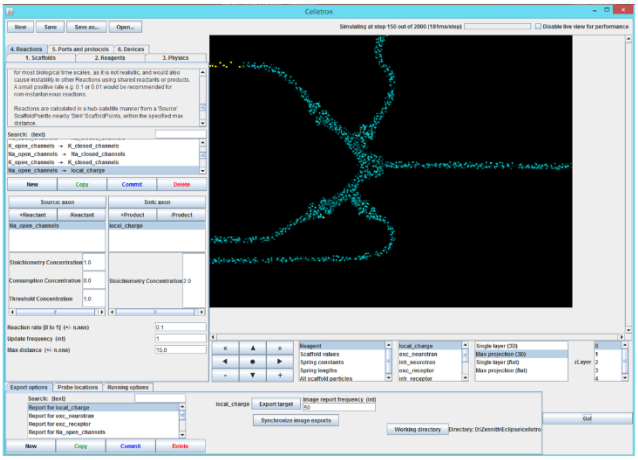

B

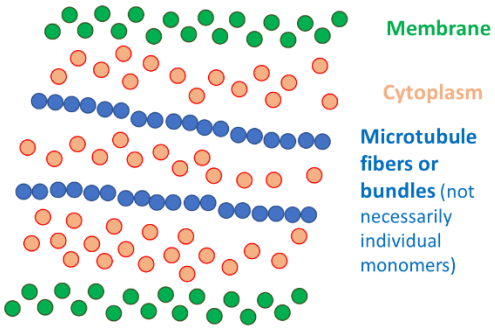

C

Modeling information, reactions, and forces in cells and tissues

Interactions are:

- Pairwise
- Within one scaffold, or between two scaffolds
- Dependent on proximity

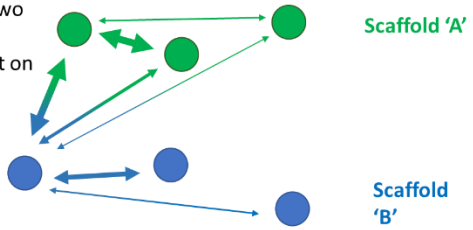

D

Interactions can exchange:

- Forces
- Concentrations of reagents/information

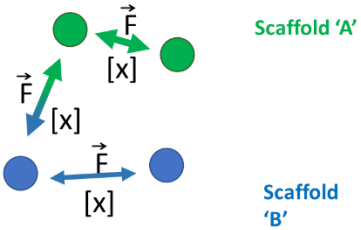

E

Physics model uses competing forces to change particle velocities

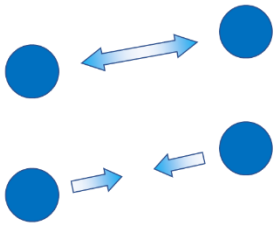

$F_{REP} = k_1 / x^2$

$F_{ATTR} = k_2 / x$

$F_{NET} = F_{ATTR} - F_{REP}$

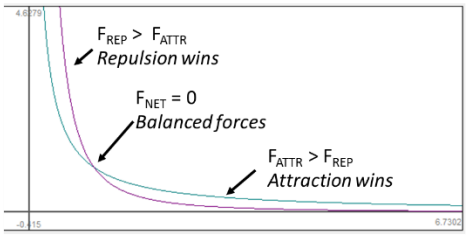

Then find acceleration due to this force:

Accel = F_{NET} / mass

(this is applied as a **vector** onto the particle's current velocity)

Information mutators

Diffusion of information

Diffusion between nearby particles is specified through a `DiffusionRule`, which allows some quantity to be exchanged between particles as a function of a user-given constant divided by the square of the distance between particles. Diffusion constants are allowed to differ if particles' polarities are aligned, or if they are anti-aligned. `DiffusionRule`s are used to define the spread of reagent values, for each scaffold that reagent is bound to, and are also used to define the spread of scaffold mass between particles, to allow local accumulations of mass to spread in a non-particulate way.

Reactions of information or particles

A `Reaction` is a user-defined relationship that converts any accessible quantity to any other accessible quantity. As well, each `Reaction` is defined as either occurring within a single scaffold, or as occurring between a 'source' scaffold and 'sink' scaffold. These allow the specification of very context-specific reactions, such as reactions limited to a cellular compartment, or reactions that must occur at the interface between cellular compartments. Reactions can observe or modify the concentrations of reagents, the mass of scaffolds, and the parameters of physical relationships, for each nearby pair of 'source' and 'sink' scaffold particles. Calculations approximately follow formal elementary reactions in chemistry, and additionally allow for the user to specify reaction rate limits, and to define particular reagents' behaviors as catalytic rather than consumable.

Physical forces and motion

Calculation of force vectors

Physical forces between any two particles is calculated as the sum of two competing force vectors. If particles are relatively nearby, then the repulsive force will overcome attraction; on the other

hand, if two particles are relatively distant, then the attractive force will dominate. The repulsive force is rationalized as representing the force between similarly-charged particles in a spherical electric field, and is calculated from a user-defined constant divided by the square of the distance between the particles. The 'attractive' force is rationalized as representing the favorable attraction two particles that may occur if they have mutually compatible binding sites. Under this regime, alignment of binding sites implies a linear (not radial) force between two points, and is therefore calculated using a user-defined constant divided by the distance between the two particles.

Forces applied to particle motion

For a single particle, all of the forces applied to it from surrounding particles are summed, resulting in a net force vector. On a given step of the simulation, that force is instantaneously translated to acceleration, according to that particle's mass. The acceleration is then applied as a vector onto the particle's already existing velocity vector. The summed velocity vector is then reduced by some fraction by a user-defined drag rate, then finally applied to determine the particle's movement at the end of the simulation step. The drag-modified velocity vector is retained for the next simulation step.

Device interfacing

Celletron has the broad, extensible capability of integrating with external devices through a USB port. These devices are 'mapped' in three-dimensional space to simulated tissue structures of interest. Currently, this has been implemented for integration with sensors and actuators controlled with an Arduino, and is designed to handle additional types of devices with minimal code modifications. This feature allows realtime communication between the simulation and real-world phenomenon. For example, I envision an array of light sensors being monitored by the simulation, where excitation of those sensors causes spatially mapped excitation of emulated rods, cones, and ip-RGCs.

Results

Synaptic Integration

Rationale

The ultimate predictive power of cellular models must come from evaluating cells' primary functions. That is, the intermediate developmental processes giving rise to cells cannot be meaningfully tested until the final results of that development are clear. Therefore, I will first demonstrate the ability of *Celletron* to model a small neural network with a combination of excitatory and inhibitory synapses. This demonstration shows that, at a morphological steady-state, the modeling method of scaffolds, reactions, particles, etc can yield reasonable multi-cellular functions.

I must emphasize that this model is currently *qualitative*, not *quantitative*, and may be subject to change at any time in either model layout or the underlying implementation of *Celletron*. My intent here is only to demonstrate feasibility, in support of further development.

Model setup

A multi-neuron test system is defined, with a neuronal cell body at its center, along with that neuron's axon projecting to the right (Figure 4.2.A). This neuron also projects dendrites to the left, which receive signals coming from presynaptic axons.

More specifically, scaffolds are defined for axons, dendrites/cell bodies, excitatory presynaptic terminals, inhibitory presynaptic terminals, excitatory postsynaptic terminals, and inhibitory postsynaptic terminals (Figure 4.2.B). Sets of reagents are defined for each of these scaffolds, and these are used in several reactions defined for specific scaffolds (Figure 4.3).

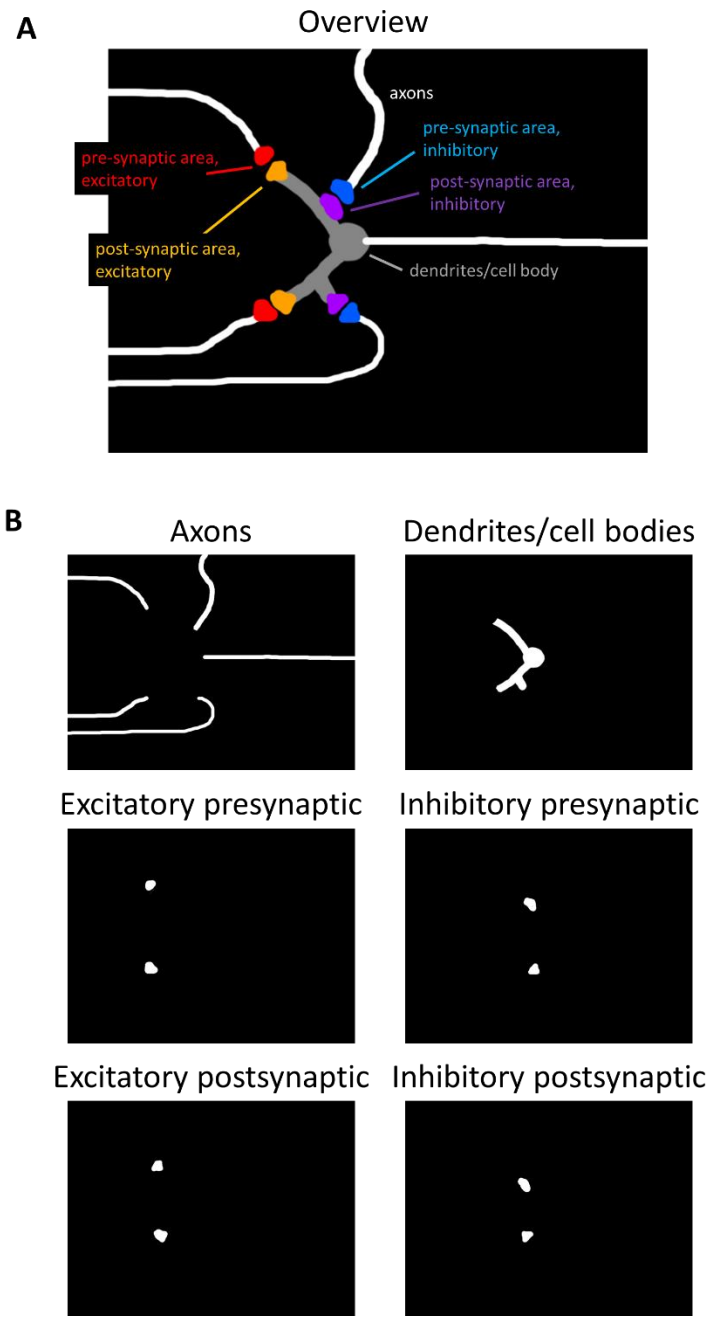

Figure 4.2: Synaptic integration scaffolds

(A) Demonstration of a set of scaffolds used to build a synaptic integration model within *Celletron*. This is a combined image, provided for clarity, and is not actually used by the simulation. (B) Individual images (as z-stacks) imported by *Celletron* to create particle-based scaffold systems.

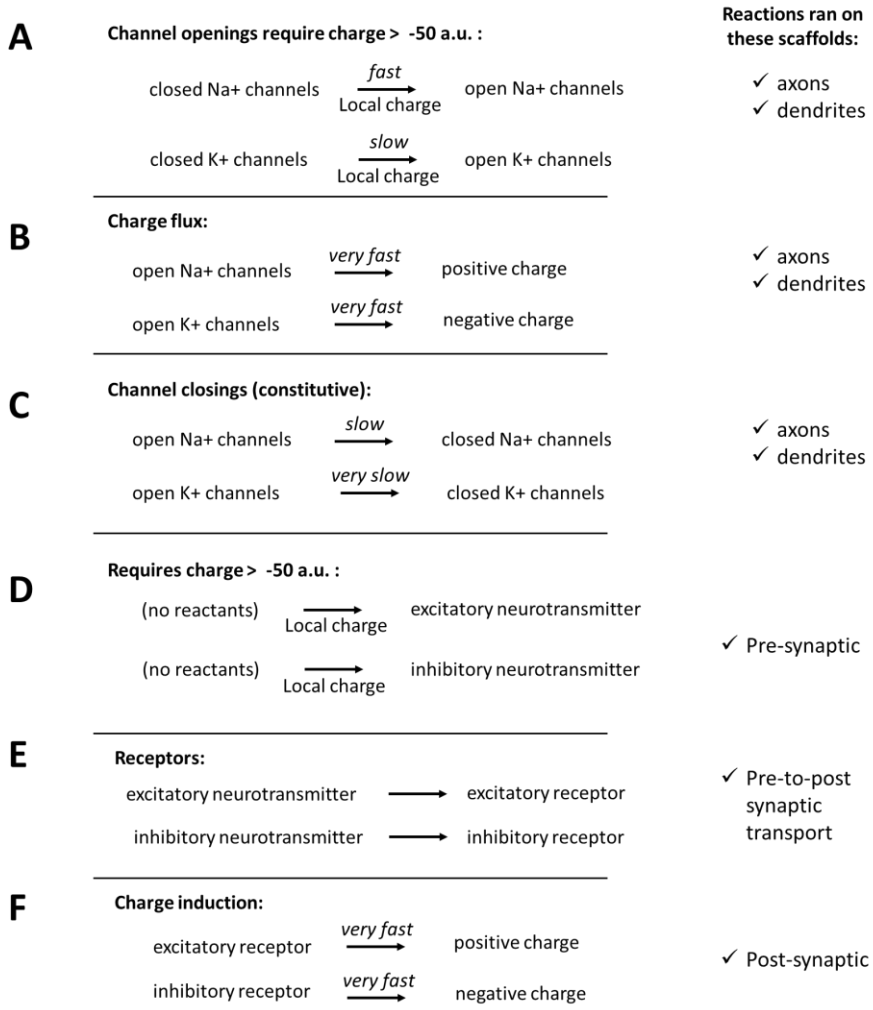

Figure 4.3: Outline of reaction systems used in synaptic integration

(A) Control of sodium and potassium channels. Closed Na and K channels are considered reagents, and consumed to produce open Na and K channels, as long as the charge is over an arbitrary threshold. Charge is not consumed in this set of reactions. (B) Open Na and K channels modify the charge, in opposing directions. Here, open channels are not consumed. (C) Open Na and K channels are gradually converted to closed Na and K channels. (D) On pre-synaptic scaffolds, local charge above an arbitrary threshold can cause secretion of neurotransmitters. Charge is not consumed for this secretory activity. (E) Neurotransmitters are received by post-synaptic scaffolds, and used to activate receptors on those scaffolds. (F) Receptors modify charge at the post-synaptic terminals.

Since this particular model is intended to demonstrate steady-state neuronal processing, no morphological physics are used, nor are any reactions specified that would result in gains or losses of scaffold mass.

Model evaluation – excitation

An experimental stimulus is applied to the indicated axon (Figure 4.4.A). As time progresses, a wave of depolarization progresses through the axon. Depolarization is eventually attenuated by slower reactions involving potassium ion flux (Figure 4.3), which eventually overshoots resting charge (Figure 4.4.B). In this way, hyperpolarization makes secondary depolarizations more difficult.

As the depolarization wave reaches the axon's presynaptic terminal, this allows charge-thresholded secretion of excitatory neurotransmitters to occur (Figure 4.3). The excitatory transmitter is received by the nearby excitatory postsynaptic terminal, which begins to depolarize nearby dendritic charge. As this charge reaches its threshold value, a new wave of depolarization travels down the dendrite, through the cell body, and down the output axon (Figure 4.4.C, see arrowhead).

Model evaluation – inhibition

Next, the ability of this model to integrate multiple incoming signals is demonstrated. The excitatory stimulus from above is paired with a simultaneous stimulus of either of two inhibitory axons (Figure 4.5.A, 4.5.C).

One might expect that a nearby, coincident inhibitory signal could prevent excitatory signaling. This situation is shown first (Figure 4.5.A). Here, an inhibitory axon is stimulated, and synapses with an inhibitory post-synaptic area. After inhibitory neurotransmitter is received, the surrounding dendrite accumulates hyperpolarizing charge (4.5.B). Despite the incoming excitatory stimulation, the hyperpolarizing charge prevents the generation of an action potential (Figure 4.5.B, arrowhead).

Figure 4.4: Evaluation of model with an excitatory synapse

(A) Experiment overview. An excitatory stimulus of charge will be applied at the top-left corner, and proceed down the excitatory axon indicated by arrows. Synaptic terminals are visible as enlargements, and the post-synaptic cell body is at the middle of this picture. (B) Time-course of action potential propagation. Red indicates depolarization (here defined as more positive charge) and yellow indicates hyperpolarization (here defined as more negative charge). The opening of Na channels progresses down the axon, and they slowly begin to close again towards frame 1000. The opening of K channels likewise progresses down the axon, but due to differently defined reaction kinetics, K channels are slower to close. (C) Overall view of the action potential inducing a post-synaptic excitation, which then causes further depolarization and emission of a new action potential (arrowhead).

Figure 4.4 (Continued)

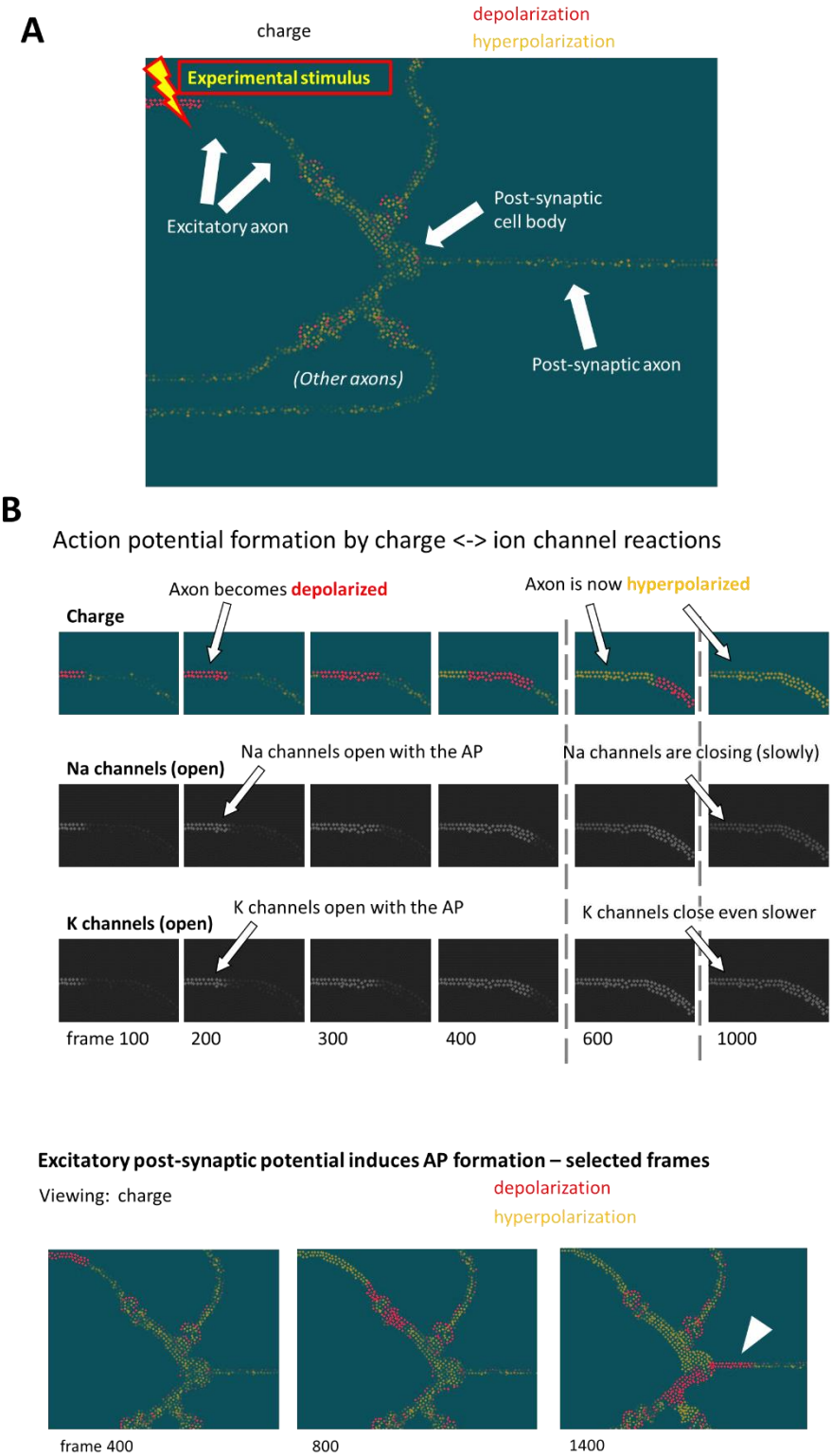

Figure 4.5: Evaluation of model with inhibitory synapses

(A) Modification of the experiment in Figure 4.4, where a second experimental stimulus is added on an inhibitory axon. (B) The inhibitory axon induces hyperpolarization in the post-synaptic neuron, and prevents action potential formation (arrowhead). (C) Modification of the experiment in Figure 4.5.A, where the second experimental stimulus is moved to a different inhibitory axon, further away. (D) This other inhibitory axon likewise produces local hyperpolarization, but is unable to prevent action potential formation (arrowhead) resulting from the excitatory synapse.

Figure 4.5 (Continued)

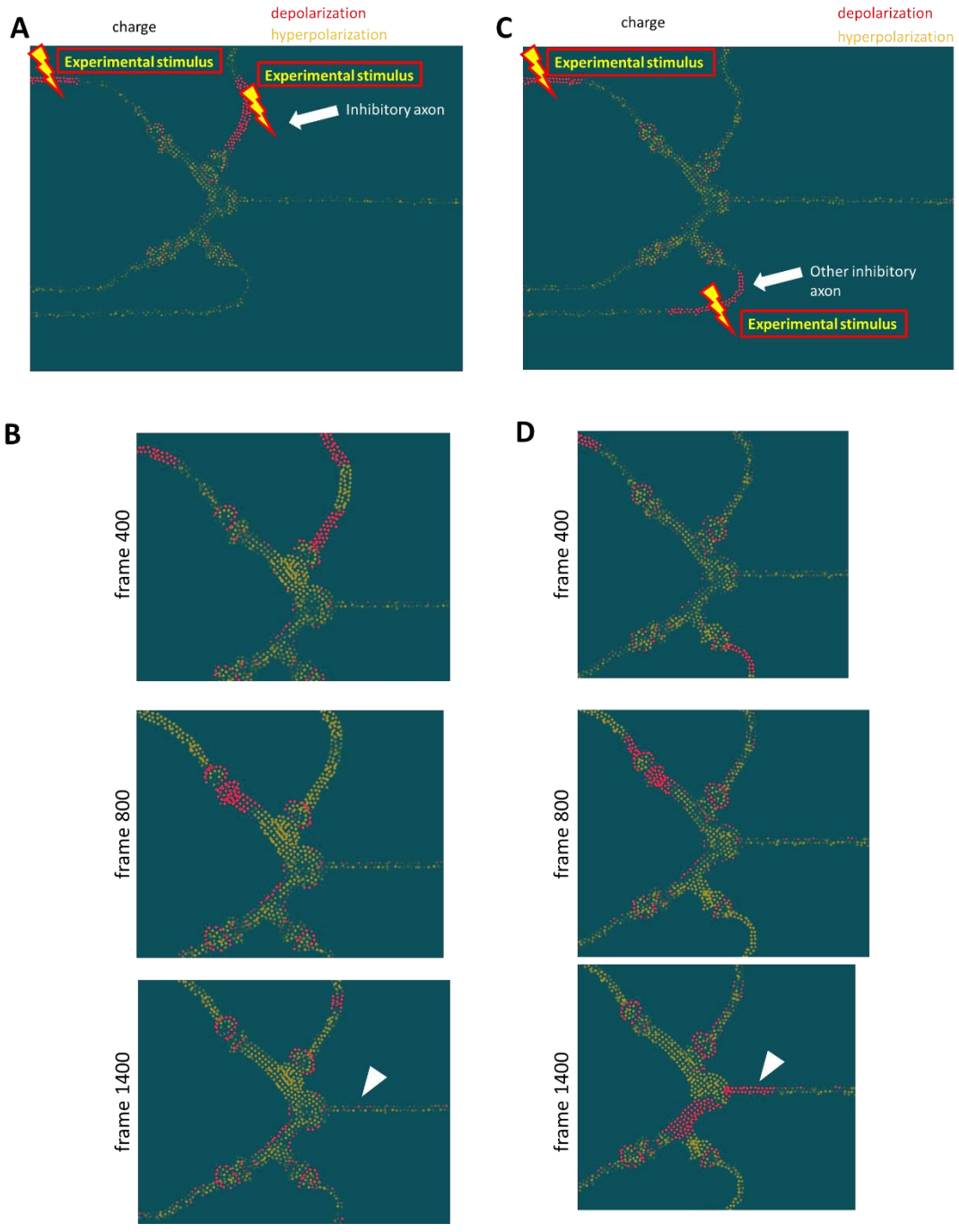

On the other hand, one might expect that a distant inhibitory signal should not affect an EPSP's ability to induce an action potential. Here, this 'irrelevant' inhibitory axon is shown synapsing on the bottom of the post-synaptic neuron's dendritic tree (Figure 4.5.C). After neurotransmission, hyperpolarization accumulates post-synaptically, but is limited in its ability to spread throughout the cell. The zone of hyperpolarization is insufficient to prevent excitatory signaling, and therefore allows action potential generation (Figure 4.5.D, arrowhead). Note that in this model depolarization spreads much more efficiently than hyperpolarization throughout the dendritic tree, likely due to the ability of the modeled reaction systems to amplify depolarization signals (Figure 4.5.D).

Growth cone navigation

Rationale

The other key aspect of predictive cellular modeling is the ability to allow cells to change over time, e.g. for the development of functional systems. Having demonstrated that scaffolds, particles, and reactions can reasonably represent functional systems, I will now demonstrate that these same abstractions can change over time in an important, regulated process during development: axon growth.

Model setup

A system is defined to represent guided axon motility along a substrate (Figure 4.6.A, 4.6.B). The most important functions of growth cone motility are embodied in the growth cone. Here, the growth cone is divided into two segments: (1) a fluid, rapidly expanding and contracting "leading edge", which binds and explores the substrate, and (2) a strong central node, or "transition zone". Trailing the growth cone is the axon itself.

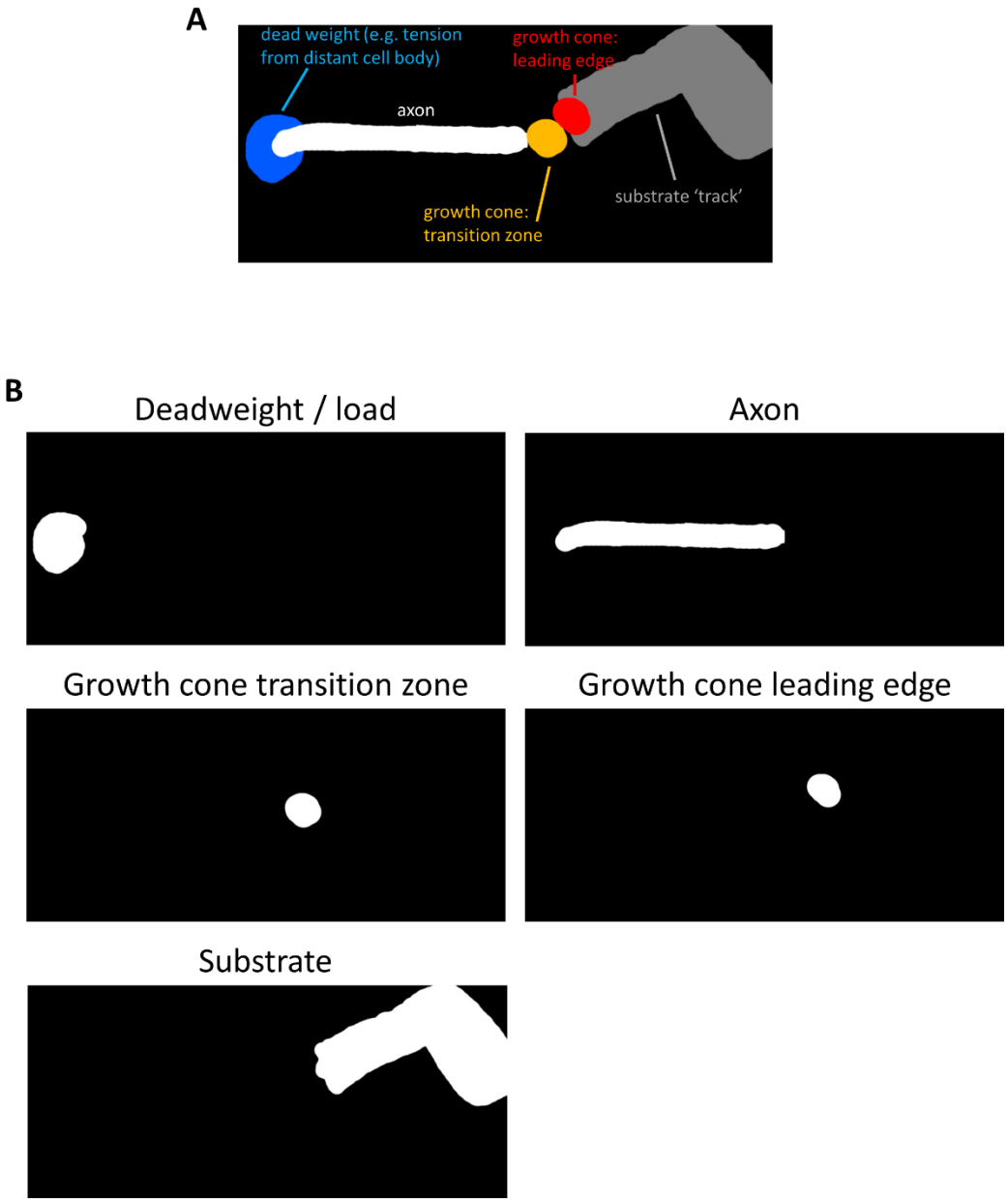

Figure 4.6: Axon outgrowth model scaffolds

(A) Demonstration of a set of scaffolds used to build a growth cone model within *Celletron*. This is a combined image, provided for clarity, and is not actually used by the simulation. (B) Individual images (as z-stacks) imported by *Celletron* to create particle-based scaffold systems.

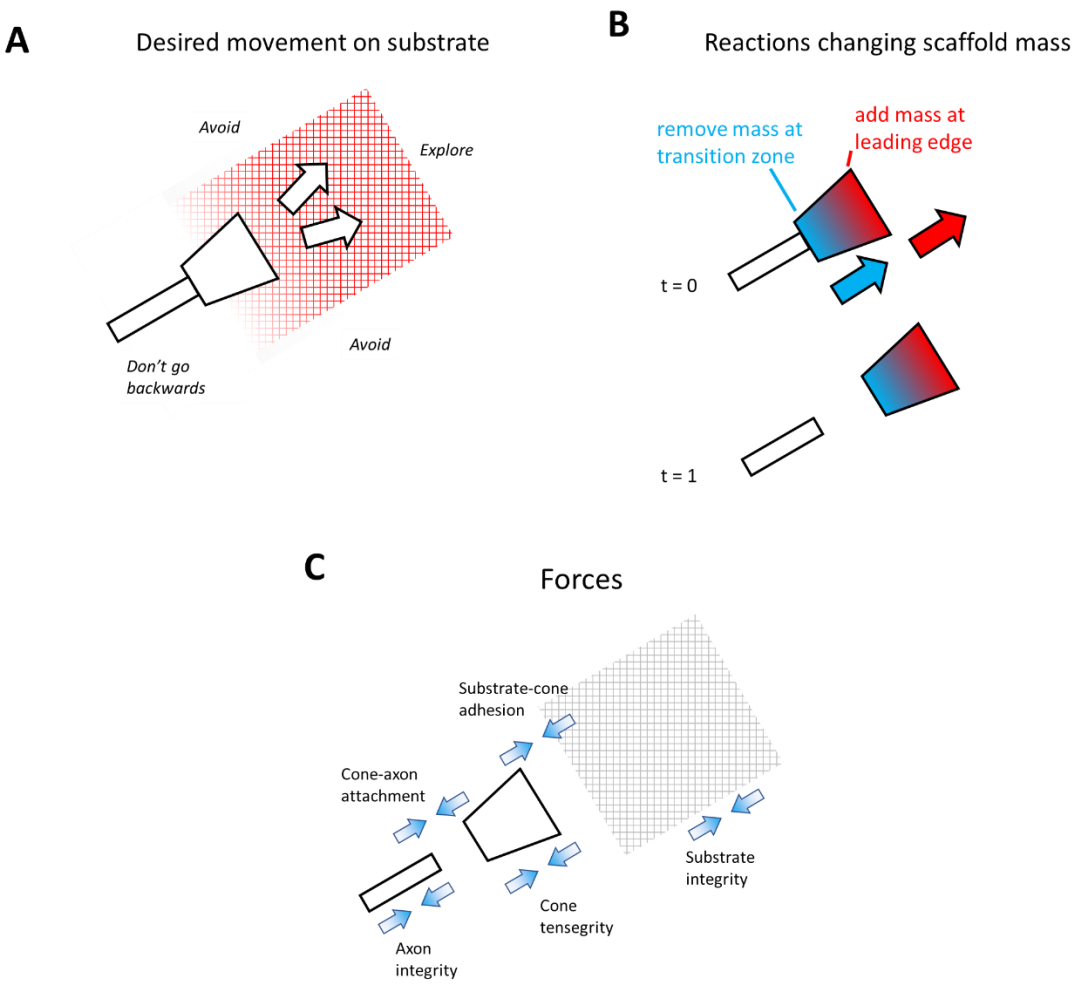

Figure 4.7: Axon outgrowth model relationships

(A) Desired behavior of the growth cone in this model, reduced to an informal set of instructions. (B) Mass-changing component of this model. Treadmilling of cytoskeleton polymers is represented by the creation of mass (the generation of new particles) at the leading edge of the growth cone, and the destruction of mass (removal of particles) at the trailing edge. (C) Some forces required within this model. Forces are specified for both intra-scaffold interactions, and inter-scaffold interactions.

In support of desired growth of the growth cone across the substrate (Figure 4.7.A), we assume that a major feature of growth cone-substrate traversal is treadmilling of cytoskeletal elements. This is represented by a set of reactions, that together have the effect of adding mass at the leading edge, and removing mass at the trailing edge (Figure 4.7.B). Mass is added to the leading edge only where that scaffold is near the substrate, and mass is only removed where the scaffold is near the growth cone's core. Furthermore, to prevent axon back-tracking on the substrate, substrate is destroyed as the growth cone traverses it.

Further, a set of physical reactions is defined, both for intra-scaffold physics, and inter-scaffold interactions. Intra-scaffold physics have the combined effects of keeping scaffolds together as a solid mass, without uncontrolled inflation or deflation. On the other hand, inter-scaffold relationships are used to adhere the distinct cellular and extracellular structures in appropriate manners (Figure 4.7.C). Two notable physical interactions are (1) the substrate – growth cone interaction, which is modeled at a short distance (relative to the other physical interactions), and (2) the growth cone core – leading edge interaction, which is modeled with relatively strong attraction in support of actin treadmilling.

Model evaluation – directional axon extension

The system described above was simulated and observed for any emergent behaviors. (Figure 4.8). Soon after the start of the simulation, the growth cone's leading edge has expanded along the substrate, while the substrate itself has begun to decay. As the simulation progresses, the leading edge continues to expand, while the decay of its trailing edge becomes visible (Figure 4.8, white see-through arrow). The core of the growth cone is continually attracted towards the leading edge, such that it follows the track specified from the substrate (Figure 4.8, yellow arrowhead).

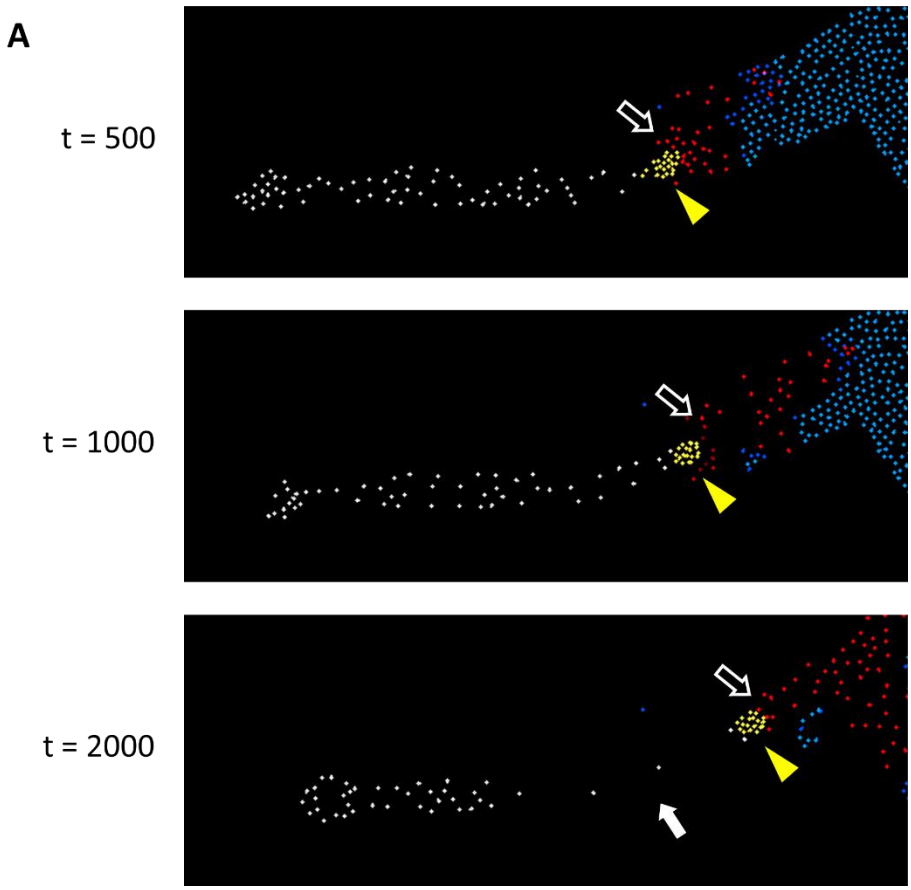

Figure 4.8: Axon outgrowth evaluation

(A) Experiment using the specified growth cone model. At t = 500, the growth cone (red) has begun to expand along the substrate (blue), and the transition zone (yellow; yellow arrowhead) has turned slightly upwards. At t = 1000, the transition zone has progressed further up and to the right (yellow; yellow arrowhead), the growth cone (red) has expanded further at the expense of the substrate (blue), and stretching of the axon itself (white) upwards and to the right is evident. Treadmilling of the trailing edge of the growth cone is also occurring (white see-through arrow). At t = 2000, the growth cone and transition zone have progressed much further along the substrate, as expected. Unfortunately, the axon appears fragmented (white arrow). Future versions of this model may benefit from further adjustment of the force parameters, as well as the local addition of mass to the axon.

Behind the growth cone, the rest of the axon follows. Encouragingly, the axon is extended, and curves upwards as the growth cone moves along the substrate. As the axon extends, it also pulls a 'deadweight' behind it in the same direction, representing load from the rest of the axon and soma. Unfortunately, the axon appears to fragment, and also appears too strongly attracted to its 'deadweight' (Figure 4.8, white solid arrow). With additional work (e.g. defining a reaction that adds new mass to the axon scaffold as the growth cone moves), this model should yield more realistic axon behavior. (Due to time constraints, I cannot test this at the time of this writing).

Discussion

Use of Celletron for modeling neural tissue development and function

Acknowledging that the current implementation of *Celletron* is not yet quantitative and needs additional work, the above examples clearly demonstrate that the current systems of particle-based scaffolds, reagents, and scaffolds can be used as building blocks to predict the functions of multi-cellular networks, and how tissues could change in regulated ways over time. Relatively simple rules can be defined that, when combined with the complex structures of tissues, give rise to emergent behaviors such as different outputs processed from various inputs, or the directed movement of a growth cone along a substrate. As further improvements are made, it should finally be possible to simulate the steps of neural development and adult functions within a single integrative model.

It's worth emphasizing the focus in *Celletron* is the methodical build-out of realistic signaling and regulatory networks, and in behaviors of cells and tissues over time, where nodes and emergent behaviors can be experimentally validated, and where network models can be a flexible resource rather than task-specific black-box. This is intended to be fairly literalistic, and not represent any form of artificial intelligence (AI). That said, AI certainly could be used to *improve* network models provided various data sources, or to *analyze* models in support of CAD/goal-seeking.

Towards decentralized construction of integrated models and neuroengineering

While partial recovery may not require addressing all sources of complexity, a full recovery almost certainly would. Such a feat is beyond my own cognitive ability, in terms of information gathering, and in designing and engineering components according to this information. I imagine others might share this view. Meanwhile, even if an interdisciplinary team of individuals was assembled that together possessed an ideal assembly of knowledge and engineering skill, the question would remain: how can this team, with its decentralized and specialized skill sets, integrate its expertise sufficiently to ultimately yield a validated nervous system restoration strategy?

The development of tools that could unload much of this complexity, and simplify collaboration between diverse researchers and engineers, would be desirable. *Celletron* is an example of an approach that could allow gradual contributions to a comprehensive tissue model, and simultaneously allow for scientists and engineers to predict how modeled tissue would respond to experimental interventions and treatments. Taking decentralization to the extreme, eventually, integration of this tool with online databases could further support these efforts.

Author contributions

Michael Norsworthy conceived a primitive first version of the described modeling method and initial implementation. Michael Norsworthy and William Immendorf implemented, tested, and improved the currently described computational tool. Michael Norsworthy designed experiments, analyzed results, and discussed modeling approaches. Michael Norsworthy assembled figures and wrote this text.

Chapter 5 – A way forward

The continuing search for restorative interventions

There are now many known examples of mechanisms and pathways which can promote regeneration. These broadly include transcription factors, intracellular pathways, and extracellular signaling environments (Butler and Tear, 2007; Liu et al., 2011; Lu et al., 2014; Moore and Goldberg, 2011; Moore et al., 2011; Patodia and Raivich, 2012). Many of these manipulations have been related to mechanisms used in normal neurogenesis of the target tissue (Blackmore et al., 2012; Moore et al., 2009; Painter et al., 2014; Park et al., 2008; Veldman et al., 2007). Additionally, the prospect of reprogramming cells to yield replacement neurons and/or supportive glia either *in vivo* or *in vitro* has been discussed (Li and Chen, 2016; Su et al., 2014). Furthermore, in the same spirit, significant progress has been made on bringing fully functional neuroprosthetics closer to the clinic (Lewis and Rosenfeld, 2016).

Nevertheless, all findings to date have limited effects, and a variety of known and unknown caveats. On axon regeneration, there have been a handful of recent reports indicating varying types of vision restoration, though even here functional restoration has generally been limited, and these might be candidates for reproducing results in confirmatory studies (Lim et al., 2016; Lima et al., 2012). The possibility of full axonal regeneration in humans has been estimated to be decades away (Crair and Mason, 2016). Meanwhile, visual neuroprosthetics have been used for eliciting phosphenes in humans and other animals, sufficient to be emotionally tantalizing to participating volunteers (Lane et al., 2013), but require much more work to integrate with tissue and properly encode image- and non-image-forming vision in order to reach a reasonable level of functional recovery. Naturally, even partial visual recovery will be valuable for patients – but to reliably restore vision to a sufficient level, while minimizing risks, remains a tall order.

***Sox11* is a double-edged sword**

From a directed screen of overexpressed neurogenic transcription factors, we found that *Sox11* promoted regeneration of RGCs, and that regeneration could span nearly the full optic nerve in mice by around 4 weeks after injury (Figure 2.1.A, 2.1.C, S.1.A, S.1.B). We implicated *DCX* and other cytoskeletal genes as being regulatory targets of *Sox11* in regeneration (Figure 2.3.C, 2.3.D). These targets held special interest, based on known importance during embryogenesis (Gleeson et al., 1999), and because recent findings identified the importance of *DCX* and its *Dclk* homologs in regeneration (Nawabi et al., 2015). Thus, *Sox11*'s regulation of cytoskeletal genes makes sense in terms of its developmental role, and links it to at least one known mechanism of axon regeneration in adults. Even more encouragingly, we found that PTEN/Sox11 combined treatment led to greatly enhanced axon regeneration, where axons reached sufficient lengths to penetrate the optic tract, and also invade the SCN (Figure 2.4.A, 2.4.B, 2.4.C, 3.2.B). These unconditionally establish *Sox11* as a potent regeneration gene, worthy of further pursuit for harnessing its beneficial mechanisms.

On the other hand, *Sox11* ablates at least alpha-RGCs (Figure 2.2), and this cannot be rescued by PTEN deletion (Figure 2.4.G, 2.4.H). Combining Sox11 with Bcl2 overexpression also does not seem to alleviate this alpha-RGC cell death (Figure S.2.B, S.2.C). While some mix of ceramide regulation (Figure 2.3.B) or oxidative stress (Figure 3.4.A, 3.4.B, 3.4.C) might be involved in this cell ablation, it is difficult to predict what treatments might rescue alpha-RGC survival, and if those treatments might have even further secondary effects.

Sox11's effect on alpha-RGCs is the first explicit demonstration of negative consequences coming from a regenerative treatment. While other treatments have been shown to act favorably on axon growth in small populations of neurons, their off-target effects have not been fully characterized (Blackmore et al., 2012; Duan et al., 2015; Wang et al., 2015). Therefore, characterizing the effects of regenerative treatments on all different subpopulations of cells (such as intrinsically photosensitive

RGCs, Figure 3.1, Figure 3.2.A) will likely be a necessary, messy effort for the field of neural regeneration – though even here, prediction of optimal therapeutic strategies would still involve challenging design within complex systems.

Modeling to facilitate interdisciplinary collaboration

Calls for interdisciplinary collaboration, for the goal of neural restoration, have been made recently (Crair and Mason, 2016). However, this may be easier said than done: keeping abreast of current knowledge is a challenge, as is integrating those findings into updated, consistent, predictive models and databases. Further, all of these collections of knowledge require deep expertise to understand, before a human-determined prediction is made – that is, current modeling approaches largely do not allow for gradual construction and refinement, often consist of network diagrams that cannot be executed by computers, cannot make predictions outside limited contexts, and do not readily permit abstraction of components and subsystems by researchers working on different portions of a shared problem.

For example, suppose there is a protein network diagram, whose 'trigger' is a membrane-bound voltage-gated ion channel, along with cytoplasmic and nuclear proteins, and a network output is a graded, quantitative transcription of several genes. Such a network might be obscure or even meaningless to an electrical engineer. This is a problem: for interdisciplinary work on a neuroprosthetic, an electrical engineer might need to know minimum, maximum, and ideal voltages to apply to a membrane to achieve, or avoid, certain genetic outputs, and would be best served by treating cellular decision-making as a 'black box'. Similarly, a biologist may want to understand how various cell types within a tissue respond to an implanted device, and predict a genetic treatment that may make cellular responses more favorable. Here, the biologist might want to evaluate a tissue-implanted device as a

'black box', and use their intuition of cellular mechanisms to determine a genetic treatment to subsequently verify *in vivo*.

As another example, suppose that a purely biological axon regeneration treatment is desired. Even here, abstraction would facilitate collaboration between biologists: one might work on genetic treatments for glia, another might work on regulation of axon growth and guidance, and another might work on modulating cell stress/cell death pathways. In this case, all components and tested interventions could be executed in a single collected model, and allow for cooperative identification of the most promising treatments in terms of the overall resulting behavior of tissue.

Complex, interdisciplinary problems rely on solving communication problems between various experts, on validation of functions in system models and in the real world, and on acknowledging that some layers of abstraction are necessary (Veeke et al., 2006). These efforts may be particularly challenging for biologists due to endemic challenges in notation, underdeveloped quantitative mathematical descriptions, siloed knowledge between biological sub-disciplines, and poorly characterized biological complexity (Lazebnik, 2002). Lazebnik (2002) leaves the reader with many impassioned and colorful statements, but this one is especially pertinent:

> *It is common knowledge that the human brain can keep track of only so many variables. It is also common experience that once the number of components in a system reaches a certain threshold, understanding the system without formal analytical tools requires geniuses, who are so rare even outside biology. In engineering, the scarcity of geniuses is compensated, at least in part, by a formal language that successfully unites the efforts of many individuals, thus achieving a desired effect, be that design of a new aircraft or of a computer program. In biology, we use several arguments to convince ourselves that problems that require calculus can be solved with arithmetic if one tries hard enough and does another series of experiments.* (Lazebnik, 2002)

There have been some movements towards the use of more capable computational tools (Hines, 1989, 1993; Karr et al., 2012; Lazebnik, 2002), but we still lack sufficiently versatile, inclusive tools that can help us break out of our specialist siloes. I have discussed an example of what one such tool might look like, which we have called *Celletron*. I hope that it, or similarly ambitious tools, will soon

help usher in a more integrative and predictive era of biological science and engineering, and facilitate collaboration towards full and complete neural restoration.

For a long time, asking “Can a biologist fix a radio?” (Lazebnik, 2002) has been answered with a quietly muttered “…nah.” – but, perhaps soon, the answer will finally be “Why, yes!”, to the benefit of society as a whole.

References

Anders, S., Pyl, P.T., and Huber, W. (2015). HTSeq-A Python framework to work with high-throughput sequencing data. Bioinformatics *31*, 166–169.

Anderson, M.G., Smith, R.S., Hawes, N.L., Zabaleta, A., Chang, B., Janey, L., and John, S.W.M. (2002). Mutations in genes encoding melanosomal proteins cause pigmentary glaucoma in DBA / 2J mice. Nat. Genet. *30*, 81–85.

Badea, T.C., and Nathans, J. (2011). Morphologies of mouse retinal ganglion cells expressing transcription factors Brn3a, Brn3b, and Brn3c: analysis of wild type and mutant cells using genetically-directed sparse labeling. Vis. Res. *51*, 269–279.

Baden, T., Berens, P., Franke, K., Roson, M.R., Bethge, M., and Euler, T. (2016). The functional diversity of retinal ganglion cells in the mouse. Nature *529*, 345–350.

Baver, S.B., Pickard, G.E., Sollars, P.J., and Pickard, G.E. (2008). Two types of melanopsin retinal ganglion cell differentially innervate the hypothalamic suprachiasmatic nucleus and the olivary pretectal nucleus. Eur. J. Neurosci. *27*, 1763–1770.

Bei, F., Lee, H.H.C., Liu, X., Gunner, G., Jin, H., Ma, L., Wang, C., Hou, L., Hensch, T.K., Frank, E., et al. (2016). Restoration of Visual Function by Enhancing Conduction in Regenerated Axons. Cell *164*, 219–232.

Belin, S., Nawabi, H., Wang, C., Tang, S., Latremoliere, A., Warren, P., Schorle, H., Uncu, C., Woolf, C.J., He, Z., et al. (2015). Injury-induced decline of intrinsic regenerative ability revealed by quantitative proteomics. Neuron *86*, 1000–1014.

Benowitz, L.I., He, Z., and Goldberg, J.L. (2017). Reaching the brain : Advances in optic nerve regeneration. Exp. Neurol. *287*, 365–373.

Bergsland, M., Werme, M., Malewicz, M., Perlmann, T., and Muhr, J. (2006). The establishment of neuronal properties is controlled by Sox4 and Sox11. Genes Dev. *20*, 3475–3486.

Berson, D.M., Dunn, F.A., and Takao, M. (2002). Phototransduction by Retinal Ganglion Cells That Set the Circadian Clock. Science (80-.). *295*, 1070–1074.

Blackmore, M.G., Wang, Z., Lerch, J.K., Motti, D., Zhang, Y.P., Shields, C.B., Lee, J.K., Goldberg, J.L., Lemmon, V.P., and Bixby, J.L. (2012). Krüppel-like Factor 7 engineered for transcriptional activation promotes axon regeneration in the adult corticospinal tract. Proc. Natl. Acad. Sci. U. S. A. *109*, 7517–7522.

Bonfanti, L., Strettoi, E., Chierzi, S., Cenni, M.C., Liu, X., Martinou, J., Maffei, L., and Rabacchi, S.A. (1996). Protection of Retinal Ganglion Cells from Natural and Axotomy-Induced Cell Death in Neonatal Transgenic Mice Overexpressing bcl-2. J. Neurosci. *16*, 4186–4194.

Bradke, F., Fawcett, J.W., and Spira, M.E. (2012). Assembly of a new growth cone after axotomy: the precursor to axon regeneration. Nat. Rev. Neurosci. *13*, 183–193.

Brindley, B.Y.G.S., and Lewin, W.S. (1968). THE SENSATIONS PRODUCED BY ELECTRICAL STIMULATION OF THE VISUAL CORTEX. J. Physiol. *196*, 479–493.

Brown, N.L., Patel, S., Brzezinski, J., and Glaser, T. (2001). Math5 is required for retinal ganglion cell and optic nerve formation. Development *128*, 2497–2508.

Butler, S.J., and Tear, G. (2007). Getting axons onto the right path: the role of transcription factors in axon guidance. Development *134*, 439–448.

Cai, D., Qiu, J., Cao, Z., McAtee, M., Bregman, B.S., and Filbin, M.T. (2001). Neuronal cyclic AMP controls the developmental loss in ability of axons to regenerate. J. Neurosci. *21*, 4731–4739.

Callier, T., Schluter, E., Tabot, G., Miller, L., F, T., and Bensmaia, S. (2015). Long-term stability of sensitivity to intracortical microstimulation of somatosensory cortex. J. Neural Eng. *12*.

Canty, A.J., Huang, L., Jackson, J.S., Little, G.E., Knott, G., Maco, B., and De Paola, V. (2013). In-vivo single neuron axotomy triggers axon regeneration to restore synaptic density in specific cortical circuits. Nat. Commun. *4*, 2038.

Casagrande, V., and Boyd, J. (1996). The neural architecture of binocular vision. Eye *10*, 153–160.

Cepko, C.L. (2014). Intrinsically different retinal progenitor cells produce specific types of progeny. Nat. Rev. Neurosci. *15*, 615–627.

Chandran, V., Coppola, G., Nawabi, H., Omura, T., Versano, R., Huebner, E.A., Zhang, A., Costigan, M., Yekkirala, A., Barrett, L., et al. (2016). A Systems-Level Analysis of the Peripheral Nerve Intrinsic Axonal Growth Program. Neuron *89*, 956–970.

Chang, X.K., Hertz, J., Zhang, X., Jin, X., Shaw, X.P., Derosa, B.A., Li, J.Y., Venugopalan, P., Valenzuela, D.A., Patel, R.D., et al. (2017). Novel Regulatory Mechanisms for the SoxC Transcriptional Network Required for Visual Pathway Development. J. Neurosci. *37*, 4967–4981.

Chen, K., Dammann, J., Boback, J., Tenore, F., Otto, K., Gaunt, R., and Bensmaia, S. (2014). The effect of chronic intracortical microstimulation on the electrode–tissue interface. J. Neural Eng. *11*.

Chen, S., Badea, T., and Hattar, S. (2011). Photoentrainment and pupillary light reflex are mediated by distinct populations of ipRGCs. Nature *476*, 92–95.

Cleland, B.Y.B.G., Levick, W.R., and Wassle, H. (1975). PHYSIOLOGICAL IDENTIFICATION OF A MORPHOLOGICAL CLASS OF CAT RETINAL GANGLION CELLS. J Physiol. *248*, 151–171.

Crair, M.C., and Mason, X.C.A. (2016). Reconnecting Eye to Brain. J. Neurosci. *36*, 10707–10722.

Crook, J.D., Peterson, B.B., Packer, O.S., Robinson, F.R., Troy, J.B., and Dacey, D.M. (2008). Y-Cell Receptive Field and Collicular Projection of Parasol Ganglion Cells in Macaque Monkey Retina. J. Neurosci. *28*, 11277–11291.

Cui, Q., Ren, C., Sollars, P., Pickard, G., and So, K.-F. (2015). The injury resistant ability of melanopsin-expressing intrinsically photosensitive retinal ganglion cells. Neuroscience *284*, 845–853.

David, S., and Aguayo, A. (1981). Axonal elongation into peripheral nervous system “bridges” after central nervous system injury in adult rats. Science (80-.). *214*, 931–933.

Davis, T., Parker, R., House, P., Bagley, E., Wendelken, S., Normann, R., and Greger, B. (2012). Spatial and temporal characteristics of V1 microstimulation during chronic implantation of a microelectrode array in a behaving macaque. J. Neural Eng. *9*.

Deiner, M.S., Kennedy, T.E., Fazeli, A., Serafini, T., Tessier-lavigne, M., and Sretavan, D.W. (1997). Netrin-1 and DCC Mediate Axon Guidance Locally at the Optic Disc : Loss of Function Leads to Optic Nerve Hypoplasia. Neuron *19*, 575–589.

Dhande, O., and Huberman, A. (2014). Retinal ganglion cell maps in the brain: implications for visual processing. Curr. Opin. Neurobiol. *24*, 133–142.

Dobelle, W., and Mladejovsky, M. (1974). Phosphenes produced by electrical stimulation of human occipital cortex, and their application to the development of a prosthesis for the blind. J Physiol. *243*, 553–576.

Dobelle, W., Mladejovsky, M., and Girvin, J. (1974). Artifical vision for the blind: electrical stimulation of visual cortex offers hope for a functional prosthesis. Science (80-.). *183*, 440–444.

Dobin, A., Davis, C.A., Schlesinger, F., Drenkow, J., Zaleski, C., Jha, S., Batut, P., Chaisson, M., and Gingeras, T.R. (2013). STAR: Ultrafast universal RNA-seq aligner. Bioinformatics *29*, 15–21.

Duan, X., Qiao, M., Bei, F., Kim, I.-J., He, Z., and Sanes, J.R. (2015). Subtype-Specific Regeneration of Retinal Ganglion Cells following Axotomy: Effects of Osteopontin and mTOR Signaling. Neuron 1–13.

Ecker, J.L., Dumitrescu, O.N., Wong, K.Y., Alam, N.M., Chen, S.-K., LeGates, T., Renna, J.M., Prusky, G.T., Berson, D.M., and Hattar, S. (2010). Melanopsin-expressing retinal ganglion-cell photoreceptors: cellular diversity and role in pattern vision. Neuron *67*, 49–60.

Ellis, E.M., Gauvain, G., Sivyer, B., and Murphy, G.J. (2016). Shared and distinct retinal input to the mouse superior colliculus and dorsal lateral geniculate nucleus. J Neurophysiol *116*, 602–610.

Enes, J., Langwieser, N., Carballosa-gonzalez, M.M., Klug, A., Traut, M.H., Ylera, B., Tahirovic, S., Hofmann, F., Stein, V., Moosmang, S., et al. (2010). Article Electrical Activity Suppresses Axon Growth through Ca v 1 . 2 Channels in Adult Primary Sensory Neurons. Curr. Biol. *20*, 1154–1164.

Erkman, L., Yates, P.A., McLaughlin, T., McEvilly, R.J., Whisenhunt, T., O’Connell, S.M., Krones, A.I., Kirby, M.A., Rapaport, D.H., Bermingham, J.R., et al. (2000). A POU Domain Transcription Factor–Dependent Program Regulates Axon Pathfinding in the Vertebrate Visual System. Neuron *28*, 779–792.

Erskine, L., and Herrera, E. (2007). The retinal ganglion cell axon ’ s journey : Insights into molecular mechanisms of axon guidance. Dev. Biol. *308*, 1–14.

Estevez, M.E., Fogerson, P.M., Ilardi, M.C., Borghuis, B.G., Chan, E., Weng, S., Auferkorte, O.N., Demb, J.B., and Berson, D.M. (2012). Form and function of the M4 cell, an intrinsically photosensitive retinal ganglion cell type contributing to geniculocortical vision. J. Neurosci. *32*, 13608–13620.

Filbin, M.T. (2006). Recapitulate development to promote axonal regeneration: good or bad approach? Philos. Trans. R. Soc. Lond. B. Biol. Sci. *361*, 1565–1574.

Fitch, M.T., and Silver, J. (2008). CNS injury , glial scars , and inflammation : Inhibitory extracellular matrices and regeneration failure. Exp. Neurol. *209*, 294–301.

Fogerson, P., and Berson, D. (2012). Outputs Of The Olivary Pretectal Nucleus In Relation To Photic Blink, Pain And Tears. Invest. Ophthalmol. Vis. Sci. *53*.

Forster, O. (1929). Beitrage zur Pathophysiologie der Sehbahn und der Sehsphare. J. Psychol. Neurol. *39*, 463–485.

Freedman, M.S., Lucas, R.J., Soni, B., Schantz, M. Von, Mun, M., and Foster, R. (1999). Regulation of Mammalian Circadian Behavior by Non-rod , Non-cone , Ocular Photoreceptors. Science (80-.). *284*, 502–505.

Gan, L., Xiangts, M., Zhout, L., Wagner, D.S., and Klein, W.H. (1996). POU domain factor Brn-3b is required for the development of a large set of retinal ganglion cells. PNAS *93*, 3920–3925.

Gao, Z., Mao, C.-A., Pan, P., Mu, X., and Klein, W.H. (2014). Transcriptome of Atoh7 retinal progenitor cells identifies new Atoh7-dependent regulatory genes for retinal ganglion cell formation. Dev. Neurobiol. *74*, 1123–1140.

Gauron, C., Meda, F., Dupont, E., Albadri, S., Quenech, N., Ipendey, E., Volovitch, M., Del, F., Joliot, A., Rampon, C., et al. (2016). Hydrogen peroxide (H 2 O 2) controls axon path finding during zebrafish development. Dev. Biol. *414*, 133–141.

Geoffroy, G., Lorenzana, A.O., Kwan, J.P., Lin, K., Ghassemi, O., Ma, A., Xu, N., Creger, D., Liu, K., He, Z., et al. (2015). Effects of PTEN and Nogo Codeletion on Corticospinal Axon Sprouting and Regeneration in Mice. J. Neurosci. *35*, 6413–6428.

Gleeson, J., Lin, P., Flanagan, L., and Walsh, C. (1999). Doublecortin Is a Microtubule-Associated Protein and Is Expressed Widely by Migrating Neurons. Neuron *23*, 257–271.

Goldberg, J.L., Espinosa, J.S., Xu, Y., Davidson, N., Kovacs, G.T. a, and Barres, B. a (2002). Retinal ganglion cells do not extend axons by default: promotion by neurotrophic signaling and electrical activity. Neuron *33*, 689–702.

Grados-munro, E.M., and Fournier, A.E. (2003). Myelin-Associated Inhibitors of Axon Regeneration. J. Neurosci. Res. *485*, 479–485.

Hammarback, J. a., Obar, R. a., Hughes, S.M., and Vallee, R.B. (1991). MAP1B is encoded as a polyprotein that is processed to form a complex N-terminal microtubule-binding domain. Neuron *7*, 129–139.

Hart, M.J., Callow, M.G., Souza, B., and Polakis, P. (1996). IQGAP1, a calmodulin-binding protein with a rasGAP-related domain, is a potential effector for cdc42Hs. EMBO J. *15*, 2997–3005.

Hattar, S., Liao, H.W., Takao, M., Berson, D.M., and Yau, K.W. (2002). Melanopsin-containing retinal ganglion cells: architecture, projections, and intrinsic photosensitivity. Science *295*, 1065–1070.

He, Z., and Jin, Y. (2016). Intrinsic Control of Axon Regeneration. Neuron *90*, 437–451.

Hines, M. (1989). A program for simulation of nerve equations with branching geometries. Int J Biomed Comput. *24*, 55–68.

Hines, M. (1993). NEURON—A program for simulation of nerve equations. Neural Syst. Anal. Model. 127–136.

Huang, W., Chen, Y., and Page, D.T. (2016). Hyperconnectivity of prefrontal cortex to amygdala projections in a mouse model of macrocephaly / autism syndrome. Nat. Commun. *7*, 1–15.

Huberman, A.D., Manu, M., Koch, S.M., Susman, M.W., Lutz, A.B., Ullian, E.M., Baccus, S.A., and Barres, B.A. (2008). Article Architecture and Activity-Mediated Refinement of Axonal Projections from a Mosaic of Genetically Identified Retinal Ganglion Cells. Neuron *59*, 425–438.

Jankowski, M.P., McIlwrath, S.L., Jing, X., Cornuet, P.K., Salerno, K.M., Koerber, H.R., and Albers, K.M. (2009). Sox11 transcription factor modulates peripheral nerve regeneration in adult mice. Brain Res. *1256*, 43–54.

Jayaprakash, N., Wang, Z., Hoeynck, B., Krueger, N., Kramer, A., Balle, E., Wheeler, D.S., Wheeler, R.A., and Blackmore, M.G. (2016). Optogenetic Interrogation of Functional Synapse Formation by Corticospinal Tract Axons in the Injured Spinal Cord. J. Neurosci. *36*, 5877–5890.

Jiang, Y., Ding, Q., Xie, X., Libby, R.T., Lefebvre, V., and Gan, L. (2013). Transcription factors SOX4 and SOX11 function redundantly to regulate the development of mouse retinal ganglion cells. J. Biol. Chem. *288*, 18429–18438.

Jing, X., Wang, T., Huang, S., Glorioso, J.C., and Albers, K.M. (2012). The transcription factor Sox11 promotes nerve regeneration through activation of the regeneration-associated gene Sprr1a. Exp. Neurol. *233*, 221–232.

Karr, J.R., Sanghvi, J.C., Macklin, D.N., Gutschow, M. V, Jacobs, J.M., Bolival, B., Assad-garcia, N., Glass, J.I., and Covert, M.W. (2012). Theory A Whole-Cell Computational Model Predicts Phenotype from Genotype. Cell *150*, 389–401.

Kay, J.N., De la Huerta, I., Kim, I.-J., Zhang, Y., Yamagata, M., Chu, M.W., Meister, M., and Sanes, J.R. (2011). Retinal ganglion cells with distinct directional preferences differ in molecular identity, structure, and central projections. J. Neurosci. *31*, 7753–7762.

Kim, I.-J., Zhang, Y., Meister, M., and Sanes, J.R. (2010). Laminar restriction of retinal ganglion cell dendrites and axons: subtype-specific developmental patterns revealed with transgenic markers. J. Neurosci. *30*, 1452–1462.

Kim, K., Perkins, G.A., Shim, M.S., Bushong, E., Alcasid, N., Ju, S., Ellisman, M.H., Weinreb, R.N., and Ju, W. (2015). DRP1 inhibition rescues retinal ganglion cells and their axons by preserving mitochondrial integrity in a mouse model of glaucoma. Cell Death Dis. *6*, 1–15.

Klier, E.M., Wang, H., and Crawford, J.D. (2001). The superior colliculus encodes gaze commands in retinal coordinates. Nat. Neurosci. *4*, 627–632.

Koser, D.E., Thompson, A.J., Foster, S.K., Dwivedy, A., Pillai, E.K., Sheridan, G.K., Svoboda, H., Viana, M., Costa, L.F., Guck, J., et al. (2016). Mechanosensing is critical for axon growth in the developing brain. Nat. Neurosci. *19*, 1592–1598.

Krieger, B., Qiao, M., Rousso, D.L., Sanes, J.R., and Meister, M. (2017). Four alpha ganglion cell types in mouse retina : Function , structure , and molecular signatures. PLoS One *12*, e0180091.

Kuwajima, T., Yoshida, Y., Takegahara, N., Petros, T.J., Kumanogoh, A., Jessell, T.M., Sakurai, T., and Mason, C. (2012). Optic Chiasm Presentation of Semaphorin6D in the Context of Plexin-A1 and Nr-CAM Promotes Retinal Axon Midline Crossing. Neuron *74*, 676–690.

Kuwajima, T., Soares, C.A., Sitko, A.A., Lefebvre, V., and Mason, C. (2017). SoxC Transcription Factors Promote Contralateral Retinal Ganglion Cell Differentiation and Axon Guidance in the Mouse Visual System. Neuron *93*, 1110–1125.

De la Huerta, I., Kim, I.-J., Voinescu, P.E., and Sanes, J.R. (2012). Direction-selective retinal ganglion cells arise from molecularly specified multipotential progenitors. Proc. Natl. Acad. Sci. U. S. A. *109*, 17663–17668.

Lane, F., Troyk, P., and Nitsch, K. (2013). Participants' experiences in a clinical trial for vision restoration: Motivation to participate, visual perception and functional use, and experience of loss following termination. In ARVO Annual Meeting Abstract,.

Lazebnik, Y. (2002). Can a biologist fix a radio ? — Or, what I learned while studying apoptosis. Cancer Cell *2*, 179–182.

Le, T.T., Wroblewski, E., Patel, S., Riesenberg, A.N., and Brown, N.L. (2006). Math5 is required for both early retinal neuron differentiation and cell cycle progression. Dev. Biol. *295*, 764–778.

Lee, J., Geoffroy, G., Chan, A.F., Tolentino, K.E., Crawford, M.J., Leal, M.A., Kang, B., and Zheng, B. (2010). Assessing Spinal Axon Regeneration and Sprouting in Nogo-, MAG-, and OMgp-Deficient Mice. Neuron *66*, 663–670.

Lee, R., Petros, T.J., and Mason, C.A. (2008). Zic2 Regulates Retinal Ganglion Cell Axon Avoidance of ephrinB2 through Inducing Expression of the Guidance Receptor EphB1. J. Neurosci. *28*, 5910–5919.

Leibinger, M., Mu, A., Andreadaki, A., Hauk, T.G., Kirsch, M., and Fischer, D. (2009). Neuroprotective and Axon Growth-Promoting Effects following Inflammatory Stimulation on Mature Retinal Ganglion Cells in Mice Depend on Ciliary Neurotrophic Factor and Leukemia Inhibitory Factor. J. Neurosci. *29*, 14334–14341.

Lewis, P.M., and Rosenfeld, J. V (2016). Electrical stimulation of the brain and the development of cortical visual prostheses : An historical perspective. Brain Res. *1630*, 208–224.

Li, H., and Chen, G. (2016). Perspective In Vivo Reprogramming for CNS Repair: Regenerating Neurons from Endogenous Glial Cells. Neuron *91*, 728–738.

Li, R., Wu, F., Ruonala, R., Sapkota, D., Hu, Z., and Mu, X. (2014). Isl1 and pou4f2 form a complex to regulate target genes in developing retinal ganglion cells. PLoS One *9*, e92105.

Lim, J.A., Stafford, B.K., Nguyen, P.L., Lien, B. V, Wang, C., Zukor, K., He, Z., and Huberman, A.D. (2016). Neural activity promotes long-distance , target-specific regeneration of adult retinal axons. Nat. Neurosci. *19*.

Lima, S. De, Koriyama, Y., Kurimoto, T., Oliveira, T., Yin, Y., Li, Y., Gilbert, H., Maria, A., Martinez, B., and Benowitz, L. (2012). Full-length axon regeneration in the adult mouse optic nerve and partial recovery of simple visual behaviors. Proc. Natl. Acad. Sci. *109*, 13465–13465.

Lin, L., Lee, V.M., Wang, Y., Lin, J.S., Sock, E., Wegner, M., and Lei, L. (2011). Sox11 regulates survival and axonal growth of embryonic sensory neurons. Dev. Dyn. *240*, 52–64.

Liu, K., Tedeschi, A., Park, K.K., and He, Z. (2011). Neuronal intrinsic mechanisms of axon regeneration. Annu. Rev. Neurosci. *34*, 131–152.

Livesey, F.J., and Cepko, C.L. (2001). Vertebrate neural cell-fate determination: lessons from the retina. Nat. Rev. Neurosci. *2*, 109–118.

Lowery, L.A., and Sive, H. (2005). Initial formation of zebrafish brain ventricles occurs independently of circulation and requires the nagie oko and snakehead / atp1a1a . 1 gene products. Development *132*, 2057–2067.

Lu, Y., Belin, S., and He, Z. (2014). Signaling regulations of neuronal regenerative ability. Curr. Opin. Neurobiol. *27*, 135–142.

Madisen, L., Zwingman, T.A., Sunkin, S.M., Oh, S.W., Hatim, A., Gu, H., Ng, L.L., Palmiter, R.D., Hawrylycz, M.J., Allan, R., et al. (2010). A robust and high-throughput Cre reporting and characterization system for the whole mouse brain. Nat Neurosci. *13*, 133–140.

Mao, C., Wang, S.W., Pan, P., and Klein, W.H. (2008a). Rewiring the retinal ganglion cell gene regulatory network : Neurod1 promotes retinal ganglion cell fate in the absence of Math5. Development *135*, 3379–3388.

Mao, C., Kiyama, T., Pan, P., Furuta, Y., Hadjantonakis, A., and Klein, W.H. (2008b). Eomesodermin , a target gene of Pou4f2 , is required for retinal ganglion cell and optic nerve development in the mouse. *1*.

Martersteck, E., Hirokawa, K.E., Evarts, M., Bernard, A., Duan, X., Ng, L., Oh, S.W., Ouellette, B., Royall, J.J., Stoecklin, M., et al. (2017). Diverse Central Projection Patterns of Retinal Ganglion Cells. Cell Rep *18*, 2058–2072.

Matynia, A. (2013). Blurring the Boundaries of Vision : Novel Functions of Intrinsically Photosensitive Retinal Ganglion Cells. J. Exp. Neurosci. *7*, 43–50.

McCreery, D., Pikov, V., and Troyk, P. (2010). Neuronal loss due to prolonged controlled-current stimulation with chronically implanted microelectrodes in the cat cerebral cortex. J Neural Eng *7*.

de Melo, J., Du, G., Fonseca, M., Gillespie, L.-A., Turk, W.J., Rubenstein, J.L.R., and Eisenstat, D.D. (2005). Dlx1 and Dlx2 function is necessary for terminal differentiation and survival of late-born retinal ganglion cells in the developing mouse retina. Development *132*, 311–322.

Mencarelli, C., and Martinez-Martinez, P. (2013). Ceramide function in the brain: When a slight tilt is enough. Cell. Mol. Life Sci. *70*, 181–203.

Moore, D.L., and Goldberg, J.L. (2011). Multiple transcription factor families regulate axon growth and regeneration. Dev. Neurobiol. *71*, 1186–1211.

Moore, D.L., Blackmore, M.G., Hu, Y., Kaestner, K.H., John, L., Lemmon, V.P., and Goldberg, J.L. (2009). KLF Family Members Regulate Intrinsic Axon Regeneration Ability. Science (80-.). *326*, 298–301.

Moore, D.L., Apara, A., and Goldberg, J.L. (2011). Krüppel-like transcription factors in the nervous system: novel players in neurite outgrowth and axon regeneration. Mol. Cell. Neurosci. *47*, 233–243.

Moore, R.Y., Speh, J.C., and Card, J.P. (1995). The Retinohypothalamic Tract Originates From a Distinct Subset of Retinal Ganglion Cells. J. Comp. Neurol. *366*, 351–366.

Morin, L.P., and Studholme, K.M. (2014). Retinofugal Projections in the Mouse.

Moujalled, D., Cook, W., Murphy, J., and Vaux, D. (2014). Necroptosis induced by RIPK3 requires MLKL but not Drp1. Cell Death Dis. *5*, e1086.

Mu, X., and Klein, W.H. (2004). A gene regulatory hierarchy for retinal ganglion cell specification and differentiation. Semin. Cell Dev. Biol. *15*, 115–123.

Mu, X., Fu, X., Sun, H., Beremand, P.D., Thomas, T.L., and Klein, W.H. (2005). A gene network downstream of transcription factor Math5 regulates retinal progenitor cell competence and ganglion cell fate. Dev. Biol. *280*, 467–481.

Murakami, M., Ichisaka, T., Maeda, M., Oshiro, N., Hara, K., Edenhofer, F., Kiyama, H., Yonezawa, K., and Yamanaka, S. (2004). mTOR Is Essential for Growth and Proliferation in Early Mouse Embryos and Embryonic Stem Cells. Mol. Cell. Biol. *24*, 6710–6718.

Nadal-Nicolás, F.M., Jiménez-López, M., Salinas-Navarro, M., Sobrado-Calvo, P., Alburquerque-Béjar, J.J., Vidal-Sanz, M., and Agudo-Barriuso, M. (2012). Whole number, distribution and co-expression of brn3 transcription factors in retinal ganglion cells of adult albino and pigmented rats. PLoS One *7*, e49830.

Naumann, J. (2012). Search for Paradise: A Patient's Account of the Artificial Vision Experiment.

Nawabi, H., Belin, S., Cartoni, R., Williams, P.R., Wang, C., Latremolière, A., Wang, X., Zhu, J., Taub, D.G., Fu, X., et al. (2015). Doublecortin-Like Kinases Promote Neuronal Survival and Induce Growth Cone Reformation via Distinct Mechanisms. Neuron *88*, 704–719.

Norsworthy, M.W., Bei, F., Kawaguchi, R., Wang, Q., Tran, N.M., Li, Y., Brommer, B., Zhang, Y., Wang, C., Sanes, J.R., et al. (2017). Sox11 Expression Promotes Regeneration of Some Retinal Ganglion Cell Types but Kills Others. Neuron *94*, 1112–1120.

Opal, P., Garcia, J.J., Propst, F., Matilla, A., Orr, H.T., and Zoghbi, H.Y. (2003). Mapmodulin/Leucine-rich Acidic Nuclear Protein Binds the Light Chain of Microtubule-associated Protein 1B and Modulates Neuritogenesis. J. Biol. Chem. *278*, 34691–34699.

Oster, S.F., Deiner, M., Birgbauer, E., and Sretavan, D.W. (2004). Ganglion cell axon pathfinding in the retina and optic nerve. Semin. Cell Dev. Biol. *15*, 125–136.

Painter, M.W., Brosius Lutz, A., Cheng, Y.-C., Latremoliere, A., Duong, K., Miller, C.M., Posada, S., Cobos, E.J., Zhang, A.X., Wagers, A.J., et al. (2014). Diminished Schwann cell repair responses underlie age-associated impaired axonal regeneration. Neuron *83*, 331–343.

Pan, L., Deng, M., Xie, X., and Gan, L. (2008). ISL1 and BRN3B co-regulate the differentiation of murine retinal ganglion cells. Development *135*, 1981–1990.

Park, K.K., Liu, K., Hu, Y., Smith, P.D., Wang, C., Cai, B., Xu, B., Connolly, L., Kramvis, I., Sahin, M., et al. (2008). Promoting axon regeneration in the adult CNS by modulation of the PTEN/mTOR pathway. Science *322*, 963–966.

Patodia, S., and Raivich, G. (2012). Role of transcription factors in peripheral nerve regeneration. Front. Mol. Neurosci. *5*, 8.

Penfield, W. (1947). Some observations on the cerebral cortex of man. Proc. R. Soc. Lond. B Biol. Sci. *134*, 329–347.

Petros, T.J., Rebsam, A., and Mason, C.A. (2008). Retinal Axon Growth at the Optic Chiasm : To Cross or Not to Cross. Annu. Rev. Neurosci. *31*, 295–317.

Piotrowska, N., and Winkler, P. (2007). Otfrid Foerster, the great neurologist and neurosurgeon from Breslau (Wrocław): his influence on early neurosurgeons and legacy to present-day neurosurgery. J Neurosurg. *107*, 451–456.

Poggi, L., Vitorino, M., Masai, I., and Harris, W.A. (2005). Influences on neural lineage and mode of division in the zebrafish retina in vivo. J. Cell Biol. *171*, 991–999.

Polleux, F., and Snider, W. (2010). Initiating and Growing an Axon. Cold Spring Harb. Perspect. Biol. *2*, 1–20.

Potzner, M.R., Tsarovina, K., Binder, E., Penzo-Méndez, A., Lefebvre, V., Rohrer, H., Wegner, M., and Sock, E. (2010). Sequential requirement of Sox4 and Sox11 during development of the sympathetic nervous system. Development *137*, 775–784.

Pudenz, R.H. (1993). Neural Stimulation : Clinical and Laboratory Experiences. Surg Neurol 235–242.

Quigley, H.A., Sanchez, R.M., Dunkelberger, G.R., Hernault, N.L.L., and Baginski, T.A. (1987). Chronic Glaucoma Selectively Damages Large Optic Nerve Fibers. Invest. Ophthalmol. Vis. Sci. *28*, 913–920.

Riesenberg, A.N., Le, T.T., Willardsen, M.I., Blackburn, D.C., Vetter, M.L., and Brown, N.L. (2009). Pax6 regulation of Math5 during mouse retinal neurogenesis. Genesis *47*, 175–187.

Ring, K.L., Tong, L.M., Balestra, M.E., Javier, R., Andrews-Zwilling, Y., Li, G., Walker, D., Zhang, W.R., Kreitzer, A.C., and Huang, Y. (2012). Direct reprogramming of mouse and human fibroblasts into multipotent neural stem cells with a single factor. Cell Stem Cell *11*, 100–109.

Risso, D., Ngai, J., Speed, T., and Dudoit, S. (2014). Normalization of RNA-seq data using factor analysis of control genes or samples. Nat. Biotechnol. *32*, 896–902.

Robinson, M.D., McCarthy, D.J., and Smyth, G.K. (2009). edgeR: A Bioconductor package for differential expression analysis of digital gene expression data. Bioinformatics *26*, 139–140.

Rodriguez, A.R., Müller, L.P. de S., and C. Brecha, N. (2014). The RNA binding protein RBPMS is a selective marker of ganglion cells in the mammalian retina. J Comp Neurol.

Rushton, D.N., Brindley, G.S., Polkey, C.E., and Browning, G. V (1989). Implant infections and antibiotic-impregnated silicone rubber coating. J. Neurol. Neurosurg. Psychiatry *52*, 223–229.

Samson, T., van Buul, J.D., Kroon, J., Welch, C., Bakker, E.N., Matlung, H.L., van den Berg, T.K., Sharek, L., Doerschuk, C., Hahn, K., et al. (2013). The Guanine-Nucleotide Exchange Factor SGEF Plays a Crucial Role in the Formation of Atherosclerosis. PLoS One *8*.

Sanes, J.R., and Masland, R.H. (2015). The Types of Retinal Ganglion Cells: Current Status and Implications for Neuronal Classification. Annu. Rev. Neurosci. *38*, 150421150146009.

Sarkar, A., and Hochedlinger, K. (2013). The Sox family of transcription factors: Versatile regulators of stem and progenitor cell fate. Cell Stem Cell *12*, 15–30.

Schaar, B.T., Kinoshita, K., and McConnell, S.K. (2004). Doublecortin Microtubule Affinity Is Regulated by a Balance of Kinase and Phosphatase Activity at the Leading Edge of Migrating Neurons. Neuron *41*, 203–213.

Schmidt, T.M., and Kofuji, P. (2011). Structure and function of bistratified intrinsically photosensitive retinal ganglion cells in the mouse. J. Comp. Neurol. *519*, 1492–1504.

Schmidt, E., Bak, M., Hambrecht, F., Kufta, C., and O'Rourke, DK Vallabhanath, P. (1996). Feasibility of a visual prosthesis for the blind based on intracortical microstimulation of the visual cortex. Brain *119*, 507–522.

Sexton, T.J., Bleckert, A., Turner, M.H., and Gelder, R.N. Van (2015). Type I intrinsically photosensitive retinal ganglion cells of early post-natal development correspond to the M4 subtype. Neural Dev. 1–15.

Shaw, J. (1955). Method and means for aiding the blind (US 2721316 A).

Skene, J.H.P., and Willard, M. (1981). Axonally Transported Proteins Associated with Axon Growth in Rabbit Central and Peripheral Nervous Systems. J. Cell Biol. *89*.

Smith, P.D., Sun, F., Park, K.K., Cai, B., Wang, C., Kuwako, K., Martinez-carrasco, I., Connolly, L., and He, Z. (2009). SOCS3 Deletion Promotes Optic Nerve Regeneration In Vivo. Neuron *64*, 617–623.

Soetedjo, R., Kaneko, C.R.S., and Fuchs, A.F. (2002). Evidence Against a Moving Hill in the Superior Colliculus During Saccadic Eye Movements in the Monkey. J. Neurophysiol. *87*, 2778–2789.

Spinelli, L., Black, F.M., Berg, J.N., Eickholt, B.J., and Leslie, N.R. (2015). Functionally distinct groups of inherited PTEN mutations in autism and tumour syndromes. Med. Genet. *52*, 128–134.

Su, Z., Niu, W., Liu, M.-L., Zou, Y., and Zhang, C.-L. (2014). In vivo conversion of astrocytes to neurons in the injured adult spinal cord. Nat. Commun. *5*.

Sun, F., Park, K.K., Belin, S., Wang, D., Lu, T., Chen, G., Zhang, K., Yeung, C., Feng, G., Yankner, B. a, et al. (2011). Sustained axon regeneration induced by co-deletion of PTEN and SOCS3. Nature *480*, 372–375.

Sweeney, N.T., Tierney, H., and Feldheim, D.A. (2014). Tbr2 is required to generate a neural circuit mediating the pupillary light reflex. J. Neurosci. *34*, 5447–5453.

Triplett, J.W., and Feldheim, D.A. (2012). Seminars in Cell & Developmental Biology Eph and ephrin signaling in the formation of topographic maps. Semin. Cell Dev. Biol. *23*, 7–15.

Triplett, J.W., Wei, W., Gonzalez, C., Sweeney, N.T., Huberman, A.D., Feller, M.B., and Feldheim, D.A. (2014). Dendritic and axonal targeting patterns of a genetically-specified class of retinal ganglion cells that participate in image-forming circuits. Neural Dev. *9*, 2.

Usui, A., Mochizuki, Y., Iida, A., Miyauchi, E., Satoh, S., Sock, E., Nakauchi, H., Aburatani, H., Murakami, A., Wegner, M., et al. (2013). The early retinal progenitor-expressed gene Sox11 regulates the timing of the differentiation of retinal cells. Development *140*, 740–750.

Veeke, H., Lodewijks, G., and Ottjes, J. (2006). Conceptual design of industrial systems : an approach to support collaboration. Res Eng Des. *17*, 85–101.

Veldman, M.B., Bemben, M.A., Thompson, R.C., and Goldman, D. (2007). Gene expression analysis of zebrafish retinal ganglion cells during optic nerve regeneration identifies KLF6a and KLF7a as important regulators of axon regeneration. Dev. Biol. *312*, 596–612.

Vetter, M.L., and Brown, N.L. (2001). The role of basic helix-loop-helix genes in vertebrate retinogenesis. Semin. Cell Dev. Biol. *12*, 491–498.

Wang, J.T., Kunzevitzky, N.J., Dugas, J.C., Cameron, M., Barres, B.A., and Goldberg, J.L. (2007). Disease Gene Candidates Revealed by Expression Profiling of Retinal Ganglion Cell Development. J. Neurosci. *27*, 8593–8603.

Wang, Z., Reynolds, A., Kirry, A., Nienhaus, C., and Blackmore, M.G. (2015). Overexpression of sox11 promotes corticospinal tract regeneration after spinal injury while interfering with functional recovery. J. Neurosci. *35*, 3139–3145.

Welsbie, D.S., Mitchell, K.L., Jaskula-ranga, V., Sluch, V., Yang, Z., Kim, J., Buehler, E., Patel, A., Martin, S., Zhang, P.-W., et al. (2017). Enhanced Functional Genomic Screening Identifies Novel Mediators of Dual Leucine Zipper Kinase- Dependent Injury Signaling in Neurons. Neuron *94*, 1142–1154.e6.

Williams, R.R., Venkatesh, I., Pearse, D.D., Udvadia, A.J., and Bunge, M.B. (2015). MASH1 / Ascl1a Leads to GAP43 Expression and Axon Regeneration in the Adult CNS. PLoS One 1–18.

Williams, S.E., Mann, F., Erskine, L., Sakurai, T., Wei, S., Rossi, D.J., Gale, N.W., Holt, C.E., Mason, C.A., and Henkemeyer, M. (2003). Ephrin-B2 and EphB1 Mediate Retinal Axon Divergence at the Optic Chiasm. Neuron *39*, 919–935.

Xiang, M., Zhoui, L., Macke, J.P., Eddy, L., Shows, T.B., and Nathansis, J. (1995). The Brn-3 Family of POU-Domain Factors : Primary Structure, Binding Specificity, and Expression in Subsets of Retinal Ganglion Cells and Somatosensory Neurons. J. Neurosci. *15*, 4762–4785.

Zhang, Y., Bo, X., Schoepfer, R., Holtmaat, A.J.D.G., Verhaagen, J., Emson, P.C., Lieberman, A.R., and Anderson, P.N. (2005). Growth-associated protein GAP-43 and L1 act synergistically to promote regenerative growth of Purkinje cell axons in vivo. Proc. Natl. Acad. Sci. *102*.

Zhu, Y., Pires, K.M.P., Whitehead, K.J., Olsen, C.D., Wayment, B., Zhang, C., Bugger, H., Ilkun, O., Litwin, S.E., Thomas, G., et al. (2013). Mechanistic Target of Rapamycin (Mtor) Is Essential for Murine Embryonic Heart Development and Growth. PLoS One *8*.

Supplementary Material

Figure S.1: *Sox11* overexpression greatly exceeds endogenous expression levels, and leads to lengthy, sustained regeneration at 4 weeks after injury

(A) Representative retinal sections stained with anti-RBPMS and anti-SOX11 antibodies from retinas injected with AAV-Control (PLAP) or AAV-Sox11, then either kept intact or given optic nerve crush for 3 days before sacrifice. Scale bar represents 50 µm.

(B) Quantification of SOX11-positive cells in GCL as in A.

(C) Representative images of optic nerve sections with CTB-labeled axons from the wild type mice at 4 weeks after injury with prior intravitreal injection of AAV-Control or AAV-Sox11. Scale bar represents 500 µm.

(D) Quantification of the numbers of regenerating axons in both groups. Data are expressed as mean ± SEM (n = 4-6). * $P < 0.05$, ** $P < 0.01$ (ANOVA with Bonferroni posttests).

Figure S.1 (Continued)

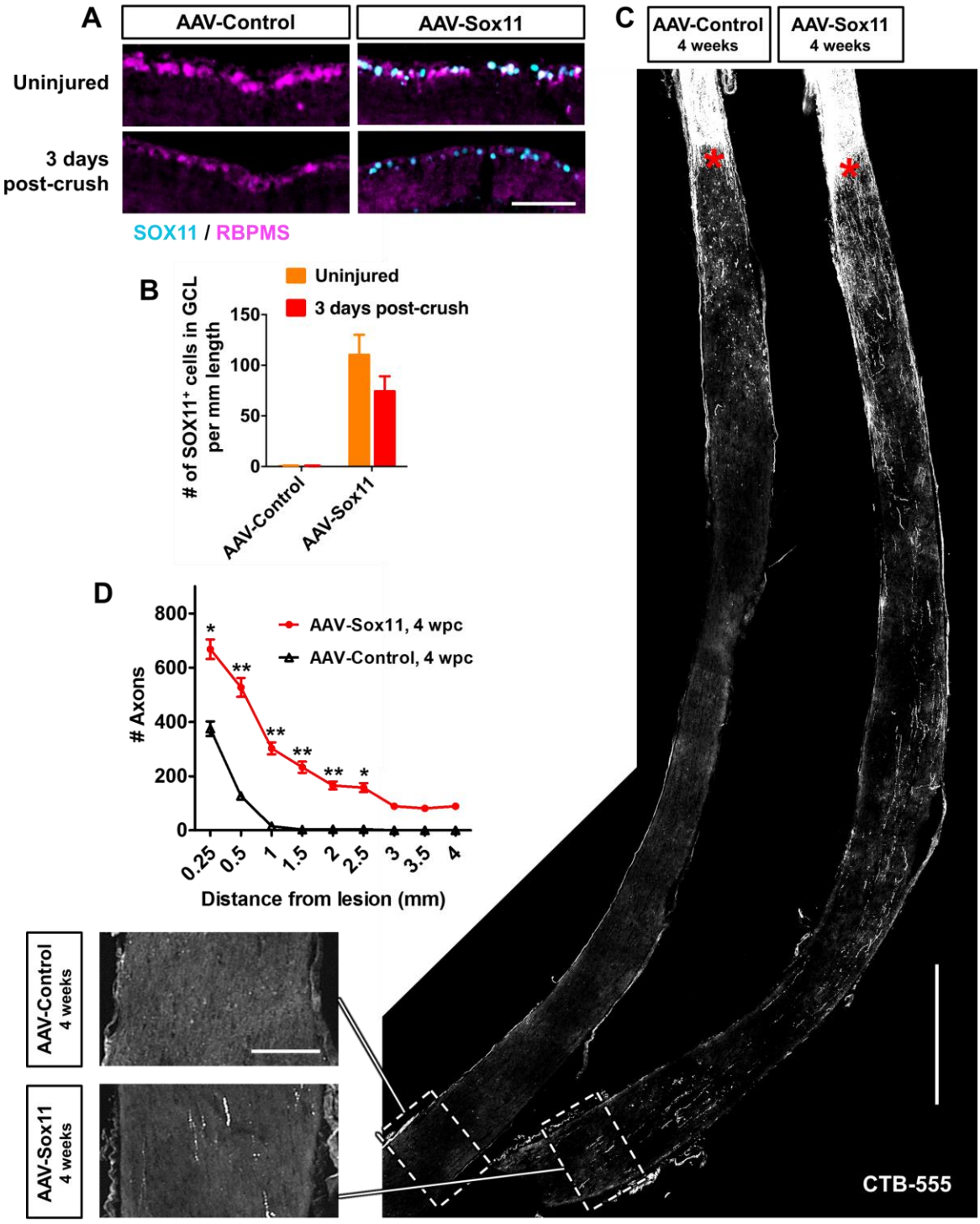

Figure S.2: *Sox11* phenotypes are insensitive to *Bcl2* overexpression and are cell autonomous

(A) Quantification of regenerating axons in mice with Bcl2 overexpression background, injected with either AAV-Control or AAV-Sox11 for 2 weeks, given optic nerve crush, allowed to regenerate for 2 weeks, and given CTB tracer injection before sacrifice.

(B) Survival of RGCs stained with TUJ1/TUBB3 in flat-mounted retinas in the same experimental conditions as A.

(C) Retinas in the same experimental conditions as A were sectioned, then stained for Osteopontin. Scalebar represents 50 μm.

(D) Vglut2-Cre mice were injected with AAV-Control or AAV-FLEX-Sox11 for 2 weeks, given optic nerve crush, regenerated 2 weeks, and given CTB-555 tracer before sacrifice. Representative sections of optic nerves are shown. Scalebar represents 250 μm.

(E) Quantification of regeneration as in D.

(F) Cell survival of the same experimental conditions as D, quantified from retinas stained with RBPMS. Numbers are relative to RBPMS counts from sections in intact retinas.

(G) Proportion of RGCs expressing SOX11 from the same conditions as D.

Figure S.2 (Continued)

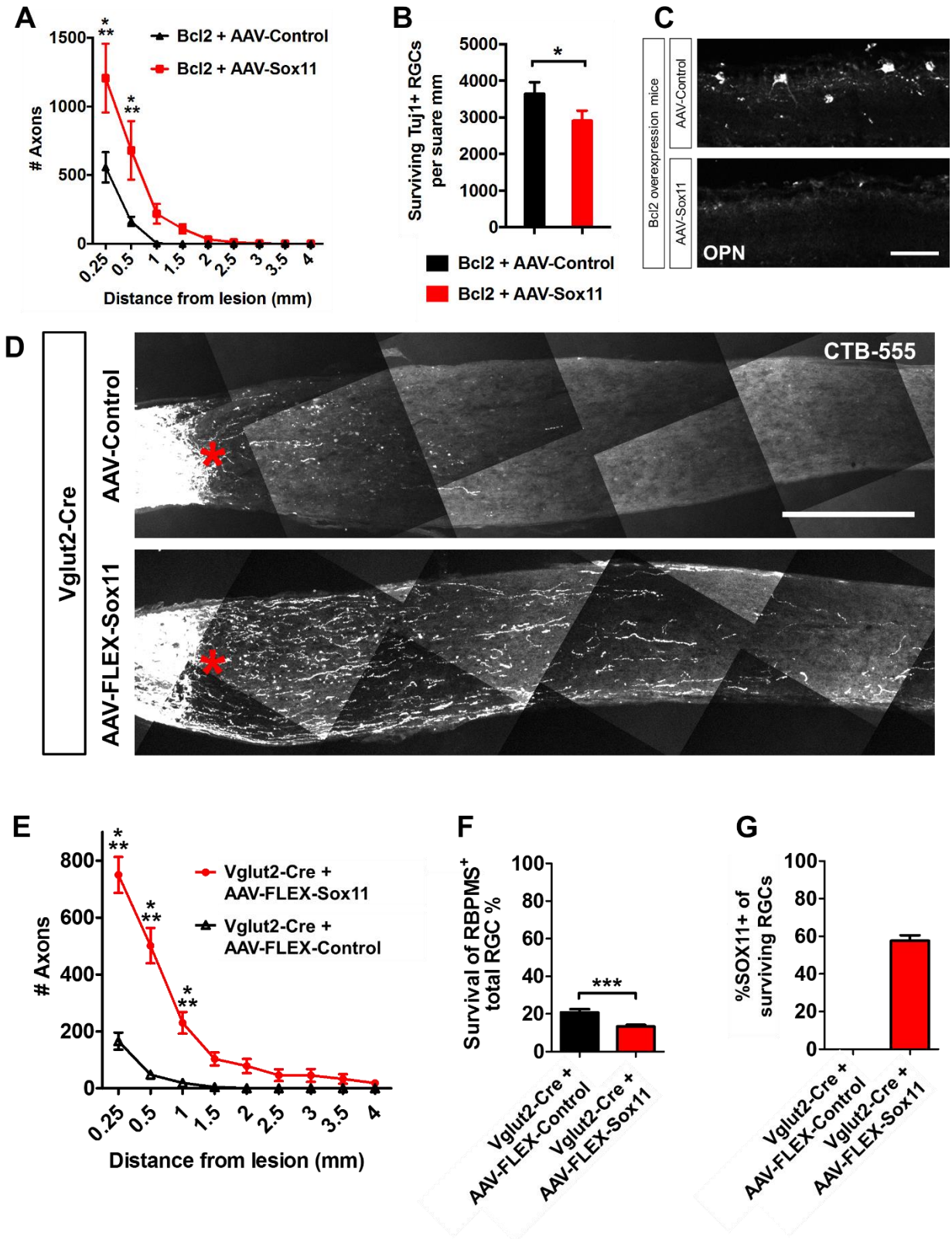

Figure S.3: Characterization of the dataset obtained from RNA sequencing for comparing AAV-PLAP to AAV-Sox11 after injury

(A) Timecourse of Alpha RGC elimination from *Sox11* expression, without optic nerve crush. Retinal sections from 1, 2, 3, or 4 weeks of *Sox11* expression, or in control eyes, were quantified for SMI32+ cells. At 2 weeks of *Sox11* overexpression, Alpha RGC ablation is underway but incomplete. We selected this timepoint to include both Alpha RGCs and non-Alpha RGCs in the dataset.

(B) Mice were injected with AAV-Control or AAV-Sox11 for 2 weeks then sacrificed at 3 days after optic nerve crush. Retinal sections were quantified for Osteopontin+ cells relative to the overall population of RBPMS+ cells in intact retinas.

(C) Heatmap based on the Pearson correlation matrix between FPKM values for all transcripts of each sample to all other samples analyzed. Dendrograms (at top and at left) indicate relations between samples, as defined by unsupervised clustering. All experimental steps through RNA extraction were performed on three different days for “A”, “B”, and “C” respectively, and all samples with the same letter were performed on the same day. Correlation values are represented in grayscale, with minimum and maximum normalized values of 0 and 1 respectively (key at bottom right).

(D) Number of differentially expressed genes at the threshold of FDR < 0.1. At this threshold, 1920 genes were down-regulated by *Sox11*, and 877 were up-regulated by *Sox11*, relative to AAV-Control.

(E) Heat map of differentially expressed genes at the threshold of p_adjusted < 0.1. Each row represents one gene’s expression profile. Genes were clustered based on similarity of expression patterns (right dendrogram). Blue to red colors indicate low to high expression respectively, according to the color key (bottom right). Columns indicate individual samples and sample similarity is given by the dendrogram (top).

Figure S.3 (Continued)

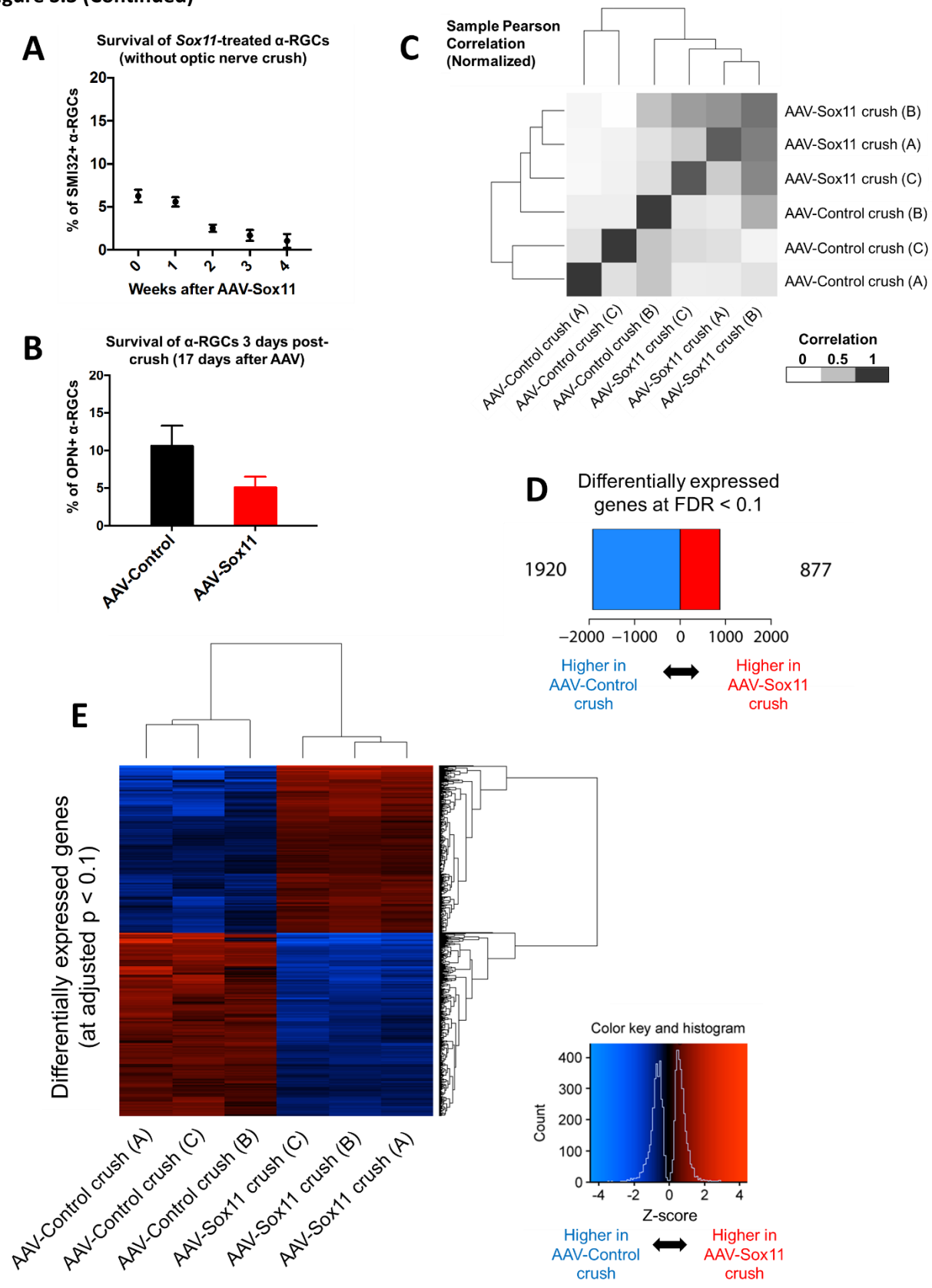

Figure S.4: Combinatorial effect of *Sox11* and *Pten* deletion at 2 weeks after injury and co-staining of RGCs retrogradely labeled by FluoroGold in intact, non-regenerative and regenerative animals

(A, B) Images (A) and quantification (B) showing CTB-labeled regenerating axons in the optic nerves at 2 weeks post crush (wpc). Scale bar in (A) represents 500 μm. Data in (B) are expressed as mean ± SEM (n = 4-5). ** $P < 0.01$ (two-way ANOVA with Bonferroni posttests).

(C) Characterization of a FluoroGold tracing method for retrogradely labeling RGCs with contiguous (intact or regenerating) axons, but not RGCs with injured axons. 4% FG was injected ~1.5 mm distal to the common crush site. In wild-type, intact mice, many RGCs are labeled as shown by the location of the FG-positive cells at the retinal ganglion cell layer as well as their co-staining with RGC marker RBPMS. When such FG tracing was performed in wild-type mice 2 weeks after optic nerve crush, no FG labeling was observed at the retinal ganglion cell layer in all mice examined, suggesting FG did not diffuse back to the injury site and was not picked up by axotomized, non-regenerative RGCs. Scale bar represents 100 μm.

(D) Co-staining of FG-traced RGCs with DCX and RBPMS in ΔPTEN/Sox11-treated animals 2 weeks after injury. Scale bar represents 20 μm.

(E) Co-staining of FG-traced RGCs with the mTOR activity marker phosphor-S6 (PS6) in ΔPTEN/Sox11-treated animals 2 weeks after injury. Scale bar represents 20 μm.

(F) Quantification of Osteopontin-expressing alpha RGCs in sections of post-crush retinas with ΔPTEN/Control or ΔPTEN/Sox11 treatments, compared to intact controls. Two sections were analyzed per animal, and numbers indicate the number of positive RGCs per millimeter of ganglion cell layer analyzed. Significance is indicated by **, $P < 0.01$; ***, $P < 0.001$ by ANOVA with Bonferroni posttests (n = 4-5 per group).

Figure S.4 (Continued)

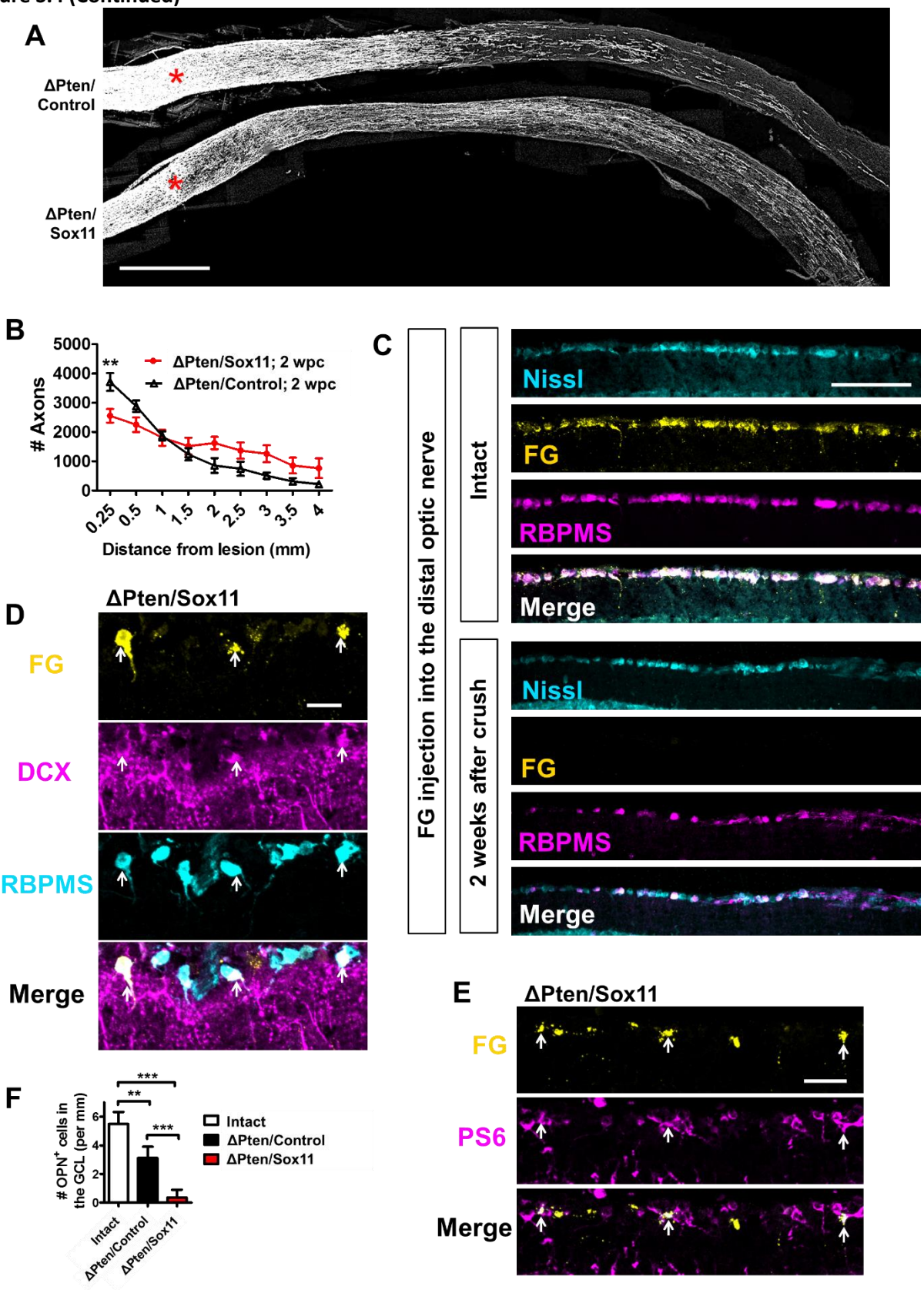

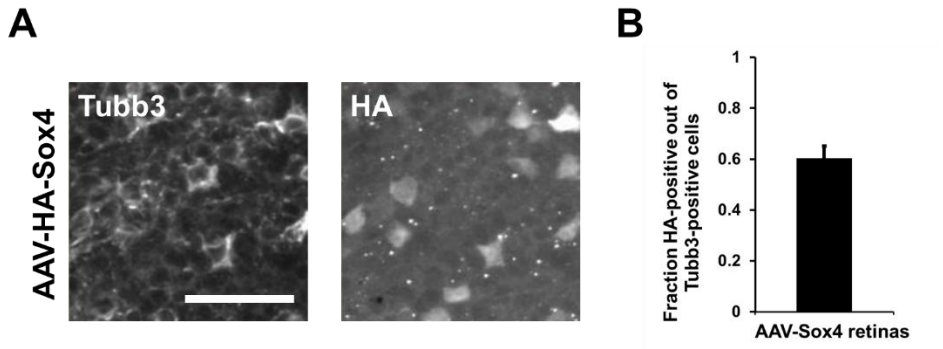

Figure S.5: Expression of AAV-Sox4

(A,B) Images (A) and quantification (B) characterizing the efficiency of AAV-Sox4 expression after two weeks of infection. Scalebar represents 50 µm.

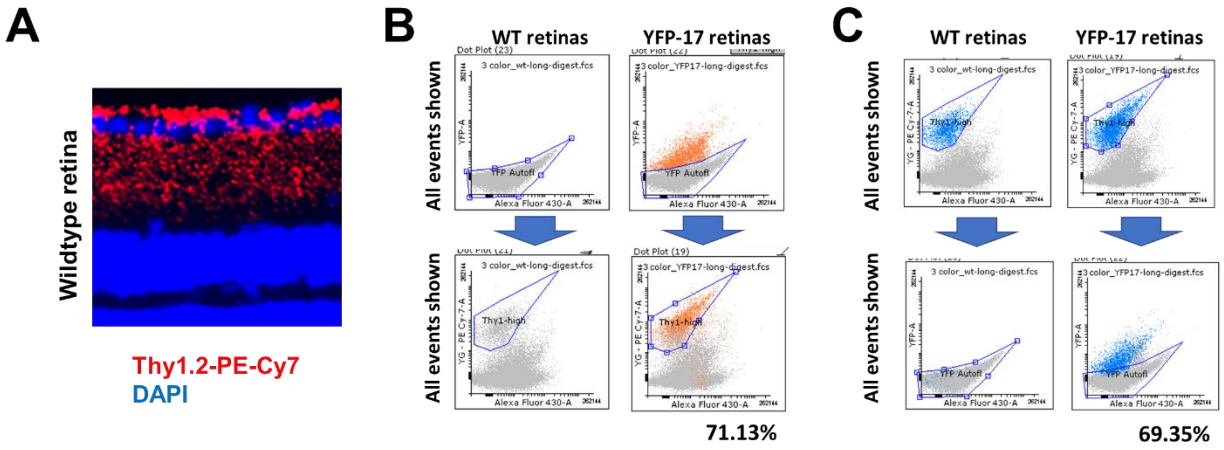

Figure S.6: Validation of FACS and antibody for extracting RNA from RGCs

(A) Staining of fixed retinal tissue sections with the Thy1.2-PE-Cy7 antibody used for sorting. Specifically, after a 10 minute rinse and 5 minutes of blocking with bovine serum albumin, the sections were stained with Thy1.2-PE-Cy7 antibody diluted 1:333 in fresh blocking solution, for 5 minutes. The labeling is appropriate for RGCs. (B-C) Flow cytometric analysis of RGCs to validate the Thy1.2-PE-Cy7 antibody. We dissociated retinal cells from either wildtype mice, or YFP-17 mice that mark RGCs with YFP fluorescence, and stained them with Thy1.2-PE-Cy7 antibody. We analyzed flow cytometric results in Flowing Software. (B) Forward-check of Thy1.2 antibody. Analyzing YFP events versus an arbitrary channel of autofluorescence revealed that YFP-high events (orange) were greatly enriched for high Thy1.2 staining. Note that coincidence of Thy1.2 and YFP should not be perfect, since YFP is generally limited to cell bodies, may not be expressed in all RGCs, and might have limited signal-to-noise performance from retinal cell autofluorescence near YFP wavelengths. (C) Reverse-check of Thy1.2 antibody. Analyzing Thy1.2-high events (blue) revealed they are enriched for YFP-high events in YFP-17 mice.

Table S.1: Significant differentially expressed genes between AAV-Sox11 and AAV-Control in RGCs

This is a large excel document. Please download from:

http://www.cell.com/cms/attachment/2105873293/2081327221/mmc2.xlsx

No login or payment is necessary.

Table S.2: Gene Ontology list of terms enriched or depleted by Sox11 versus Control in RGCs

This is a large excel document. Please download from:

http://www.cell.com/cms/attachment/2105873293/2081327219/mmc3.pdf

No login or payment is necessary.